2010-09

Frequency diverse array radar

Aytun, Alper

Monterey, California. Naval Postgraduate School

NAVAL POSTGRADUATE SCHOOL

MONTEREY, CALIFORNIA

THESIS

FREQUENCY DIVERSE ARRAY RADAR

by

Alper Aytun

September 2010

Thesis Advisor: David C. Jenn
Second Reader: Terry Smith

Approved for public release; distribution is unlimited

THIS PAGE INTENTIONALLY LEFT BLANK

REPORT DOCUMENTATION PAGE		Form Approved OMB No. 0704-0188

1. AGENCY USE ONLY *(Leave blank)*	2. REPORT DATE September 2010	3. REPORT TYPE AND DATES COVERED Master's Thesis

4. TITLE AND SUBTITLE Frequency Diverse Array Radar	5. FUNDING NUMBERS
6. AUTHOR(S) Alper Aytun	
7. PERFORMING ORGANIZATION NAME(S) AND ADDRESS(ES) Naval Postgraduate School Monterey, CA 93943-5000	8. PERFORMING ORGANIZATION REPORT NUMBER
9. SPONSORING /MONITORING AGENCY NAME(S) AND ADDRESS(ES) N/A	10. SPONSORING/MONITORING AGENCY REPORT NUMBER

11. SUPPLEMENTARY NOTES The views expressed in this thesis are those of the author and do not reflect the official policy or position of the Department of Defense or the U.S. Government. IRB Protocol number _____.

12a. DISTRIBUTION / AVAILABILITY STATEMENT Approved for public release; distribution is unlimited	12b. DISTRIBUTION CODE

13. ABSTRACT (maximum 200 words)

Electronic scanning is the most desirable feature of state-of-the-art radar systems. With electronic scanning, it is possible to steer the main beam of an array antenna instantaneously into a desired direction where no mechanical mechanism is involved in the scanning process. Electronic scanning methods including phase scanning, time delay scanning, and frequency scanning have been used in various radar applications; however new and cheaper scanning methods are still being investigated. It is the purpose of this thesis to investigate an array configuration called frequency diverse array (FDA), which gives rise to range-, time-, and angle-dependent scanning without using phase shifters.

In this thesis, first, frequency diverse array as a time-modulated array is presented. A general analysis and the theory of time domain scanning is given. Equations derived for a time-modulated frequency diverse array are simulated using MATLAB. Amplitude tapering and Fourier series expansion is implemented in MATLAB and the results are provided for comparison.

Secondly, analysis of a frequency diverse array is presented. Time-, range-, and angle-dependent electronic scanning is achieved by applying a small amount of frequency shift among the antenna elements. The simulation results for radiation patterns with various excitation types are given.

Lastly, the radar applications of FDA are considered. The received power from a target at a fixed range is simulated in MATLAB and the results are presented.

14. SUBJECT TERMS Array Antenna, Frequency Diversity, Frequency Scanning, Frequency Diverse Array, Radar	15. NUMBER OF PAGES 131
	16. PRICE CODE

17. SECURITY CLASSIFICATION OF REPORT	18. SECURITY CLASSIFICATION OF THIS PAGE	19. SECURITY CLASSIFICATION OF ABSTRACT	20. LIMITATION OF ABSTRACT
Unclassified	Unclassified	Unclassified	UU

NSN 7540-01-280-5500 Standard Form 298 (Rev. 2-89)
Prescribed by ANSI Std. 239-18

THIS PAGE INTENTIONALLY LEFT BLANK

Approved for public release; distribution is unlimited

FREQUENCY DIVERSE ARRAY RADAR

Alper Aytun
Lieutenant Junior Grade, Turkish Navy
B.S., Turkish Naval Academy, 2003

Submitted in partial fulfillment of the
requirements for the degree of

MASTER OF SCIENCE IN ELECTRONIC WARFARE SYSTEMS ENGINEERING

from the

NAVAL POSTGRADUATE SCHOOL
September 2010

Author: Alper Aytun

Approved by: Dr. David C. Jenn
Thesis Advisor

Lt. Col. Terry Smith
Second Reader

Dr. Dan Boger
Chairman, Department of Information Sciences

THIS PAGE INTENTIONALLY LEFT BLANK

ABSTRACT

Electronic scanning is the most desirable feature of state-of-the-art radar systems. With electronic scanning, it is possible to steer the main beam of an array antenna instantaneously into a desired direction where no mechanical mechanism is involved in the scanning process. Electronic scanning methods including phase scanning, time delay scanning, and frequency scanning have been used in various radar applications; however new and cheaper scanning methods are still being investigated. It is the purpose of this thesis to investigate an array configuration called frequency diverse array (FDA), which gives rise to range-, time-, and angle-dependent scanning without using phase shifters.

In this thesis, first, frequency diverse array as a time-modulated array is presented. A general analysis and the theory of time domain scanning is given. Equations derived for a time-modulated frequency diverse array are simulated using MATLAB. Amplitude tapering and Fourier series expansion is implemented in MATLAB and the results are provided for comparison.

Secondly, analysis of a frequency diverse array is presented. Time-, range-, and angle-dependent electronic scanning is achieved by applying a small amount of frequency shift among the antenna elements. The simulation results for radiation patterns with various excitation types are given.

Lastly, the radar applications of FDA are considered. The received power from a target at a fixed range is simulated in MATLAB and the results are presented.

THIS PAGE INTENTIONALLY LEFT BLANK

TABLE OF CONTENTS

LIST OF FIGURES

THIS PAGE INTENTIONALLY LEFT BLANK

LIST OF TABLES

THIS PAGE INTENTIONALLY LEFT BLANK

LIST OF ACRONYMS AND ABBREVIATIONS

AF	array factor
ASK	amplitude shift keying
CAD	computer-aided-design
CW	continuous wave
EF	element factor
ESA	electronically scanned array
FDA	frequency diverse array
FFT	fast Fourier transform
GMTI	ground moving target indication
HPBW	half-power beamwidth
LFMCW	linear frequency modulation continuous wave
LNA	low noise amplifier
MTI	moving target indication
NRL	navy research lab
OOK	on-off keying
RAM	random-access-memory
RF	radio frequency
SAR	synthetic aperture radar
SF	subarray factor
SNR	signal-to-noise ratio
SNR	signal-to-noise ratio
TWT	travelling wave tube

THIS PAGE INTENTIONALLY LEFT BLANK

ACKNOWLEDGMENTS

First of all, I would like to express my gratitude to the great Turkish Nation, Turkish Armed Forces, and especially the Turkish Navy for providing this great opportunity to pursue my Master of Science degree in the United States at the Naval Postgraduate School.

I would like to express my sincere thanks to Prof. David Jenn and my second reader Lt. Col. Terry Smith for their help, professional guidance, and patience during the thesis process. I would have never been able to complete this thesis without their support and comments.

I would also like to thank to my parents, Arif Aytun and Bahtiyar Aytun, and my sister, Işıl Aytun, for their patience and endless support during my two-year journey at the Naval Postgraduate School. I always felt their love and support in my heart and I would like to dedicate this thesis to my beloved family.

THIS PAGE INTENTIONALLY LEFT BLANK

DISCLAIMER

The views expressed in this thesis are those of the author and do not reflect the official policy or position of Turkish Republic, Turkish Armed Forces, Turkish Army, Turkish Navy, Turkish Air Force, U.S. Navy or the Naval Postgraduate School.

THIS PAGE INTENTIONALLY LEFT BLANK

I. INTRODUCTION

A. BACKGROUND

One of the most desirable features of modern radar systems is the capability of performing beam scanning by electronic methods. An electronically scanned array (ESA) is state-of-the-art in radar technology and has been used in many systems on various platforms. It has major advantages compared to mechanically steered radars. These advantages include increased data rate, instantaneous positioning of the radar beam, and elimination of mechanical errors, beam agility, multi-mode operation and simultaneous multi-target tracking.

A considerable amount of effort has been expended in the investigation of the methods for electronic scanning of antenna systems. Techniques that have been studied in this connection include frequency variation, phase shift scan (using ferrites, travelling wave tubes (TWTs), delay lines, etc.), and in a minor way, the ideas of space time equivalence [1]. Generally, all of these are narrowband systems that use amplitude or phase modulated waveforms that are applied to all elements in the array. A more nontraditional approach is to vary the excitation across the array in either the time or frequency domain. This leads to frequency diverse arrays (FDAs), where the phase shifter is eliminated.

It is the purpose of this thesis to investigate the characteristics of frequency scanning and frequency diverse arrays. With radar and electronic warfare as a focus, this thesis researches the applications of frequency diverse arrays and explores its potential capabilities.

In the next subsections, there is a brief introduction to radar and electronic warfare systems, the role of radar antenna, desired antenna properties, performance measures, gain, beamwidth pattern, and bandwidth of a radar system.

1. The Historical Development of Radar

The word “radar” is the acronym of *ra*dio *d*etection and *r*anging; however, due to its wide use, the word has become a standard noun in English, and almost all people have had an experience with radar [2].

The history of radar extends back to 1885 when German physicist Heinrich Hertz conducted several experiments and demonstrated the reflection of waves. In 1904, another German, Christian Hulsmeyer, designed an apparatus known to be monostatic radar that detected ships. However, the importance of his invention was not realized at that time.

In 1922, S. G. Marconi, who is known as the pioneer of wireless radio, observed the radio detection of targets. In the same year, L. C. Young and A. H. Taylor of the U.S. Naval Research Laboratory (NRL) demonstrated ship detection by radar. In 1930, Hyland accidentally detected aircrafts by radar, and in 1934, first continuous wave (CW) radar was designed and used.

The development of radar accelerated and spread during World War II independently in countries including the United States, United Kingdom, Germany, Soviet Union, France, Italy, Japan and the Netherlands [2, 3]. By the end of the war, the value of radar and the advantages of microwave frequencies and pulsed waveforms were widely recognized [2].

Since those early days of radar system experiments, a number of developments have taken place in the world of radar. Use of Doppler effect on moving target indication (MTI) radar, pulse compression, pulse Doppler concepts, use of solid state transistor, klystron, TWTs, and electronically scanned array antennas can all be counted as the major developments in the radar arena. However, the importance of the digital signal and data processing should also be noted, which has led to many theoretical capabilities to be realized practically.

Today, applications of radar include military applications, remote sensing (weather observation), air traffic control, law enforcement and highway safety, aircraft safety and navigation, ship safety, and space vehicles. Radar has also been found in many

applications in industry to measure speed and distance and with special care, the identification of physical features of a system of interest.

2. Basic Radar Functions

Radar is an electromagnetic system for the detection and location of objects such as aircrafts, ships, spacecraft, vehicles, and people, as well as sensing the natural environment [3]. Radar radiates electromagnetic energy using the directionality of its antenna and then detects the presence of the target by thresholding the received echo signal that is reflected from the target. A time-shared single antenna is usually used for both transmitting and receiving. This type of radar is called monostatic radar. If the transmitter and receiver antennas are not co-located, then it is classified as bistatic radar. Most radars used in modern applications are monostatic. After a pulse is transmitted, the monostatic radar antenna is switched to receiver mode via a duplexer and the receiver literally listens to the arrival of the pulse transmitted. The basic principle of radar is depicted in Figure 1.

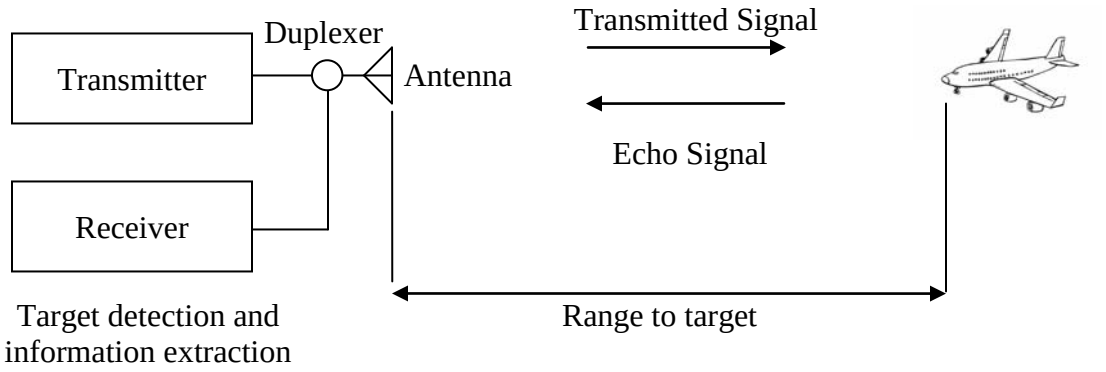

Figure 1. Basic Principle of Radar (From [3])

The most important information that radar provides is the range, although one can extract more information from the received radar signal than a target's range. The range of the target is found by measuring the time elapsed between the transmitted and received

pulse. Electromagnetic waves travel with the speed of light ($c = 3\times10^8$ m/s). Thus, the time for the signal to travel to a target located at a range R and return back to radar after reflection is $2R/c$. The range to a target is then

$$R = \frac{cT_R}{2} \tag{1}$$

where T_R is the time for the signal to travel to the target and back.

Tracking radars employ narrow pencil beams, so that the target's location in angle or bearing can be approximated from the direction that the radar antenna points, when the received signal is of maximum amplitude. If the target is in motion, then the reflected wave experiences a frequency shift due to the Doppler effect. For closing targets, the frequency of the reflected signal becomes greater than that of the transmitted signal, while the opposite happens when the target moves away from the target and frequency decreases. Since the frequency shift is proportional to the velocity of the target, this information is used to determine the velocity. The amount of the Doppler shift presented to a monostatic radar caused by the movement of the target with a radial velocity of v_r is

$$f_d = \frac{2fv_r}{c} \tag{2}$$

where f_d is Doppler frequency shift, f is the radar frequency, and c is the speed of light.

For a pulsed radar, once a pulse is transmitted by the radar antenna, the transmitter must wait for a sufficient amount of time in order for the received pulse (echo) to be returned from the target without any ambiguity. Due to this reason, the pulse repetition rate plays a critical role in establishing a radar's unambiguous range. If the time between pulses T_p is too short, an echo signal from a long-range target might arrive after the transmission of the next pulse and be mistakenly associated with the second pulse rather than the actual pulse transmitted earlier that created the received echo. This can result in an incorrect and or ambiguous range measurement [2]. The maximum unambiguous range can be written as

$$R_{un} = \frac{cT_p}{2} = \frac{c}{2f_p} \tag{3}$$

where T_p is the pulse repetition period and f_p is the pulse repetition frequency (PRF).

The concept of a resolution cell arises frequently in radar nomenclature. A resolution cell is the volume in space that contributes to the echo received by radar at any one instant [2]. The resolution cell can be considered as the volume covered by the angular resolution and the range resolution. The range resolution depends on the duration of the pulse transmitted. For a monostatic radar to resolve two closely spaced targets, they must be separated by a distance

$$\Delta R = \frac{c\tau}{2} \tag{4}$$

where ΔR is the range resolution and τ is the pulse duration.

Cross-range resolution, which is in fact angular resolution defined in terms of range, depends on the 3 dB beamwidth of the antenna. Since most radars employ pencil beams, the 3 dB beamwidth of the antenna is usually small in terms of angle. Therefore, small-angle approximations can be used to derive an approximate cross-range resolution equation, which is given by

$$\Delta CR \approx R\theta_{3dB} \tag{5}$$

where ΔCR is the cross-range resolution for two scatterers located at the edges of the beam, R is the range, and θ_{3dB} is the 3 dB beamwidth of the antenna (in radians).

3. Radar Antenna

As indicated by Equation (5), the antenna plays an important role in terms of sensitivity and the angular resolution of radar. Most radar antennas employ pencil beams in order to have a good angular resolution. Different types of antennas including parabolic reflectors, scanning feed antennas, lens antennas, and phased array antennas have been used in various radar systems.

The most important properties of an antenna are its gain, beamwidth, and sidelobe levels. Antennas direct the radiated energy in the desired direction by their narrow beamwidths. Antenna gain is the ratio of power per unit solid angle radiated by the antenna to power per unit solid angle radiated by an isotropic antenna. Isotropic antennas radiate uniformly in all directions. A useful rule of thumb for a typical high-gain antenna used in practice is

$$G \approx \frac{26000}{\theta_{3dB}\phi_{3dB}} \tag{6}$$

where θ_{3dB} and ϕ_{3dB} are 3 dB beamwidths in azimuth and elevation in degrees, respectively [2]. If an antenna has a gain greater than one in some directions, it must have a gain less than one in other directions, since energy is conserved by the antenna. An antenna designer must take into account the application for the antenna when determining the gain. In radar applications, high-gain antennas have the advantage of longer range and better signal quality, but must be pointed carefully in a particular direction. On the other hand for most frequencies of interest, they are large, heavy, and generally expensive.

The angular resolution of the antenna is determined by its main lobe and is conventionally expressed in terms of 3 dB or half power beamwidth (HPBW). The 3 dB beamwidth can be defined as the angular width where the normalized main lobe amplitude drops down to 0.707. The 3 dB beamwidth in radians can be approximated by the following formula:

$$\theta_{3dB} \approx 0.89\frac{\lambda}{D} \tag{7}$$

where D is the diameter of the antenna. From this equation it can be seen that a smaller beamwidth requires a larger aperture or a shorter wavelength (i.e., higher frequency) [2]. This is one of the reasons that radars usually use frequencies greater than about 1 MHz.

The peak sidelobe of the antenna pattern affects how echoes from angles other than the antenna main lobe can affect the detection of targets. Sidelobe signals can be intentional (i.e., jamming) or unintentional (i.e., clutter) interference signals. For the uniform illumination pattern, the peak side lobe level is 13.2 dB below the main lobe

peak. This is often considered too high in radar systems [2]. Antenna sidelobes can be reduced by the use of tapering of the excitation current amplitudes. Amplitude tapering is similar to windowing functions used in digital signal processing. The consequence associated with tapering the antenna currents to reduce the sidelobes is that the antenna gain will be reduced as well.

Bandwidth is the difference between the upper and lower cut-off frequencies of a radar receiver, and is typically measured in Hertz. In case of a baseband channel or video signal that is near zero frequency, the bandwidth is equal to its upper cut-off frequency. In a radar receiver, the bandwidth is mainly determined by the width of the filtering and signal amplification in the IF strip right before detection. The receiver must be able to process the signal bandwidth of the backscattered pulse.

The wider the bandwidth means the greater the degree of noise that will be input to the receiver. Since the typical background noise is white noise, which exists at all frequencies, the broader the frequency range to which the receiver bandpass filters are tuned, the higher the intensity level of the noise and the lower the signal-to-noise ratio (SNR), and so the receiver's sensitivity.

The bandwidth is roughly proportional to the amount of information carried by the signal. To detect a rectangle pulse with the Fast Fourier Transformation (FFT) the bandwidth of the receiver is equal to the highest sine wave frequency component that is significant. The higher the receiver's bandwidth, the slower is the rise time of the edges of the rectangular signal.

Generally, the necessary bandwidth of a pulse with the shape of a half-wave sine signal of duration τ is assumed as [4].

$$B = \frac{1}{\tau} \tag{8}$$

4. Radar Range Equation

The radar equation relates the range of a radar to the characteristics of the transmitter, receiver, antenna, target, and the environment. It is useful not only for determining the maximum range at which a particular radar can detect a target, but it can serve as a means for understanding the factors affecting radar performance [3]. In its simplest form, the radar range equation can be derived from the received power, which can be written as

$$P_R = \left(\frac{P_t G}{4\pi R^2} \right) \left(\frac{\sigma}{4\pi R^2} \right) \cdot A_e \tag{9}$$

where P_R is the received power, P_t is the transmitted power, G is the gain of the transmit antenna, σ is the radar cross section of the target, and A_e is the effective aperture of the receive antenna. From Equation (9), range R can be written as

$$R = \left[\frac{P_t G A_e \sigma}{(4\pi)^2 P_r} \right]^{1/4} \tag{10}$$

Equations (9) and (10) clearly show that the received power is inversely proportional to R^4 and that the received power is far lower than the transmitted power. Since most radars have a long-range performance requirement, this equation also shows that the sensitivity of the receiver should be good enough to receive very weak signals reflected from the target.

B. PREVIOUS RESEARCH

As was previously mentioned, the main objective of this thesis is to investigate frequency diverse arrays that employ novel electronic scanning techniques. Unlike conventional arrays, frequency diverse arrays do not use phase shifters to generate phase shifts among the elements of the array in order to point the beam to desired directions. The cost of phase shifters can be up to nearly half the entire cost of an electronically scanning phased array. In addition, most of the gallium arsenide-based semiconductor phase shifters usually have high insertion loss (up to -13 dB). The phase shifters

introduce uncertainty and error in reliably transmitting and receiving pulses in specific directions. Moreover, modern systems are emphasizing aspects of simplicity, reliability, and versatility. Consequently, more attention is paid to new concepts for electronic beam scanning [5].

The time-modulated array antenna, which used a new technique for electronic scanning, was introduced by H. E. Shanks in his paper, which was published in 1962 [1]. In his paper, Shanks discussed the theory of simultaneous scanning using time modulation techniques and showed that the required complex pattern was generated by a progressive-pulse aperture excitation. He derived the fundamental equations and relationships concerning the form of pulse excitation and scanning coverage. This paper established the basics of a frequency diverse array where Shanks used a small amount of frequency increment among the array elements. He also showed that by using this technique, it was no longer necessary to use phase shifters to scan the main beam into the desired direction.

Due to new advances in digital signal processing, the use of frequency diversity in array theory started to get more attention. Antonik et al. [6] presented the generalized structure for the frequency diverse array radar in 2006. They showed that when a frequency increment is applied across the array elements, the resulting pattern depends on the range. They also demonstrated how the scan angle changed with frequency increment and generated an apparent scan angle.

In another paper [7], Antonik et al. described the use of multi-mode waveform diversity to enable the execution of two different missions at the same time. They particularly focused on the use of a frequency diverse array in synthetic aperture radar (SAR) and moving target indication (MTI) radar in their paper and proposed a hardware configuration for a frequency diverse array that could perform both of these tasks.

Secmen et al. [8] presented a frequency diverse array antenna with a periodic time-modulated pattern in range and angle in 2007. In their paper, they demonstrated the periodic manner of the pattern in three domains, namely time, angle and range. They also provided the expressions for determining the position and the angular bearing of a target for a frequency diverse array.

In 2008, Huang et al. [9] simulated a frequency diverse array using an eight-element microstrip patch array on Microwave Studio and generated the theoretical array pattern on a computer aided design (CAD) program. Their work proves that the frequency increment across the array determines the scanning speed of a frequency diverse array.

In a recent paper, which has not been published yet, Secmen et al. presented the design and implementation of a frequency diverse array using linear frequency modulated continuous waveform (LFMCW). In their work, they analyzed the frequency diverse array concept in terms of a mathematical foundation. Their work also justified the important parameters. In their effort, they revealed the similarity between frequency scanning and the LFMCW-based frequency diverse array.

C. OBJECTIVES

The main purpose of this thesis is to investigate frequency diverse arrays, their characteristics, and their use in radar applications. First, array theory is introduced as a building block and then the concept of frequency diverse arrays is investigated in detail. Also in this thesis, the question of what kind of waveforms one can use to implement frequency diversity is addressed.

Ultimately, this thesis may be helpful to electronic warfare officers and technical personnel to understand frequency diverse arrays and their implementation in the field of radar. The theoretical concepts introduced in this thesis can be used in a hardware implementation of a frequency diverse array antenna. Moreover, the results of this thesis can be the basis of further developments and research.

D. ORGANIZATION OF THE THESIS

This thesis consists of six chapters. Chapter I provides an introduction to electronic scanning and its advantages.

Chapter II presents the background for the notion of an array, uniform linear arrays, beam steering, and image theory that is used in subsequent chapters. This chapter also discusses the frequency scanning concept and phase shifters.

Chapter III introduces a time-modulated antenna and time domain scanning where antenna elements are switched on and off periodically with a small frequency increment. This chapter also provides the far-field pattern of a time-modulated antenna and the possible array configuration.

Chapter IV presents a general analysis of a frequency diverse transmit antenna with a periodically modulated pattern in range, angle and time. The expressions for determining the position and the angular bearing of the target for this type antenna are given.

Chapter V provides the radar implementations of a frequency diverse array and deals with the range detection of the target.

Chapter VI gives the conclusions of the thesis and recommends areas for future work.

THIS PAGE INTENTIONALLY LEFT BLANK

II. ANTENNA ARRAY THEORY

A. ARRAY ANTENNAS

Several electrically small, low-gain antennas can be arranged in space and interconnected to produce a high-gain directional radiation pattern. Such a configuration is referred to as an array antenna, or simply an array. Arrays offer the unique capability of electronic scanning of the main beam. By changing the phase of the exciting currents in each antenna element of the array, the radiation pattern can be scanned through space. The array is then called a phased array [10].

Most arrays consist of identical antenna elements such as dipoles, horns, or reflectors. However, there certainly might be arrays consisting of different types of antenna elements. In general, array elements can be distributed in linear arrangement, on a surface, or throughout a volume. The most common configurations for antenna arrays are linear arrays and planar arrays. For the purpose of this thesis, only linear arrays that have identical antenna elements are considered. The frequency diverse array (FDA) concepts developed for linear arrays can be extended to other array configurations.

In the far-field region, the electric field from a radiating antenna element can be expressed as the multiplication of two functions. The first function is the spherical propagation factor $\frac{e^{-jkR}}{R}$, which depends on the range, and the second function is $f_e(\theta,\phi)$, which is a normalized function that accounts for the directional dependence of the element's electric field [11].

With regards to the elements in the array shown in Figure 2, the far electric field from the elements of the array can be written as †

$$E_n = a_n e^{j\psi_n} \frac{e^{-jkR_n}}{R_n} f_e(\theta,\phi) \tag{11}$$

† In this section, phasor quantities are used with a $e^{j\omega t}$ time dependence assumed and suppressed.

where a_n represents the amplitude and ψ_n represents the phase of the excitation which gives rise to the radiated electric field [11]. The angle theta is the angle from the normal with respect to the axis of the array (i.e., the *z*-axis in Figure 2)

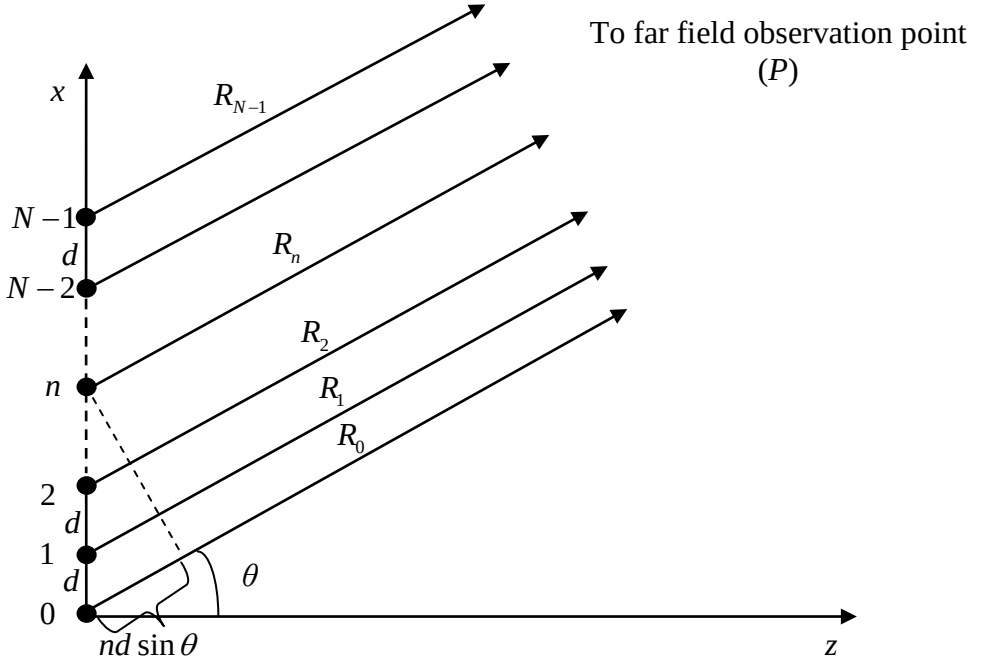

Figure 2. Linear Array Configuration and Geometry (After [11])

In most radar applications, only the far field is of interest, and therefore some approximations can be made. In an amplitude sense, differences in distances from individual antenna elements can be ignored and approximated by $R_n \approx R_0$. However, a small difference in the distances can generate significant phase shifts. If we restrict P to lie in the *x*-*z* plane the range dependence in the e^{-jkR_n} term can be approximated by

$$R_n \approx R_0 - nd\sin\theta \tag{12}$$

Using Equations (11) and (12), the superposition of all electric fields from N individual antenna elements at a far-field observation point P can be written as

$$E_n = f_e(\theta,\phi)\left(\frac{e^{-jkR_0}}{R_0}\right)\left(\sum_{n=0}^{N-1} a_n e^{j\psi_n} e^{jnkd\sin\theta}\right) \tag{13}$$

The array factor (AF) is defined as

$$AF = \left(\sum_{n=0}^{N-1} a_n e^{j\psi_n} e^{jnkd\sin\theta}\right) \tag{14}$$

The array factor is a function of the positions of the antenna elements and their current (or voltage) excitation coefficients, but not a function of the specific type of radiators used. The array factor represents the far-field radiation pattern of the N elements, in the case where the individual elements are isotropic radiators [11].

The array factor is governed by two input (excitation) functions. The first one is the array amplitude distribution given by the coefficients $\{a_n\}$. The second one is the array phase distribution given by the phases $\{\psi_n\}$. By changing the amplitude or phase distribution one can control the sidelobe levels or steer the main beam of the array.

1. Uniformly Excited, Equally Spaced Linear Arrays

One important case is the equally spaced and uniformly excited linear array. This array is excited by equal current amplitudes so

$$a_0 = a_1 = a_2 = ... = a_{N-1} \tag{15}$$

The element phases are considered to be equal, and can arbitrarily be set to zero $(\psi_n = 0)$. The array factor is then

$$AF = a_0 \sum_{n=0}^{N-1} e^{jnkd\sin\theta} = a_0 \sum_{n=0}^{N-1} e^{jn\gamma} \tag{16}$$

where $\gamma = kd\sin\theta$. Equation (16) is a geometric series and the array factor turns out to be

$$AF = a_0 \frac{\sin(N\gamma/2)}{\sin(\gamma/2)} e^{j(N-1)\gamma/2} \tag{17}$$

The phase factor $e^{j(N-1)\gamma/2}$ is not important unless the array output signal is further combined coherently with the output from another antenna. In fact, if the array was centered about the origin, the phase factor would not be present since it represents the phase shift of the array phase center relative to the origin [10]. Neglecting the phase factor in Equation (17) gives

$$AF = a_0 \frac{\sin(N\gamma/2)}{\sin(\gamma/2)} \tag{18}$$

The magnitude of the array factor has its maximum value when γ is equal to zero and the maximum value is Na_0. The normalized array factor magnitude for the uniformly excited, equally spaced linear array is then

$$\left|AF_{norm}\right| = \left|\frac{\sin(N\gamma/2)}{N\sin(\gamma/2)}\right| \tag{19}$$

The array factor of a 6-element array of $\frac{\lambda}{2}$ spaced elements given in Equation (19) is plotted in Figure 3, and it shows that when the array is uniformly excited with the same current amplitudes and zero phase shift across the elements of the array, the main beam points in the broadside direction ($\theta = 0^\circ$).

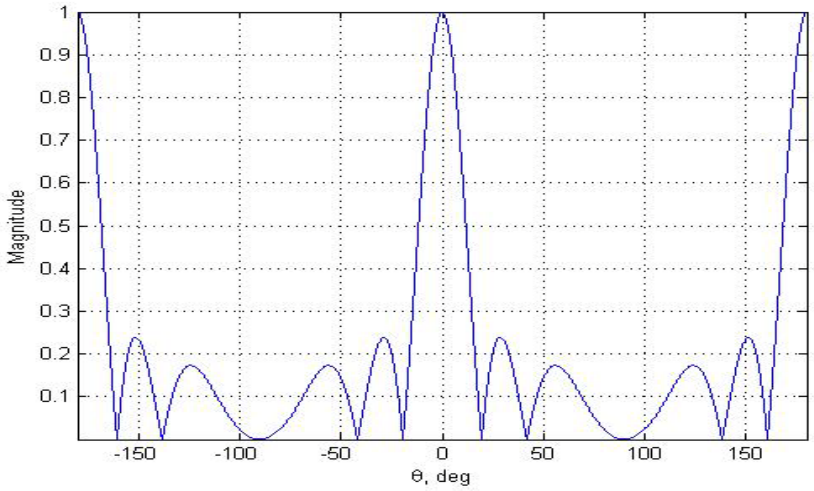

Figure 3. Array Factor of 6-element Array with $d = \frac{\lambda}{2}$, $\theta_0 = 0^\circ$

2. Pattern Multiplication

In the previous section, uniformly excited and equally spaced linear arrays were discussed. The radiators were considered to be isotropic antennas that radiate equal power in all directions and have no directionality. This is not the case in the real-world applications of radar. Actual arrays have element antennas that are not isotropic.

If the array elements are similar in the sense that they are in the same direction, of the same length, and have the same distribution, then patterns of all antenna elements will be similar and simplifications can be made. Although antenna elements may have different amplitudes and phases, they will have the same spatial variation. When all antenna elements are identical, the electric field can be written as a product of an element pattern and an array factor. The process of factoring the pattern of an array into an element pattern and an array factor is referred to as the *principle of pattern multiplication*. It can be summarized that the electric field pattern of an array consisting of similar elements is the product of the pattern of the elements and the pattern of an array of isotropic point sources with the same locations, relative amplitudes, and phases as the original array.

Based on the principle of pattern multiplication, the complete (normalized) pattern of an array antenna can be written as

$$F_{norm}(\theta,\phi) = EF_{norm} \cdot AF_{norm} = f_e(\theta,\phi) \cdot AF_{norm} \tag{20}$$

where EF_{norm} stands for the element factor [10].

3. Electronic Scanning of Arrays

In Section 1, it was shown that when a linear array is excited uniformly, which means identical current amplitudes and zero interelement phase, the resulting array pattern has a peak or main lobe at the broadside of the antenna. Beam steering refers to changing the direction of the main beam of the array pattern. Electronic scanning is achieved by applying linearly progressive phase shifts from element to element across the

array such that the maximum value of the pattern now occurs at the angle theta instead of broadside to the array axis. This concept is illustrated in Figure 4.

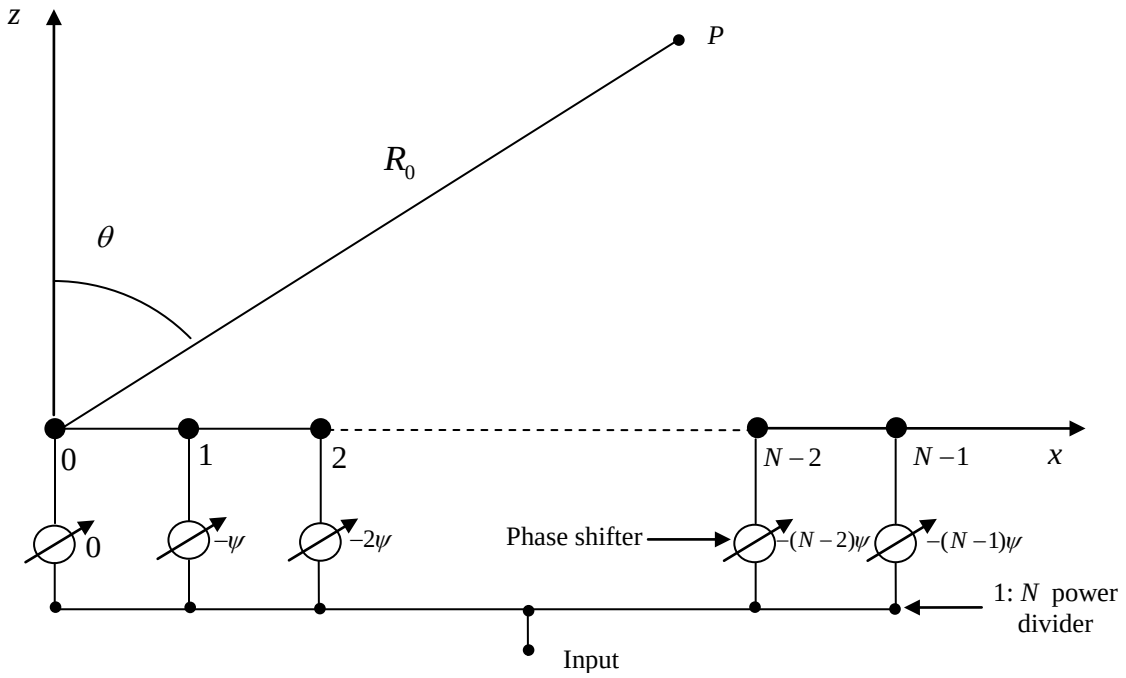

Figure 4. The Application of a Linear Phase

The array factor of the array depicted in Figure 4 can be written as

$$AF = a_0 \sum_{n=0}^{N-1} e^{-jn\psi} e^{jnkd\sin\theta} = \sum_{n=0}^{N-1} e^{jn(kd\sin\theta-\psi)} = a_0 \sum_{n=0}^{N-1} e^{jn\gamma'} \tag{21}$$

If we restrict *P* to lie in the *x*-*z* plane as before, then $\gamma = kd\sin\theta - \psi$. The interelement phase shift ψ is defined in terms of angle θ_0, which can be called the scan angle which is the direction for the pattern maximum value,

$$\psi = kd\sin\theta_0 \tag{22}$$

Then,

$$\gamma' = kd(\sin\theta - \sin\theta_0) \tag{23}$$

Since the array factor becomes a maximum when γ' is equal to zero, the scan angle must be equal to the pointing direction of the main beam $(\theta_0 = \theta)$. When the phase is uniform (in other words, when $\psi = 0^\circ$), θ_0 must be 0°. This corresponds to the broadside direction. Similarly, to steer the beam to the endfire direction (along the array axis), which corresponds to $\theta = 90^\circ$, one should apply an incremental phase shift to all elements of the array of kd radians. In general, by applying a linear phase across the array, the main beam can be steered to any desired direction.

Figure 5 depicts the array factor of an electronically scanned half wavelength-spaced 6-element array when a linear phase progression of $\frac{\pi}{9}$ radians (i.e., 20 degrees) is applied. It is clearly seen that the main beam of the antenna points 20° and beam steering to the desired direction is achieved. Observe also that the only parameter that has changed from the previous unscanned array is the scan angle (i.e., linear phase). When comparing the two outputs, it can be noted that scanning an array increases that pattern width (i.e., decreased the directivity of the antenna output).

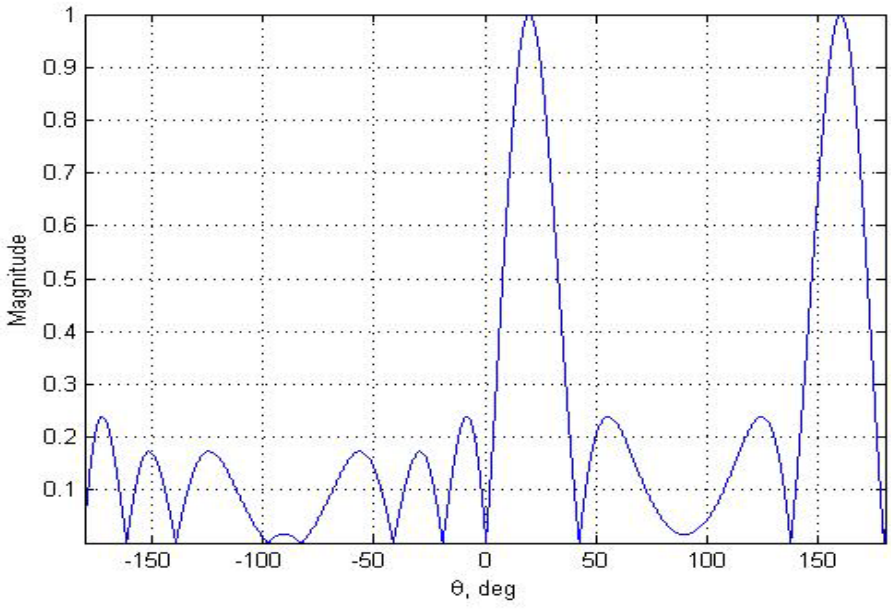

Figure 5. Array Factor for an Electronically Scanned 6-element Array with $d = \frac{\lambda}{2}$,

$$\theta_0 = \frac{\pi}{9} = 20^\circ$$

A linear phase distribution can be accomplished by controlling the excitation of each radiating element individually through the use of electronically controlled phase shifters. Alternatively, another technique known as frequency scanning can be used [11]. The next section briefly discusses frequency scanning and provides the basic idea behind the frequency diverse array concept.

4. Frequency Scanning

The outstanding feature of frequency scanning is that it is a means for providing inertialess beam scanning, which in comparison with other inertialess scanning techniques, is economical, relatively simple, and reliable. This is extremely desirable in modern radars that have as performance objectives the rapid detection and accurate position measurement of multiple targets at widely different positions, including cases where the targets have high velocities and acceleration and hence require rapid updating.

So far, the widest application for frequency scanning has been found in the fields of air surveillance and aircraft control. Radars for these applications have been advantageously designed and produced with, in most cases, antennas mechanically rotated in azimuth and frequency scanned in elevation to provide three-dimensional aircraft position data. Many other configurations have been conceived to cover a relatively broad spectrum of applications ranging from such diverse fields as airborne surveillance and mapping, mortar shell detection, and aircraft landing precision radars [12].

To establish the basic technique of frequency scanning, consider an electromagnetic wave of frequency f propagating through a transmission line of length l with a velocity of v. The electromagnetic wave experiences a phase shift as follows:

$$\phi = kl = \frac{2\pi}{\lambda} l = 2\pi \frac{f}{v} l \tag{24}$$

Therefore, a change in the frequency of the electromagnetic wave propagating at constant velocity along the transmission line introduces a phase shift as seen in Equation (24). In this manner, it is possible to get an electronic phase shift (ψ) relatively easy compared to other methods. Frequency scanned arrays mostly use equal length series feed structures to very simply introduce linear phase across elements. Since no phase shifting devices are required, there is no insertion loss due to phase shifters. The series feed arrangement is illustrated in Figure 6.

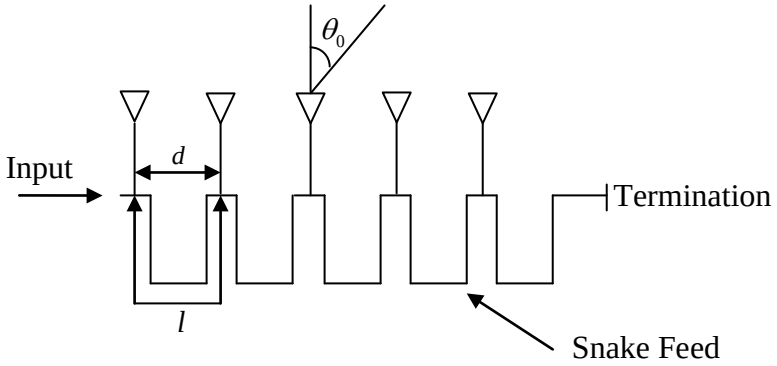

Figure 6. Series–fed, Frequency Scanned Linear Array (From [3])

If the beam is to point in a direction θ_0, the phase difference between elements should be $kd\sin\theta_0$. In frequency scanned arrays, usually an integral number of 2π radians is added. This permits a scan angle to be obtained with a smaller frequency change. Equating phase difference to phase shift obtained from a line of length l gives [3]

$$\frac{2\pi}{\lambda}d\sin\theta_0 + 2\pi m = \frac{2\pi}{\lambda}l \tag{25}$$

$$\sin\theta_0 = -\frac{m\lambda}{d} + \frac{l}{d} \tag{26}$$

When $\theta_0 = 0^\circ$, which corresponds to the broadside beam direction, Equation (25) results in $m = l/\lambda_0$, where λ_0 corresponds to the wavelength and f_0 is the frequency at the broadside direction. Using this information, Equation (26) can be rewritten as

$$\sin\theta_0 = \frac{l}{d}\left(1-\frac{\lambda}{\lambda_0}\right) = \frac{l}{d}\left(1-\frac{f_0}{f}\right) \tag{27}$$

If the beam is steered between $\pm\theta_1$, the wavelength excursion $\Delta\lambda$ turns out to be

$$\sin\theta_1 = \frac{l}{2d}\frac{\Delta\lambda}{\lambda_0} \tag{28}$$

An examination of Equation (26) shows that as the frequency is changed, one beam after another will appear and disappear, with each beam corresponding to a different value of m [3]. As the delay gets larger in the transmission line compared to the spacing of the elements, one can change the beam-pointing angle more rapidly as a function of wavelength. For this reason, in frequency scanned arrays usually tapped delay lines or slow wave structures are used, which may be folded, helically wound, or dielectrically loaded in form.

With antennas having such a delay line, the beam-pointing angle can be made to be an accurately controlled function of RF frequency. Volumetric aerial coverage can be obtained in radar systems using these antennas by radiating an orderly progression of sequentially generated transmitter signals, each at a different RF frequency [12]. This concept is illustrated in Figure 7. Beamwidths typically range from 0.5° to 5° in the frequency scanned plane. Angular coverage provided by frequency scan ranges from as low as 10° to well over 90° and is commonly achieved with frequency bands of between one and ten percent of the carrier frequency [12].

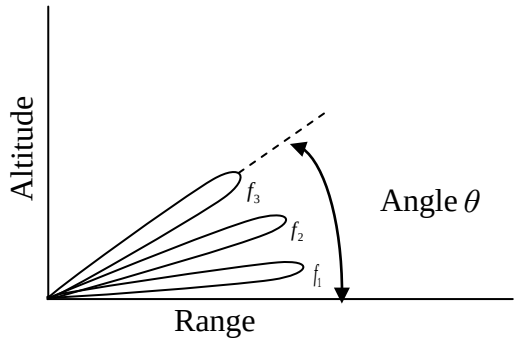

Figure 7. Frequency Scanning (From [12])

Generally, a snake feed configuration is used to scan a pencil beam in elevation, with mechanical rotation providing the azimuth scan. The AN/SPS-48 is a frequency scanned radar used on U.S. Navy ships for the measurement of the elevation and azimuth of aircraft targets [3]. A block diagram of a typical frequency scan is depicted in Figure 8.

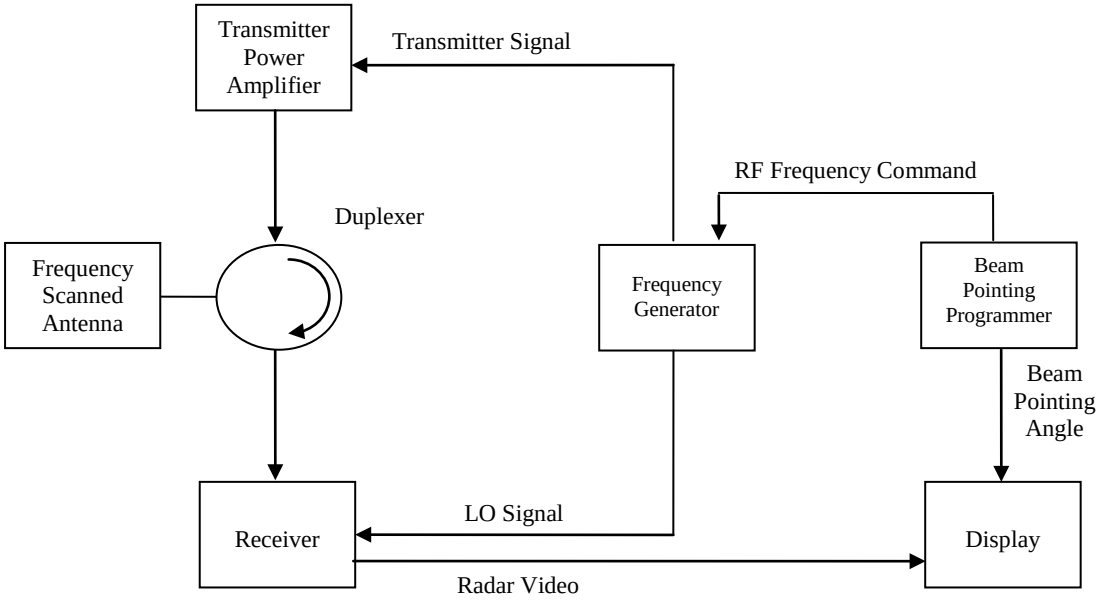

Figure 8. Block Diagram of a Frequency Scan Radar (After [12])

B. GROUND PLANES AND THE METHOD OF IMAGES

Most radar antennas use a conducting ground plane to limit radiation to a hemispherical region. Image theory can be used to compute the radiation pattern of elements above a ground plane. Image theory states that any given current configuration above an infinite, perfectly conducting plane is electrically equivalent to the combination of the source current configuration and its image configuration, with the conducting plane removed [11]. Even if the ground plane is not infinite and perfectly conducting, image theory can still provide useful pattern data.

1. Arrays with Elements Above a Ground Plane

In Section A above, linear arrays were discussed. The radiation patterns of linear arrays are axially symmetric. Here we have aligned the array along the *z* axis rather than the *x* axis, to be consistent with the FDA formulation in Chapter IV. For practical radar applications, a ground plane is added to provide a hemispherical radiation pattern in the +*x* direction. To obtain the complete array factor for an array with a ground plane, first consider a linear array that consists of *N* isotropic point sources in the *y*-*z* plane as shown in Figure 9. Assuming that the array elements are centered at the origin, element locations can be found from the following equation:

$$z_n = \frac{2n-(N+1)}{2}d\ ,\ n=1,...,N \tag{29}$$

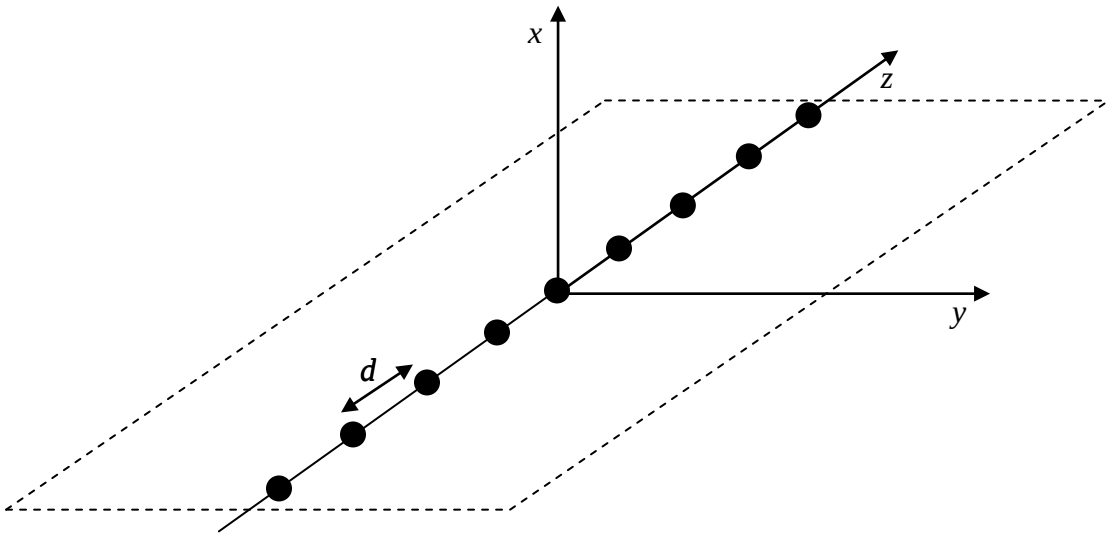

Figure 9. Linear Array Centered at the Origin (After [13])

The array factor of a uniformly excited and equally spaced linear array is given in Equation (17). If the excitation current amplitudes are all equal to one, then the array factor becomes

$$AF = \frac{\sin(N\gamma/2)}{\sin(\gamma/2)} \tag{30}$$

where $\gamma = kd\cos\theta - \psi$ [13].

Most radar antennas are placed above a perfect electric ground plane of finite extent. However, if the ground plane extends sufficiently beyond the elements then it can be approximated by an infinite ground plane. The array above an infinite, perfectly conducting ground plane is equivalent to a linear array with new elements comprised of the real source elements and their images in free space that are separated by a distance of 2*h*. This new "element" is sometimes referred to as a subarray. Figure 10 illustrates the concept.

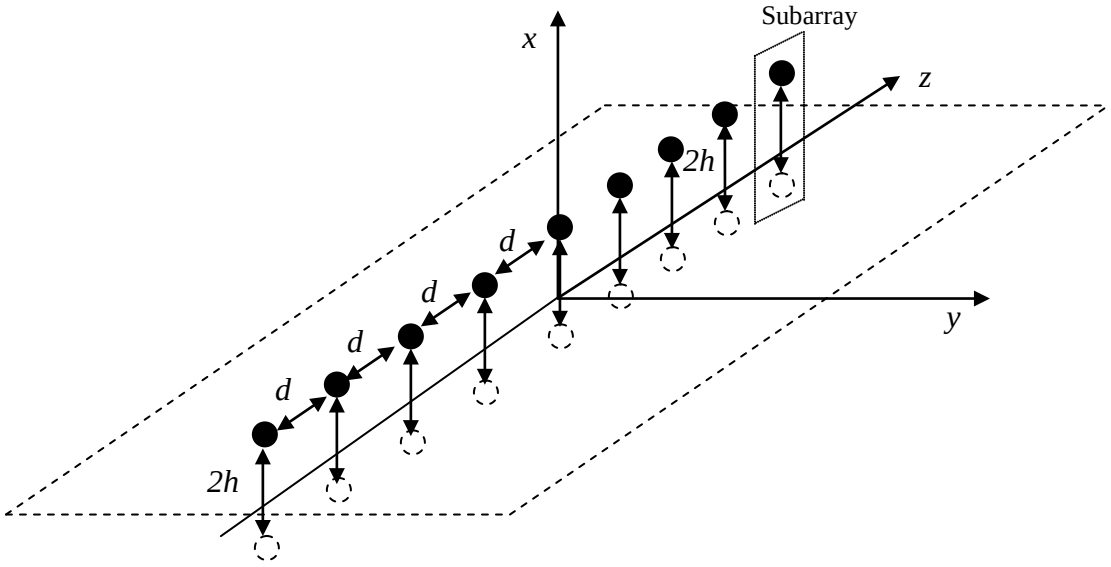

Figure 10. Two-element Linear Array (Subarray) Along the *z*-axis Using Image Theory (After [13])

The subarray factor (*SF*) for a two-element linear array along the *x*-axis, with images out of phase with sources, is

$$SF = e^{jkh\sin\theta\cos\phi} - e^{-jkh\sin\theta\cos\phi} \tag{31}$$

where h is the distance from the antenna elements to the ground plane. If Euler's trigonometric identity is used,

$$\sin\theta = \frac{1}{2j}(e^{j\theta} - e^{-j\theta}) \tag{32}$$

then Equation (31) becomes

$$SF = 2j\sin(kh\sin\theta\cos\phi) \tag{33}$$

The total normalized pattern factor is obtained using the principle of pattern multiplication

$$F_{norm}(\theta,\phi) = (AF_{norm}\cdot SF_{norm}\cdot EF_{norm}) = \frac{\sin(N\gamma/2)}{N\sin(\gamma/2)}\sin(kh\sin\theta\cos\phi)EF_{norm} \tag{34}$$

In general, the element factor (*EF*) has both θ and ϕ components. For a half-wave dipole with maximum current I_m along the *y*-axis, the far electric field components can be written as [15]

$$E_\theta = \frac{j\eta_0 I_m e^{-jkR}}{2\pi R}\left[\frac{\cos\left(\frac{\pi}{2}\sin\theta\sin\phi\right)}{1-\sin^2\theta\sin^2\phi}\right]\cos\theta\sin\phi \tag{35}$$

$$E_\phi = \frac{j\eta_0 I_m e^{-jkR}}{2\pi R}\left[\frac{\cos\left(\frac{\pi}{2}\sin\theta\sin\phi\right)}{1-\sin^2\theta\sin^2\phi}\right]\cos\phi \tag{36}$$

To normalize the element factors, one should remove the leading factor $\frac{j\eta_0 I_m e^{-jkR}}{2\pi R}$ in the equations. If the dipoles are ideal dipoles (i.e., uniform current I_m and length L) the terms in the brackets reduce to 1 and *L* is added to the leading factor [13].

In this chapter, the basic array antenna theory was presented and the means of beam steering with the use of electronically controlled phase shifters was explained. In addition to this, another beam steering technique, namely frequency scanning, was

introduced as a building block to understand frequency diverse arrays. Lastly, image theory and its use in array applications were discussed. Also, the equations for a half-wave dipole along the *y*-axis were given. All of these results will be used in the implementation of a frequency diverse array above a ground plane, where the elements of the array are the half-wave dipoles directed in the *y*-direction (parallel) and separated along the *x*-axis (array axis).

In the next chapter, a frequency diverse array, which employs a time-modulated pulse excitation, will be discussed.

THIS PAGE INTENTIONALLY LEFT BLANK

III. TIME DOMAIN SCANNING

A. INTRODUCTION

Perhaps the most desired feature of phased arrays is electronic scanning. In Chapter II, two techniques of electronic scanning were introduced, namely, phase scanning and frequency scanning. However, time domain techniques can be applied to antennas to provide a means for quasi-electronic scanning. Generally, because of the ease of analysis and implementation there is a bias towards frequency domain techniques. However, time domain techniques, especially periodic time domain modulation of one or more antenna parameters, can provide advanced radiation characteristics including sidelobe reduction, multiple beamscanning, and multi-mode operation. The pattern of an antenna is a function of three spatial dimensions; therefore, the time domain can be considered as the fourth dimension of an antenna.

If a wave of energy is incident on an antenna whose parameters are modulated in a periodic manner, the voltage across the output terminals will be of the following form:

$$E(\theta,t) = As(t)\left\{b_0(\theta) + b_1(\theta)\cos\omega_0 t + b_2(\theta)\cos 2\omega_0 t + ...\right\} e^{j\omega t} \tag{37}$$

where *A* contains the radial dependence, θ denotes the spatial variation in the signal, and the Fourier series containing $b_n(\theta)$, which are Fourier coefficients, is the time-dependent radiation pattern with ω_0 as the fundamental modulation frequency. Symmetry in the terminal voltage as a function of time is assumed (otherwise the series expansion shown above will also have sinusoidal terms). One can refer to ω as the center frequency or carrier frequency although it is not a carrier frequency in the traditional sense. The modulation frequency is assumed to be much less than the center frequency (i.e., $\omega_0 \ll \omega$). In Equation (37), $s(t)$ represents the input information. For radar applications $s(t)$ can be considered as a pulse waveform [14]. The following paragraphs develop the time-space relationship as explained by Shanks and Bickmore [1, 14].

Consider a distribution of radiating sources spread over a surface S_0. Then, its radiation pattern can be written as

$$g(\theta) = \int_{S_0} \xi(S_0) G(\theta, S_0) dS_0 \tag{38}$$

where $\xi(S_0)$ is the complex distribution of energy over the surface and $G(\theta, S_0)$ is Green's function. Green's function can be thought of as spatial impulse function [10]. A sample Green's function for a spherical wave $\frac{e^{jkR_n}}{R_n}$ was shown earlier in Equation (11). If $\xi(S_0)$ varies with time then it can be denoted as $\xi(S_0, t)$, and if $g(\theta)$ depends on the time variable it becomes $g(\theta, t)$. Equation (38) can be written as

$$g(\theta, t) = \int_{S_0} \xi(S_0, t) G(\theta, S_0) dS_0 \tag{39}$$

Due to the periodic nature of $\xi(S_0, t)$, it can be decomposed into a Fourier series expansion and the Fourier series coefficients can be calculated. The Fourier series expansion of $\xi(S_0, t)$ is

$$\xi(S_0, t) = \zeta_0(S_0) + \zeta_1(S_0)\cos\omega_0 t + \zeta_2(S_0)\cos 2\omega_0 t + \ldots \tag{40}$$

where $\zeta_n(S_0)$ are the Fourier coefficients of the series and ω_0 is the fundamental modulation frequency. Substituting Equation (40) into Equation (39) yields the equation

$$g(\theta, t) = \sum_{n=0}^{\infty} \left\{ \int_{S_0} \zeta_n(S_0) G(\theta, S_0) dS_0 \right\} \cos n\omega_0 t \tag{41}$$

The expression inside the curly brackets represents the time-dependent radiation pattern that can be denoted as $b_n(\theta)$ [14]

$$b_n(\theta) = \int_{S_0} \zeta_n(S_0) G(\theta, S_0) dS_0 \tag{42}$$

From the derivation of $b_n(\theta)$, one can conclude that harmonic coefficients $\zeta_n(S_0)$ give rise to the corresponding Fourier coefficients, $b_n(\theta)$, in Equation (37).

By examining Equation (37), it can be seen that the time varying radiation pattern can be written as the superposition of the time- and angle-dependent harmonic coefficients that are tagged with a different frequency. Due to this independent nature of ω_0 harmonics, each term in Equation (37) provides a way to detect the target independently. This can be used as a direct indication of the presence and the strength of a target in the direction associated with the beam pointing in that direction when pencil beams are used. This characteristic is of importance for electronic scanning.

1. Time Domain Array Theory

In order to understand electronic scanning using time domain antennas, consider a continuously excited linear array. Assume that $2N+1$ pencil beams are desired from an array of length $2l_0$ and beams are spaced angularly by θ_0 [1]. In order to accomplish this, let

$$b_n(\theta) = A_n \frac{\sin(kl_0 \sin\theta)}{\sin\theta} \tag{43}$$

which corresponds to a pencil beam directed at the boresight of the antenna $\left(\theta = 0^\circ\right)$. In order to steer the pencil beams, it is required to introduce a phase shift that is analogous to the beam steering of the array. Therefore, for each pencil beam, a scan angle θ_0 is introduced to produce the aforementioned phase shift. Equation (43) can be written as

$$b_n(\theta) = A_n \frac{\sin(kl_0 \left[\sin\theta - \sin\theta_0\right])}{\left[\sin\theta - \sin\theta_0\right]} \tag{44}$$

From Equation (37) the time varying radiation pattern can be extracted as

$$g(\theta, t) = \left(\sum_{n=0}^{\infty} b_n(\theta) \cos n\omega_0 t \right) e^{j\omega t} \tag{45}$$

Using Equation (44) and Euler's identity for $2N+1$ pencil beams, Equation (45) can be rewritten as [1]

$$g(\theta,t)=\sum_{n=-N}^{N}\frac{\sin[kl_0(v-nv_0)]}{v-nv_0}e^{j(\omega+n\omega_0)t} \tag{46}$$

where $g(\theta,t)$ = desired time varying complex pattern

ω_0 = fundamental modulation frequency

v = $\sin\theta$

v_0 = $\sin\theta_0$ (scan angle)

The time varying pattern given in Equation (46) demonstrates the characteristics of a non-scanning antenna, which can detect and locate targets over a wide angular region through the 2N+1 pencil beams separated by θ_0. This is an extremely useful characteristic for an antenna in radar applications. Here, $2N+1$ beams define the angular coverage while v_0 provides a means for detection accuracy. Equation (46) is basically the superposition of the $2N+1$ pencil beams each tagged with a different frequency. As n changes, the harmonic frequency changes and the linear array generates a beam whose direction is determined by the scan angle θ_0. In addition, the second term in the equation tags the beams with different frequencies. Therefore, a target in the vicinity of the angular direction nv_0 is directly associated with the frequency $n\omega_0$. From another viewpoint, since the Fourier transform of a sine wave gives two Dirac delta functions at the same frequency with opposite signs in the frequency spectrum, Equation (46) represents a frequency spectrum in which the upper and lower sideband magnitudes indicate the strength of the targets in the associated directions. This concept is illustrated in Figure 11.

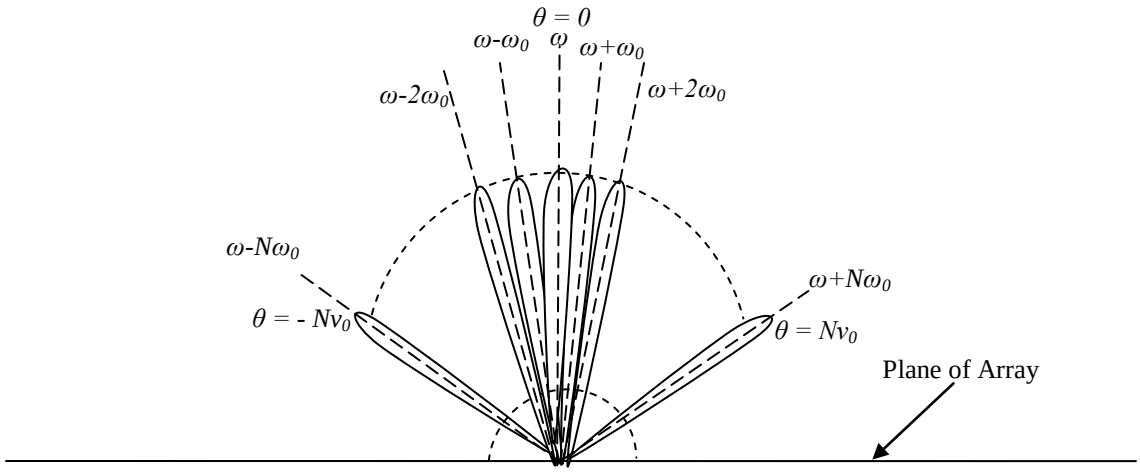

Spatial Representation

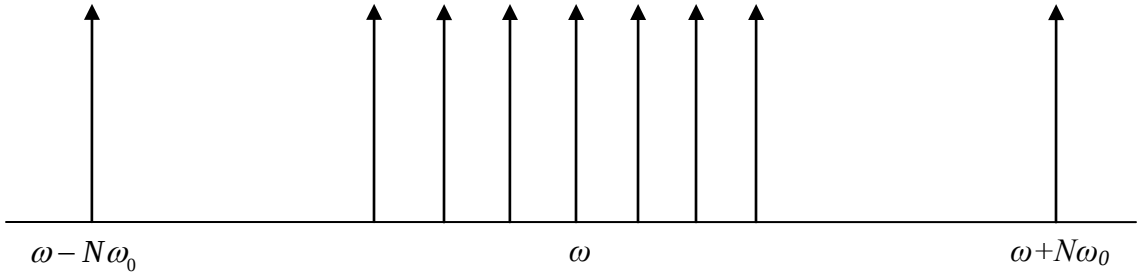

Frequency Representation

Figure 11. Time Domain Electronic Scanning (After [1])

Equation (46) presents the pattern of the array. From antenna theory, it is well known that an inverse Fourier transform of the far-field pattern gives the current distribution of the antenna. Therefore, one can apply the Fourier integral to the complex pattern given in Equation (46). By applying the Fourier integral to the aperture distribution, the following is obtained [1]:

$$f(x,t) = \sum_{n=-N}^{N} e^{-j(kv_0 nx - n\omega_0 t)} \tag{47}$$

Equation (47) can be written as

$$f(x,t) = \sum_{n=-N}^{-1} e^{-j(kv_0 nx - n\omega_0 t)} + 1 + \sum_{n=1}^{N} e^{-j(kv_0 nx - n\omega_0 t)} \tag{48}$$

Changing the sign of the index and the exponent, Equation (48) becomes

$$f(x,t) = \sum_{n=1}^{N} e^{j(kv_0 nx - n\omega_0 t)} + 1 + \sum_{n=1}^{N} e^{-j(kv_0 nx - n\omega_0 t)} \tag{49}$$

Equation (49) can be rewritten as

$$f(x,t) = 1 + 2\sum_{n=1}^{N} \cos\left[n\left(kv_0 x - \omega_0 t\right)\right] \tag{50}$$

where Euler's trigonometric identity

$$\cos\theta = \frac{1}{2}\left(e^{j\theta} + e^{-j\theta}\right) \tag{51}$$

is used.

Equation (50) can be thought of as a series of travelling amplitude waves moving from left to right along the array with the same speed. Because of the equality of these wave amplitudes, the complete sum resembles a pulse travelling across the array. It can be seen that when *N* tends to infinity, the traveling pulse becomes a Dirac delta function.

An examination of Equation (50) reveals that in order to realize the pattern given in Equation (46) and depicted in Figure 11, the linear array must be excited progressively a small portion at a time. From this viewpoint, it will be considered that the linear array is excited with a rectangular pulse travelling across the array, to see whether it produces the complex pattern given in Figure 11. For this purpose, an array of N elements, where each element is excited for a particular period of time, will be assumed. This is equivalent to on-off switching of antenna elements in sequence. Each antenna element is excited for T / N seconds and then turned off, starting from the leftmost element and moving in time to the rightmost element. This excitation cycle is repeated for every T seconds where T represents the period of the excitation. The generated pulse travels all the array elements in T seconds, and then returns back to the leftmost element of the array. Switching an antenna element on for a particular time and then turning it off generates a rectangular-

shaped pulse modulated with the carrier frequency, which is similar to the on-off keying (OOK) or amplitude shift keying (ASK) in communication theory. This concept is illustrated in Figure 12.

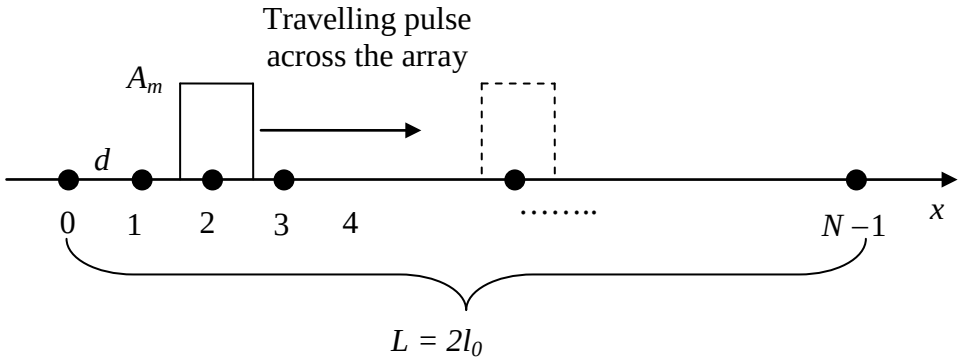

Figure 12. Excitation of the Time Domain Scanned Array

Each element is turned on with excitation current amplitude A_m during the time defined by

$$\frac{mT}{N} \le t \le (m+1)\frac{T}{N} \tag{52}$$

where m is the symbol used for sequence numbering the array elements (i.e., $m = 0,1,2,3,...,N-1$) as it is illustrated in Figure 12. Using Equation (52) the aperture excitation can be written as a piecewise function as follows:

$$a(t) = \begin{cases} A_m, & \frac{mT}{N} \le t \le (m+1)\frac{T}{N} \\ 0, & \text{else} \end{cases} \tag{53}$$

where $a(t)$ is the aperture excitation. The resulting pattern from the excitation given in Equation (45) can be written in the form of

$$g(\theta,t) = h_m(\theta)e^{j\omega t} \tag{54}$$

where

$$h_m(\theta) = A_m e^{jmkd\sin\theta} \tag{55}$$

Therefore, Equation (54) can be rewritten as

$$g(\theta, t) = A_m e^{jmkd\sin\theta} e^{j\omega t} \tag{56}$$

The time delay for a pulse to arrive to the observation point at the far field has to be taken into consideration. In Chapter II, it was shown that due to the spacing between antenna elements, each wave radiated from an element has to travel a distance of $d\sin\theta$ compared to the wave radiated from the adjacent element in the direction of θ, where the observation point is located. This path length difference also introduces a time delay for the signal to arrive at the observation point. The time delay experienced by waves can be written in general for all elements by simply subtracting the time delay from both sides of Equation (52), and thus it becomes [1]

$$\frac{mT}{N} - \frac{md}{c}\sin\theta \;\le\; t \;\le\; (m+1)\frac{T}{N} - \frac{md}{c}\sin\theta \tag{57}$$

where *d* is the interelement spacing along the array.

Equation (54) shows the periodicity of the complex pattern since the angle-dependent function is multiplied with a periodic complex signal $e^{j\omega t}$. From Fourier analysis, it is well known that any periodic function can be expanded into its Fourier coefficients by simply taking the Fourier series. The Fourier series of a periodic function can be written as [16]

$$x(t) = \sum_{q=-\infty}^{\infty} c_q e^{j(2\pi/T_0)qt} \tag{58}$$

where c_q represents the Fourier coefficients and T_0 is the fundamental period of the signal. Equation (58) is also known as the Fourier synthesis equation in which the signal

is reconstructed from the harmonics of the complex sinusoidal wave with Fourier coefficient weighting. The complex Fourier coefficients can be found using the following Fourier analysis equation [16]

$$c_q = \frac{1}{T_0}\int_0^{T_0} x(t)e^{-j(2\pi/T_0)qt}dt \tag{59}$$

However, Equation (54) is a function of two variables, namely angle (θ) and time (t). For this reason, the Fourier series of a two-variable function is needed. Using a similar approach as in the one-dimensional case and applying Equations (58) and (59) to Equation (56) results in the transform pair [1]

$$g(\theta,t) = \sum_{n=-\infty}^{\infty} f_n(\theta)e^{j\omega t}e^{j(2\pi/T)nt} \tag{60}$$

and

$$f_n(\theta) = \frac{1}{T}\int_0^{T} g(\theta,t)e^{-j\omega t}e^{-j(2\pi/T)nt}dt \tag{61}$$

where $f_n(\theta)$ are simply equal to $b_n(\theta)$, which are the pencil beams directed in different angles defined in Equation (44). Substituting Equations (54), (55) and (56) gives the result

$$f_n(\theta) = \frac{1}{T}\sum_{m=0}^{N-1} A_m e^{jkmd\sin\theta}\int_{(mT/N)-(md/c)\sin\theta}^{(m+1)(T/N)-(md/c)\sin\theta} e^{-j(2\pi nt/T)}dt \tag{62}$$

After the integration term-by-term, Equation (62) reduces to

$$f_n(\theta) = (-1)^n \frac{\sin\left(\frac{n\pi}{N}\right)}{n\pi}\sum_{m=0}^{N-1} A_m e^{\left\{jm\left[\frac{(\omega+n\omega_0)}{c}d\sin\theta-\frac{2n\pi}{N}\right]\right\}} \tag{63}$$

The summation in Equation (63) assumes the form of the conventional array factor discussed in Chapter II. The maximum value of the array factor occurs when the exponent is equal to zero; hence, setting the exponent to zero

$$(k + nk_0)d \sin\theta - \frac{2n\pi}{N} = 0 \tag{64}$$

where $k = \frac{\omega}{c}$ and $k_0 = \frac{\omega_0}{c}$. Then, the angle at which the array factor is maximized can be found from Equation (64) as

$$\sin\theta = \frac{2n\pi}{Nd(k + nk_0)} \tag{65}$$

Since k_0 depends on ω_0, and it is assumed that $\omega_0 \ll \omega$, one can conclude that $k_0 \ll k$. Therefore, the scan angle is related by the following:

$$\sin\theta = \frac{2n\pi}{Nkd} \tag{66}$$

Equation (66) shows that the direction of a beam is associated with the Fourier coefficient number or frequency mode number n. This is particularly important because it allows the beams to be associated with their corresponding frequencies.

Now for the sake of simplicity, assume that the array is excited with uniform excitation (i.e., $A_m = 1$) and the spacing between the array elements is a half wavelength. Then, Equation (63) can be written as [1]

$$f_n(\theta) = (-1)^n \frac{\sin\left(\frac{n\pi}{N}\right)}{\frac{n\pi}{N}} \sum_{m=0}^{N-1} (1) e^{j(\gamma + \gamma_n)m} \tag{67}$$

where the exponent

$$\gamma + \gamma_n = \left[\frac{(\omega + n\omega_0)}{c} d \sin\theta - \frac{2n\pi}{N} \right] \tag{68}$$

can be simplified to

$$\gamma + \gamma_n = kd\sin\theta + nk_0 d\sin\theta - \frac{2\pi}{N}n \tag{69}$$

Combining the terms dependent on *n*, Equation (69) becomes

$$\gamma + \gamma_n = kd\sin\theta + n\left(k_0 d\sin\theta - \frac{2\pi}{N}\right) \tag{70}$$

Recalling the earlier approximation that $k_0 \ll k$, one can write Equation (70) as

$$\gamma + \gamma_n \approx kd\sin\theta - \frac{2\pi}{N}n \tag{71}$$

The wave number k can be expressed as $k = \frac{2\pi}{\lambda}$ and the interelement spacing is assumed to be half wavelength, namely $d = \frac{\lambda}{2}$. In Equation (71), the product kd reduces to π and Equation (71) can be written as

$$\gamma + \gamma_n \approx \pi\sin\theta - \frac{2\pi}{N}n \tag{72}$$

In Equation (67), the summation is a geometric series and similar to the derivation of the array factor of a uniform linear antenna array and it can be written as a Dirichlet function. Therefore, Equation (67) reduces to

$$f_n(\theta) = (-1)^n \frac{\sin\left(\frac{n\pi}{N}\right)}{\frac{n\pi}{N}} e^{j\frac{N-1}{2}(\gamma+\gamma_n)} \frac{\sin\left[\frac{N(\gamma+\gamma_n)}{2}\right]}{\sin\left[\frac{\gamma+\gamma_n}{2}\right]} \tag{73}$$

Substituting Equation (72) into Equation (73) results in as the following:

$$f_n(\theta) = (-1)^n \frac{\sin\left(\frac{n\pi}{N}\right)}{\frac{n\pi}{N}} e^{j\frac{N-1}{2}\left(\pi\sin\theta - \frac{2\pi}{N}n\right)} \frac{\sin\left[\frac{N\pi}{2}(\sin\theta - \frac{2n}{N})\right]}{\sin\left[\frac{\pi}{2}\left(\sin\theta - \frac{2n}{N}\right)\right]} \tag{74}$$

The exponent in Equation (74) can be written as

$$\frac{N-1}{2}\left(\pi\sin\theta-\frac{2\pi n}{N}\right)=\frac{N-1}{2}\pi\sin\theta-\frac{N-1}{2}\frac{2\pi n}{N}\approx\frac{N-1}{2}\pi\sin\theta-n\pi \tag{75}$$

and since $e^{jn\pi}=\pm1$,

$$f_n(\theta)=(-1)^n\frac{\sin\left(\frac{n\pi}{N}\right)}{\frac{n\pi}{N}}e^{j\frac{N-1}{2}\pi\sin\theta}\left\{\frac{\sin\left[\frac{N\pi}{2}(\sin\theta-\frac{2n}{N})\right]}{\sin\left[\frac{\pi}{2}\left(\sin\theta-\frac{2n}{N}\right)\right]}\right\} \tag{76}$$

The last factor in the curly brackets is the array factor that has the form of $\frac{\sin(N\varsigma)}{\sin(\varsigma)}$.

Substituting Equation (76) into Equation (60) gives the complete complex pattern as

$$g(\theta,t)=\sum_{n=-\infty}^{\infty}(-1)^n\frac{\sin\left(\frac{n\pi}{N}\right)}{\frac{n\pi}{N}}e^{j\frac{N-1}{2}\pi\sin\theta}\frac{\sin\left[\frac{N\pi}{2}(\sin\theta-\frac{2n}{N})\right]}{\sin\left[\frac{\pi}{2}\left(\sin\theta-\frac{2n}{N}\right)\right]}e^{j(\omega+n\omega_0)t} \tag{77}$$

From the array factor, it is clearly seen that the phase shift required to steer the beam to the desired directions is defined by [1]

$$\sin\theta=\frac{2n}{N} \tag{78}$$

Equation (78) explicitly shows the relation among the number of elements, number of beams, and the scan angle θ. In order to understand how some antenna parameters affect the system capabilities, suppose that fifty beams are desired from -25° to 25° and each beam is separated by one degree [1]. Using Equation (78), where $n=25$ and $\theta=50^\circ$, forces the number of elements to be 118. Therefore, to realize the requirements given above, one must use 118 antenna elements. In this way, one can get the desired beamwidth of one degree, which plays a key role in the angular resolution of radar.

2. Application of Formulas

In Section A.1, the theory of a time modulated antenna array to achieve electronic scanning was discussed. In order to visualize the theory, MATLAB programming language is used because of its convenient easy-to-use plotting functions.

In this section, Equations (76) and (77), which are the closed form equations derived for a rectangular pulse excitation, are used to illustrate the theory of a time modulated antenna and electronic scanning. Next, to compare the results with those of the closed form expressions, theory is implemented via MATLAB programming language step-by-step. This step-by-step procedure also lets the user to investigate the effects of amplitude tapering. MATLAB scripts, which are used to implement theory, are given in the appendix of this thesis.

Due to the memory limitations of the computers used in this study (Microsoft Windows with 4 GB of RAM) and the time elapsed to run the MATLAB scripts, the number of beams desired was limited to twenty. Therefore, suppose that twenty beams are desired over angles from -10° to 10° with the beams separated by one degree. From Equation (78), the number of antenna elements required can be readily found, and it turns out to be 115 elements for these particular requirements. Implementing Equation (76) in MATLAB gives the pattern plots displayed in Figure 13.

Figure 14 is the zoomed-in version of Figure 13 in which the sidelobe level, angle separation, and the number of beams generated can be seen more clearly. This plot shows that Equation (72) generates the desired number of simultaneous pencil beams, which are separated approximately by one degree. If the desired number of beams were set to 180 with angle separation of one degree, then it would provide a way to cover a wide range of directions in terms of angles. In this simulation, the modulation frequency was set to 10 kHz and the carrier frequency was 10 MHz. Since each beam is tagged with a different frequency, it provides a means of detecting targets simultaneously, which are also tagged with the frequency associated with the beam. In addition, note that the sidelobe level is approximately 13.3 dB down from the main lobe as expected for a uniformly excited array.

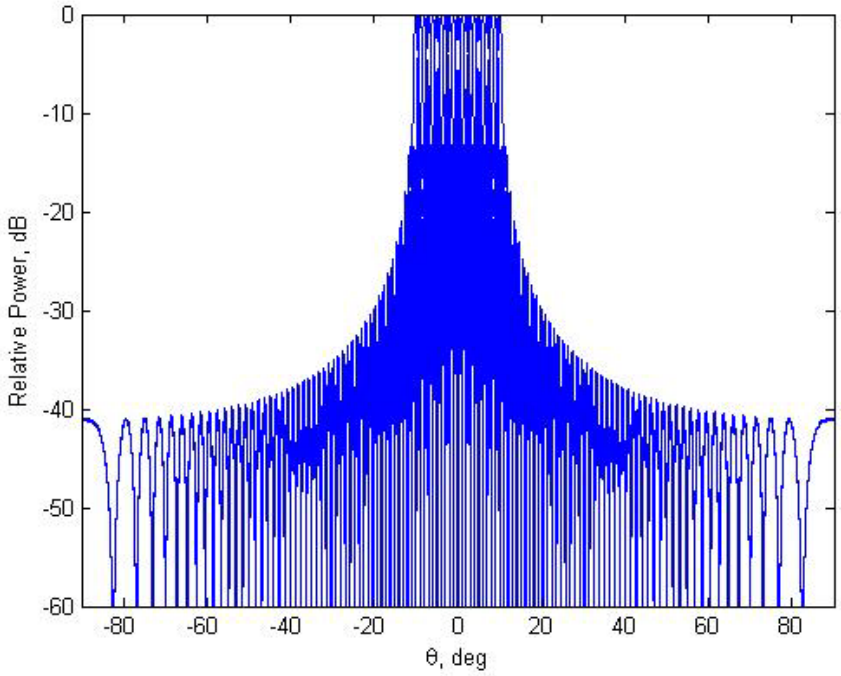

Figure 13. Multiple Beams from a Time Modulated Antenna with a Closed Form Expression

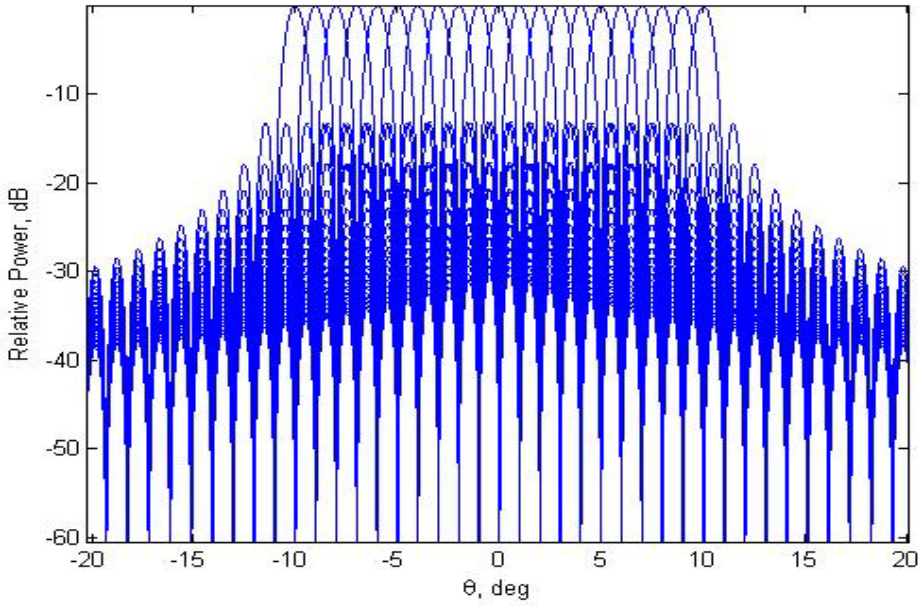

Figure 14. Multiple Beams from a Time Modulated Antenna with a Closed Form Expression (Zoomed in)

Figures 13 and 14 only demonstrate the spatial dependence of the complex pattern, not the time-dependent pattern complex. To obtain a more detailed picture of the time varying pattern, Equation (77) is implemented in MATLAB. A carrier frequency of 10 MHz and a modulation frequency of 10 kHz are used in order to satisfy the requirement for $f_0 \ll f$ along with the same requirements for the number of the beams and angle separation as mentioned previously. In the MATLAB script, after computation of the time-dependent pattern, a fast Fourier transform (FFT) is implemented and a mesh plot of the pattern vs. frequency angle is plotted. Figures 15 and 16 depict the plots of the time varying pattern in the frequency domain with linear units and dB, respectively.

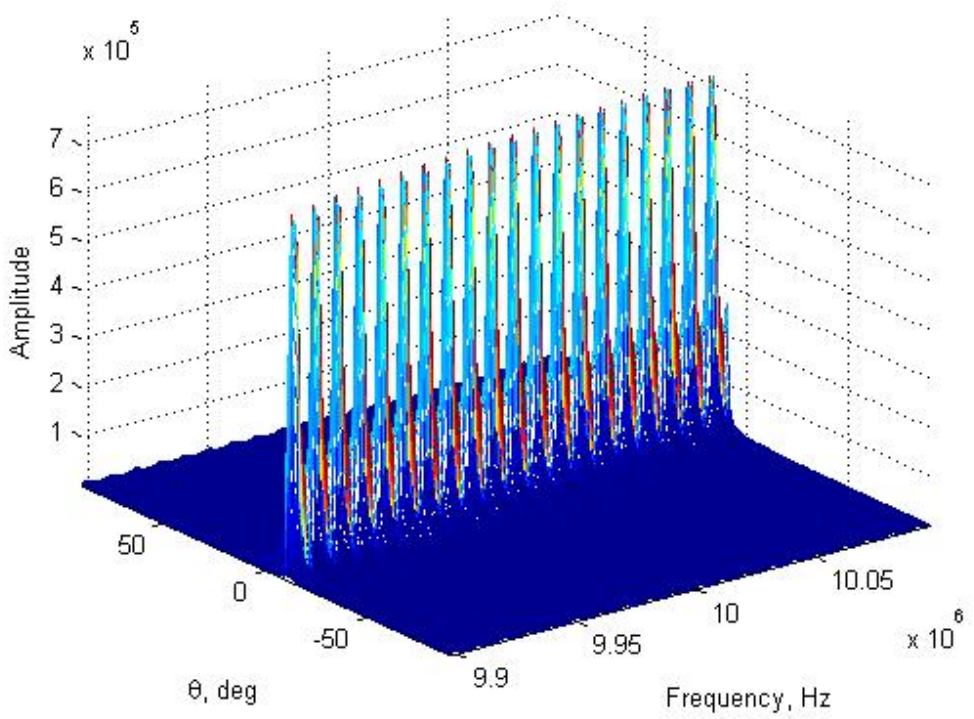

Figure 15. Plot of the Time Varying Complex Pattern vs. Frequency and Angle θ in Linear Units

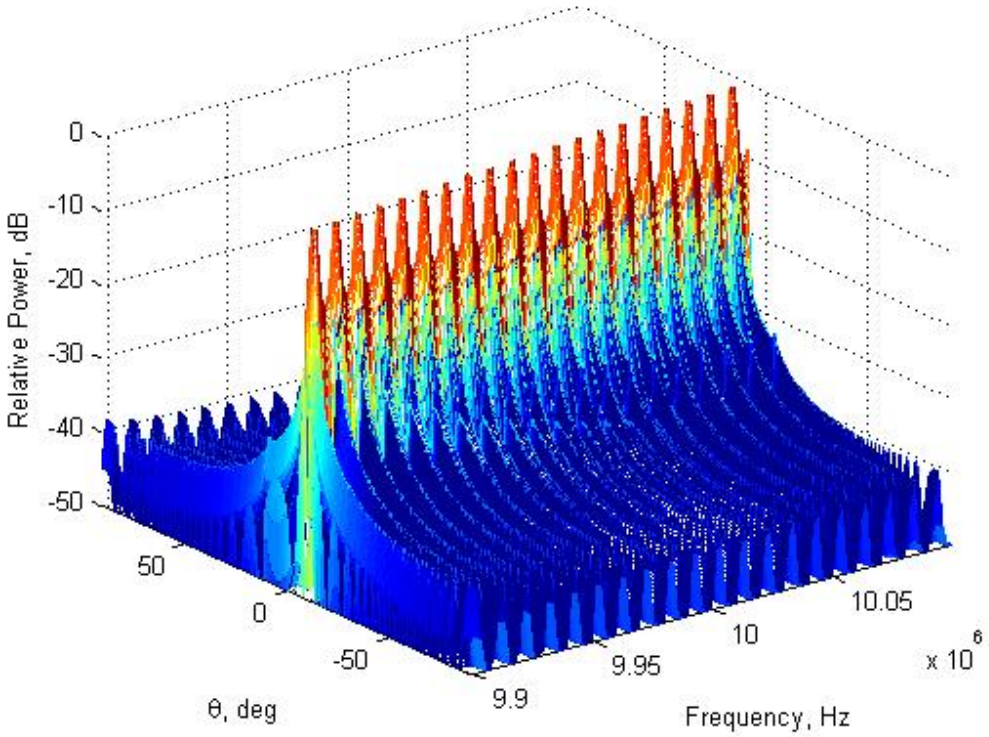

Figure 16. Plot of the Time Varying Complex Pattern vs. Frequency and Angle θ in dB

Figures 15 and 16 show that each beam generated has a different scan angle and is also tagged with a different frequency value that is determined by the modulation frequency f_0 and its harmonics. Therefore, this implementation presents a FDA as a time modulated array that creates multiple beams. Figure 17, which is top view of Figure 16, delineates the frequency increment as a linearly increasing line and clearly reveals the connection between the scan angle and frequency tagging. As seen from Figure 17, the first beam has a scan angle of -10° and is associated with 9.9 MHz frequency, and as the beam number increases, the frequency associated with the beam increases by 10 kHz as expected. In Figure 17, the frequencies associated with the beams appear to be slightly shifted due to the limitations of the computer's RAM and insufficient data points.

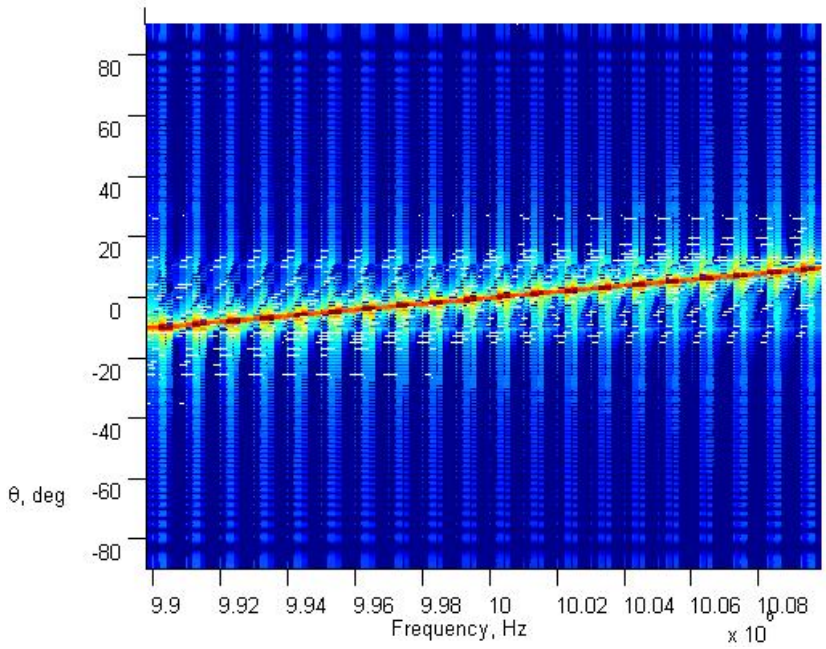

Figure 17. Top View of the Time Varying Complex Pattern vs. Frequency and Angle θ in dB

In order to see the effects of amplitude tapering, the steps followed to derive the closed form equations must be implemented in MATLAB. Closed form equations are valid only for uniform excitation where all the current amplitudes are equal to one. In uniform excitation of an array, the highest sidelobe is 13.26 dB down from the main peak. One can use the amplitude tapering to reduce the sidelobe levels; however, there is a trade-off between the reduced sidelobe level and beamwidth. As the sidelobe level decreases, the main beam broadens. Therefore, an antenna designer should carefully decide between the desired sidelobe level and the beamwidth that defines both the gain and the angular resolution of a radar.

Figures 18 and 19 (zoomed-in version) show the result obtained from MATLAB by following the same procedure to derive the closed form equations. The only difference between Figure 13 and 18 is the way they are computed. Figure 13 was plotted with a closed form equation, which is in fact an approximation of Figure 18. The closed form solution was derived based on the assumption of a uniform array. On the other hand, Figure 18 is the more generalized result and is derived based on a Fourier series

expansion of the complex pattern where on-off switching of antenna elements is used as discussed in the theory section. In addition, note that the sidelobe level for the uniform excitation is approximately the same theoretical value. A comparison of Figures 13 and 18 show minor differences. However, in general the same pattern and values are obtained for modeling of a uniformly excited array from both the closed form equations and the Fourier series expansion.

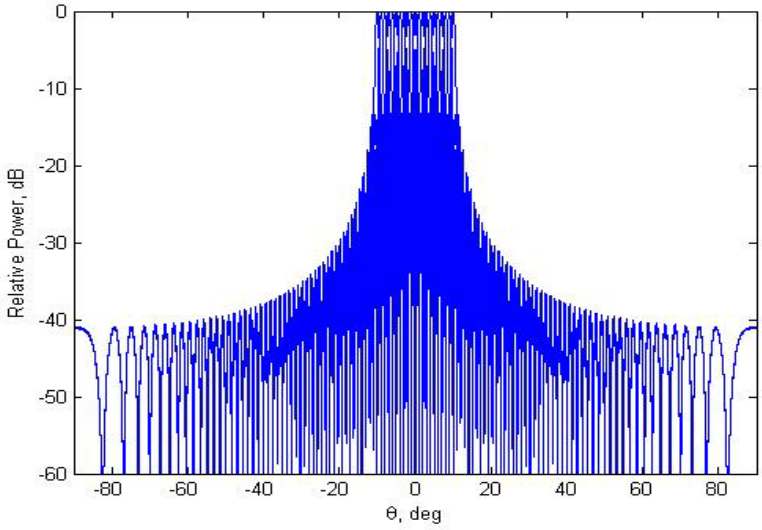

Figure 18. Fourier Series Expansion of the Complex Pattern

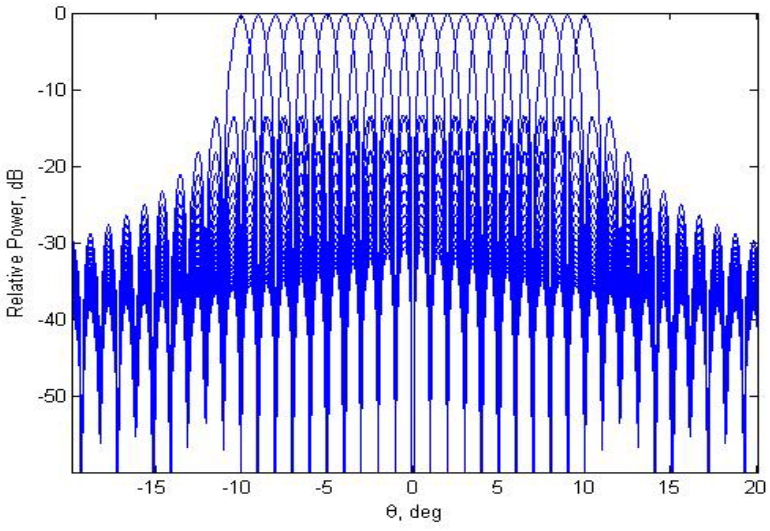

Figure 19. Fourier Series Expansion of the Complex Pattern (Zoomed in)

Similarly, Figures 20 and 21 demonstrate the same characteristics as Figures 16 and 17. The slight frequency shift problem the author had in Figure 17 is eliminated in Figure 20 due to the step-by-step implementation of the formulas.

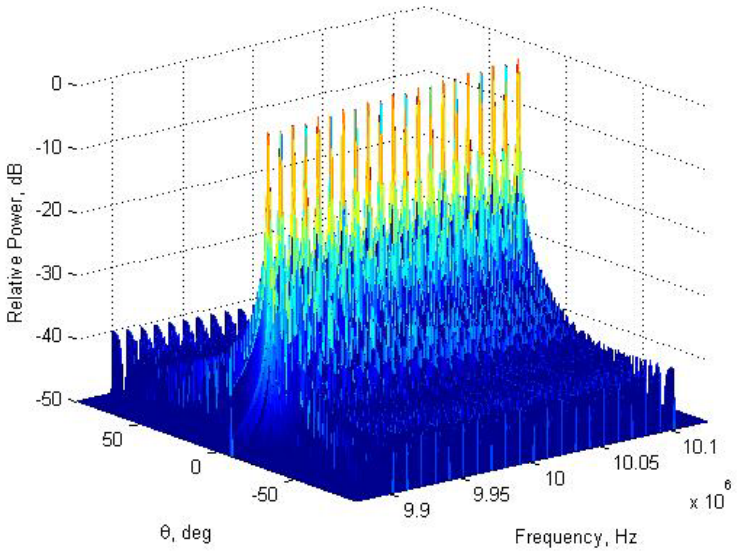

Figure 20. Plot of the Time Varying Complex Pattern vs. Frequency and Angle θ in dB Using Fourier Series Expansion

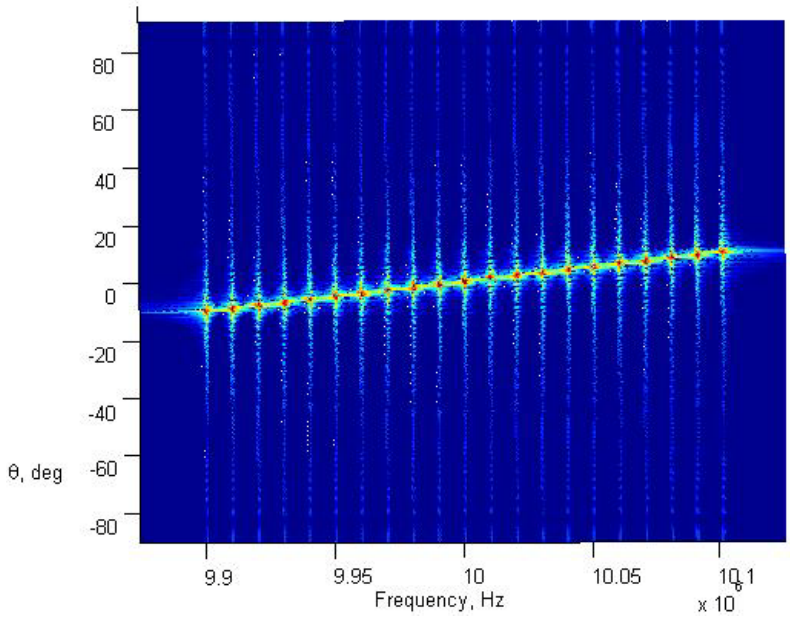

Figure 21. Top View of the Time Varying Complex Pattern vs. Frequency and Angle θ in dB Using Fourier Series Expansion

In Figure 18 through Figure 21, the complex pattern is depicted with uniform excitation; in other words, all current amplitudes for all elements are equal to one. However, as mentioned before, amplitude tapering can be used to reduce the sidelobe levels. The greater the taper of the aperture illumination as it approaches the edges of the antenna aperture the lower the sidelobe level will be, but at the cost of a wider beamwidth and a lower maximum gain [3]. Widely used amplitude aperture distribution types and radiation pattern characteristics produced by these distributions are given in Table 1.

Type of Distribution, $\|z\| < 1$	**Relative Gain**	**Half-power beamwidth, degree**	**Sidelobe Level**
Uniform, *A(z)=1*	1	$51\lambda/D$	13.2
Cosine, $A(z) = \cos^n(\pi z/2)$			
n = 0	1	$51\lambda/D$	13.2
n = 1	0.810	$69\lambda/D$	23
n = 2	0.667	$83\lambda/D$	32
n = 3	0.575	$95\lambda/D$	40
n = 4	0.515	$111\lambda/D$	48
Parabolic, $A(z) = 1-(1-\Delta)z^2$			
$\Delta = 1.0$	1	$51\lambda/D$	13.2
$\Delta = 0.8$	0.994	$53\lambda/D$	15.8
$\Delta = 0.5$	0.970	$56\lambda/D$	17.1
$\Delta = 0$	0.833	$66\lambda/D$	20.6
Triangular, $A(z) = 1-\|z\|$	0.75	$73\lambda/D$	26.4
Circular, $A(z) = \sqrt{1-z^2}$	0.865	$58.5\lambda/D$	17.6
Cosine-squared-plus-pedestal			
$0.33 + 0.66\cos^2(\pi z/2)$	0.88	$63\lambda/D$	25.7
$0.008 + 0.92\cos^2(\pi z/2)$	0.74	$76.5\lambda/D$	42.8

Table 1. Various Aperture Distribution Types (After [3])

As the last step of the implementation, a radiation complex pattern is plotted using cosine aperture distribution, where *n* is chosen to be one with cosine-squared-plus-pedestal aperture excitation in order to check the validity of the MATLAB code. First, a cosine aperture distribution is used for the 115 elements in a linear array to generate 20 beams with one-degree separation. The cosine aperture excitation is shown in Figure 22. The Fourier series expansion of the time varying pattern due to the cosine aperture excitation is given in Figure 23. It is clearly seen from Figure 23 that the peak sidelobe level is approximately 23 dB less than the main beam as expected by theory according to Table 1. Also note that the beams are no longer as narrow as in the uniform excitation case; in other words, reduced sidelobe levels are realized at the expense of broadened beams.

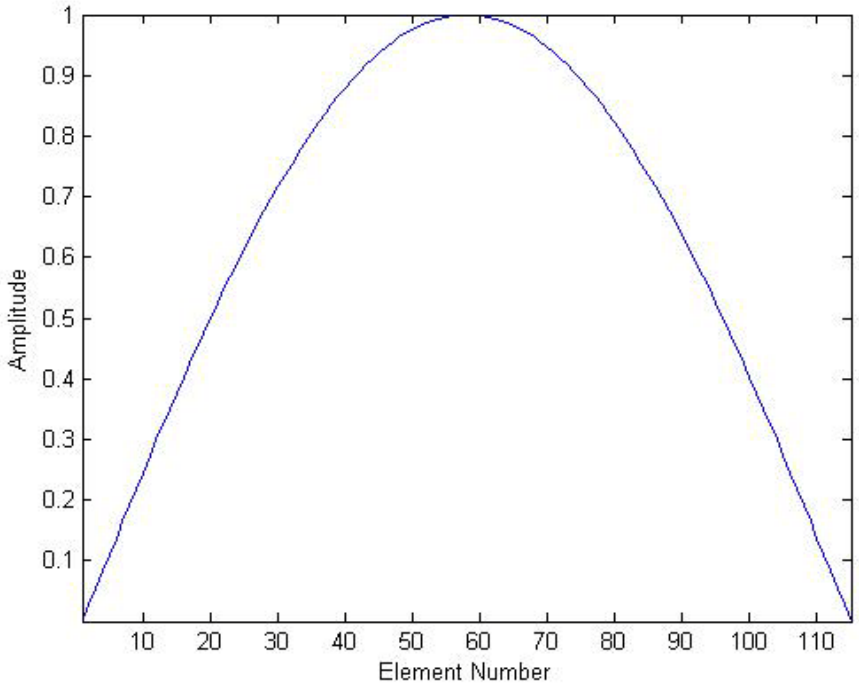

Figure 22. Cosine Aperture Excitation $\left(A(z)=\cos^{n}(\pi z/2)\right)$ for 115 Elements, $n=1$

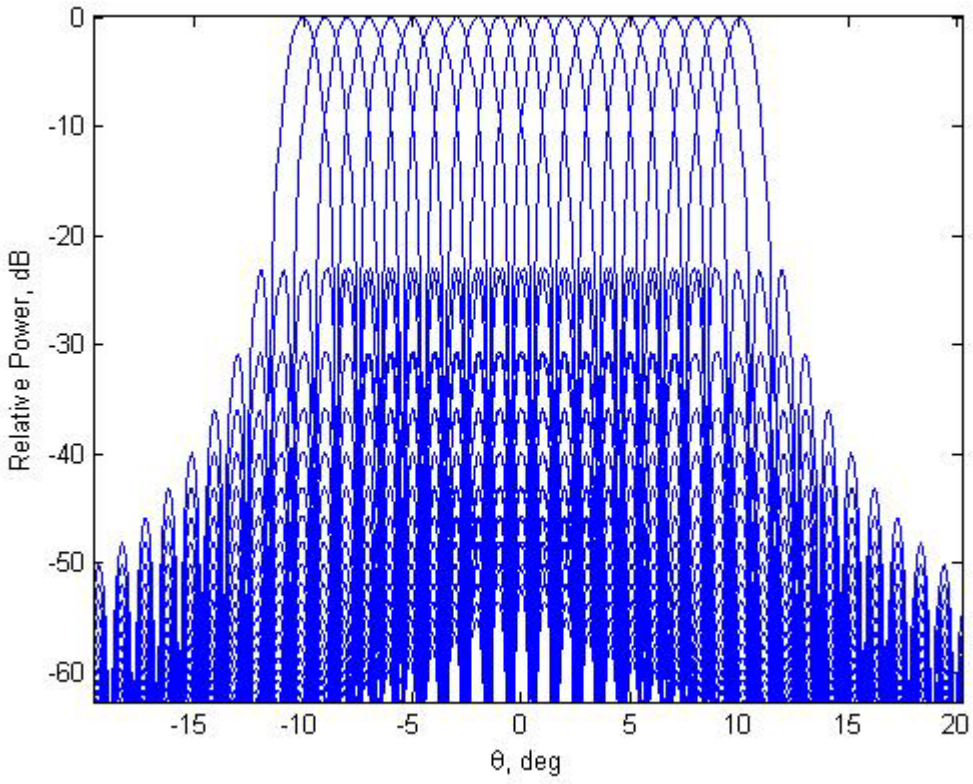

Figure 23. Radiation Pattern of a Time Modulated Array Where the Excitation is a Cosine Function

Lastly, a cosine-squared-plus-pedestal aperture excitation is used where the excitation is given by $0.33+0.66\cos^2(\pi z/2)$ and is illustrated in Figure 24. The resulting pattern due to cosine-squared-on-a-pedestal excitation is shown in Figure 25. The results match with the theoretical values given in Table 1 as expected, and sidelobe level appears to be approximately 26 dB down from the main peak level.

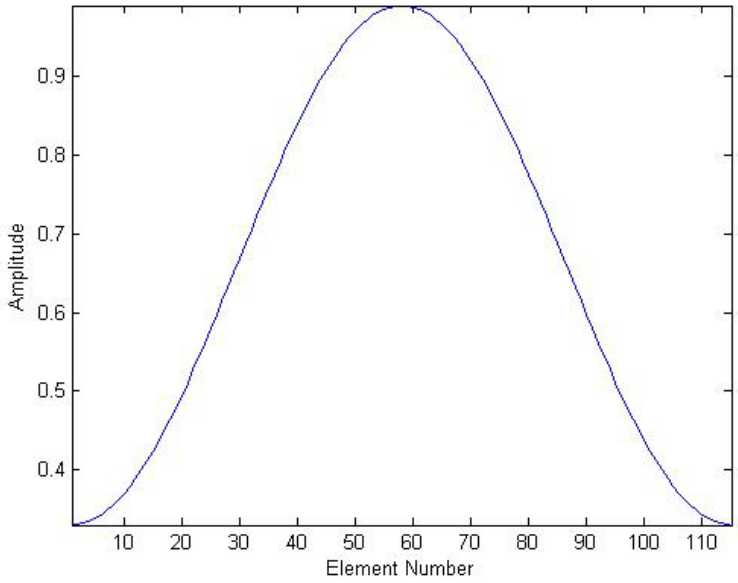

Figure 24. Cosine-squared-on-a-pedestal Aperture Excitation $\left(A(z) = 0.33 + \cos^2(\pi z / 2)\right)$ for 115 Elements, $n = 1$

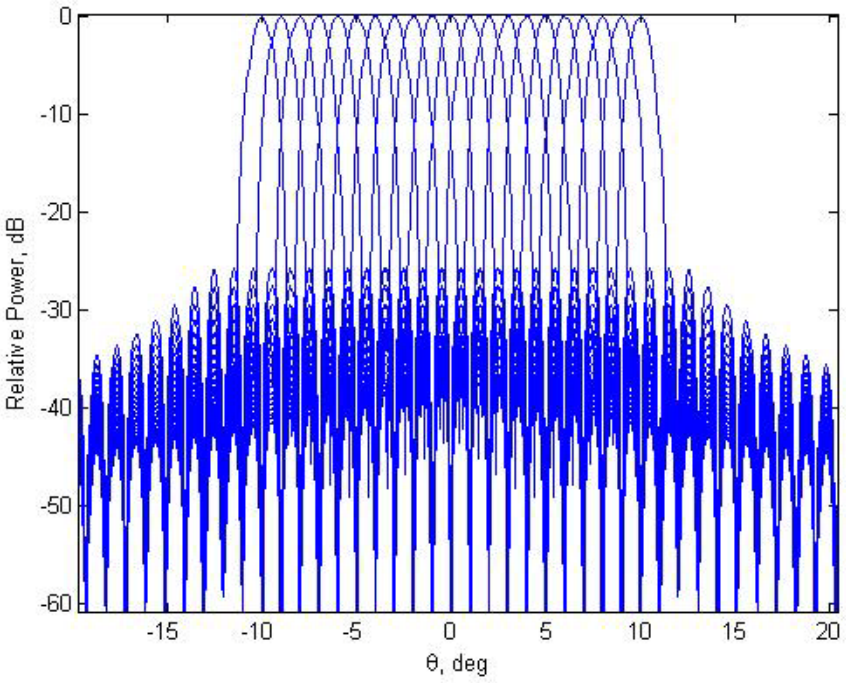

Figure 25. Radiation Pattern of a Time Modulated Array Where the Excitation is a Cosine-squared-on-a-pedestal Function

In this chapter, the theory behind time modulated antennas and how they can be used in radar applications to generate a quasi-electronic scanning mechanism was discussed. Since all pencil beams appear simultaneously, it provides a way to achieve wide-angle coverage. In addition, it should be noted that frequency tagging of beams creates the distinct advantage of finding the direction of a target easily. The analytical theory was supported by MATLAB programming to illustrate the effects of amplitude tapering.

The concept given in this chapter in essence shows some characteristics of a frequency diverse array as a time modulated array to decrease sidelobe levels and create multiple beams. In the next chapter, the frequency diverse array concepts, which basically rely on the feeding of each antenna in an array structure with a progressive incremental (or decremental) frequency shift, will be introduced [8].

IV. FREQUENCY DIVERSE ARRAYS

A. CONCEPT

A frequency diverse array is a new and novel electronic scanning technique. The elements of the array can be either excited with the same waveform or different types of waveforms. In this thesis, for simplicity the same waveform use will be assumed. The most important difference of a frequency diverse array from a conventional array is that a small amount of frequency increment compared to the carrier frequency is used across the array elements instead of a linear phase shift. Use of frequency increment generates a far electric field pattern that is a function of range, time, and angle. Range-dependent beamforming is of importance because one can get local maxima at different ranges, and this can be used for multiple target detection with the use of advanced signal processing techniques, although the range ambiguities might be a problem.

1. Theory

Conventional array theory was discussed in Chapter II in detail. A frequency diverse array is particularly different from a conventional array due to the use of frequency increment across the array elements. In conventional arrays, it is assumed that the waveform radiated by the array elements is identical, excluding the current amplitudes and current phases. Recall that amplitude tapering reduces the sidelobe levels and progressive phase increment steers the main beam to the desired direction.

Now, assume that the waveform radiated from each antenna element is identical with a frequency increment of Δf Hz applied across the elements. In a conventional array (see Figure (26)), the phase shift due to the path length is defined by

$$\psi = \frac{2\pi}{\lambda} d \cos\theta \tag{79}$$

where angle θ defines the direction of the target from the axis of the array. The concept of a frequency diverse array is illustrated in Figure 26.

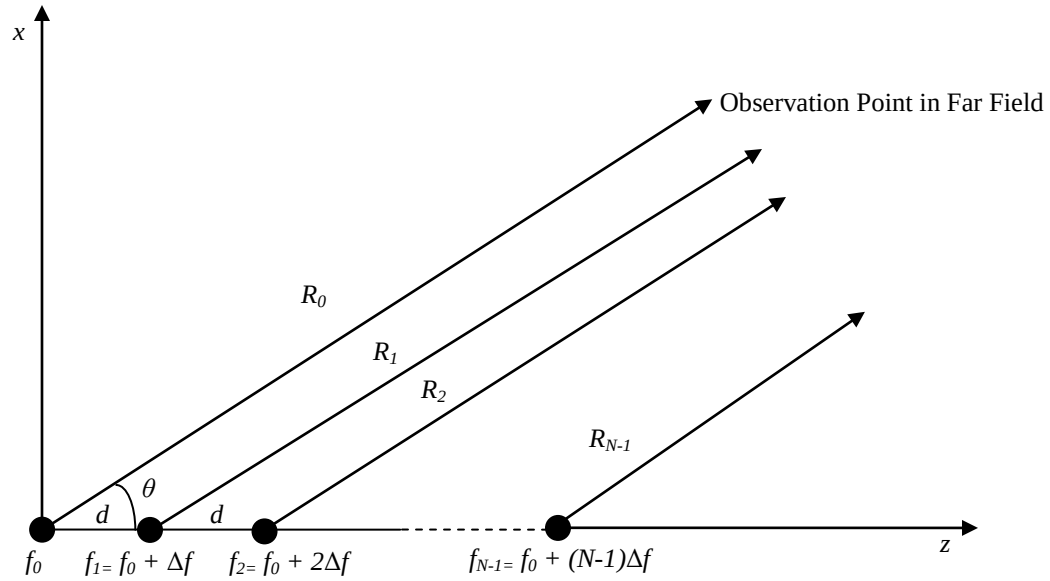

Figure 26. Frequency Diverse Linear Array Antenna Concept (After [8])

The phase of the signal arriving at element zero, which is located at the origin of the coordinate system depicted in Figure 26, is

$$\psi_0 = \frac{2\pi}{\lambda} R_0 = \frac{2\pi f_0}{c} R_0 \tag{80}$$

where f_0 is the frequency of the waveform radiated from element zero and R_0 is the path length between the element and the far-field observation point. Similarly, the phase of the signal arriving at element one can be written as

$$\begin{aligned} \psi_1 &= \frac{2\pi f_1}{c} R_1 = \frac{2\pi(f_0 + \Delta f)}{c}\left(R_0 - d\cos\theta\right) \\ \psi_1 &= \frac{2\pi f_0 R_0}{c} + \frac{2\pi(\Delta f) R_0}{c} - \frac{2\pi f_0 d\cos\theta}{c} - \frac{2\pi(\Delta f) d\cos\theta}{c} \end{aligned} \tag{81}$$

where the approximation $R_{N-1} \approx R_0 - (N-1)d\cos\theta$ is used from array theory [17].

The phase difference between the signals arriving at element zero and element one results in

$$\psi_0 - \psi_1 = \frac{2\pi f_0}{c} R_0 - \left(\frac{2\pi f_0 R_0}{c} + \frac{2\pi (\Delta f) R_0}{c} - \frac{2\pi f_0 d \cos\theta}{c} - \frac{2\pi (\Delta f) d \cos\theta}{c} \right)$$

$$\Delta\psi = \frac{2\pi f_0 d \cos\theta}{c} + \frac{2\pi (\Delta f) d \cos\theta}{c} - \frac{2\pi (\Delta f) R_0}{c} \tag{82}$$

The first term in Equation (82) is simply the conventional array factor seen frequently in array theory where $\frac{f_0}{c} = \frac{1}{\lambda}$, assuming that the waves are radiating in free space. The last term is of importance because it shows that the radiation pattern of the array depends on the range and the frequency increment. Frequency scanning and frequency diverse arrays have similarities in terms of frequency diversity; however, frequency scanned arrays use the frequency increment as a function of time for all elements, while frequency diverse arrays use the frequency increment at the discrete points of the aperture [17].

The new terms introduced in Equation (82) generate an apparent angle contradictory to the scan angle that one normally sees. This apparent scan angle can be derived using the same approach used in Chapter II. Due to the change in the angle, progressive phase shift must be defined in terms of the apparent angle as follows [6]:

$$\Delta\psi = \frac{2\pi}{\lambda} d \cos\theta_a \tag{83}$$

where θ_a is the apparent angle. Equating Equation (83) to Equation (82) results in

$$\Delta\psi = \frac{2\pi f}{c} d \cos\theta_a = \frac{2\pi f_0 d \cos\theta}{c} + \frac{2\pi (\Delta f) d \cos\theta}{c} - \frac{2\pi (\Delta f) R_0}{c} \tag{84}$$

Solving Equation (84) for the angle yields the following [6]:

$$\cos\theta_a = \frac{f_0 \cos\theta}{f} + \frac{\Delta f \cos\theta}{f} - \frac{\Delta f R_0}{fd}$$
$$\theta_a = \arccos\left(\frac{f_0 \cos\theta}{f} + \frac{\Delta f \cos\theta}{f} - \frac{\Delta f R_0}{fd} \right) \tag{85}$$

From array antenna theory discussed in Chapter II, it is known that a progressive phase shift of $\Delta\psi$ across the elements must be applied for scanning. In addition to this, a scan angle θ_0 must be defined to steer the main beam to desired direction. Equation (84) defines the amount of phase shift for a FDA, and the array factor can be calculated readily using a similar approach. Assume the desire is to steer the main beam to broadside where $\theta_0 = 90^\circ$. This means that there is no phase shift due to the path length and the first term in Equation (84) vanishes. Additionally, assume that the frequency increment across the array is not applied (i.e., $\Delta f = 0$) and uniform excitation is used. It can be clearly seen that when $\theta_0 = 0$ and $\Delta f = 0$, the interelement phase shift becomes zero ($\Delta\psi = 0$). This is nothing more than a uniform linear array. If the carrier frequency is set to 100 kHz and ten antenna elements are used, where the spacing between antenna elements is $d = \frac{\lambda}{2}$, the pattern shown in Figure 27 is obtained when $\theta_0 = 0$ and $\Delta f = 0$.

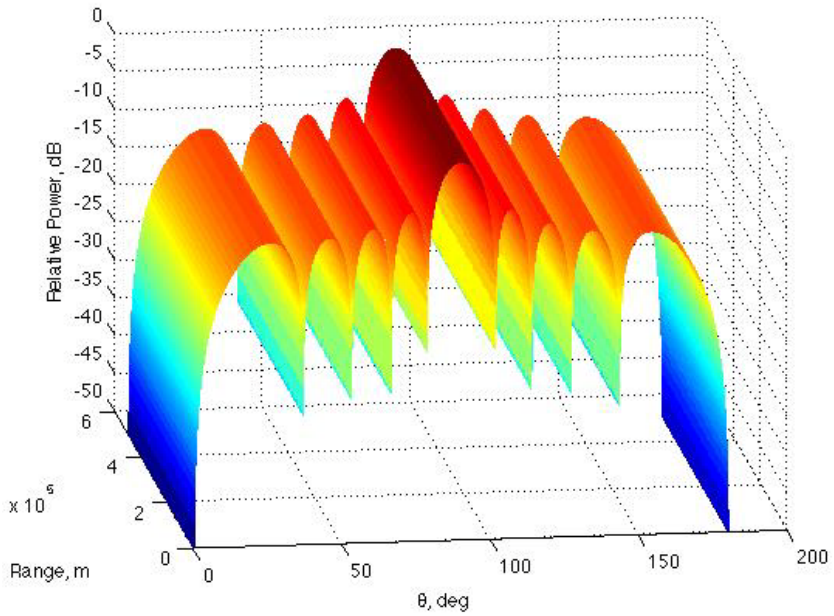

Figure 27. Array Pattern when no Frequency Increment is Applied (After [6])

If the frequency increment Δf is chosen to be 500 Hz for the same array configuration, the second and third terms become nonzero and the array pattern is affected by these terms, as demonstrated by the pattern shown in Figure 28.

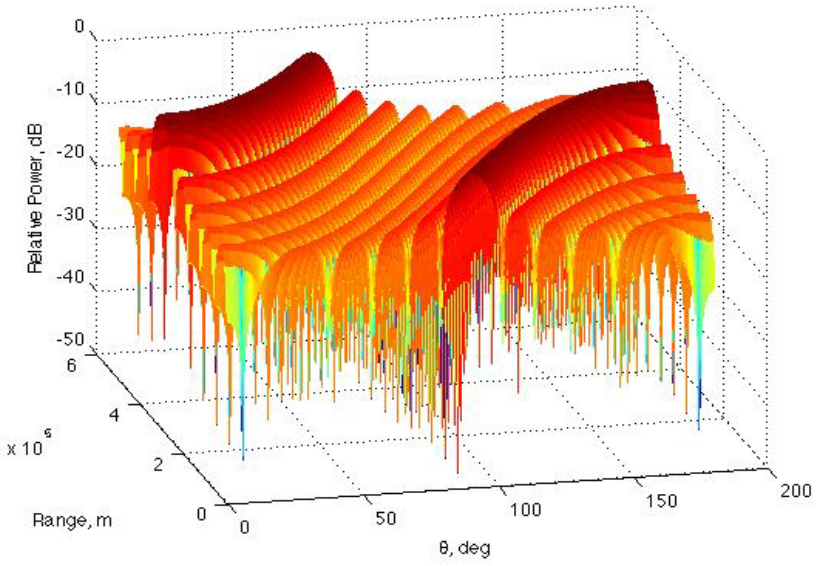

Figure 28. Array Pattern when a Frequency Increment of $\Delta f = 500$ Hz is Applied (After [6])

Figure 28 shows that the array pattern is not only a function of time, but also a function of angle and range. As shown, the array pattern reaches its maximum at different ranges and angles. This leads to the definition of the apparent angle because the main beam is no longer directed at a fixed scan angle. This flexible beam scan option can decrease the effects of multipath and be used in synthethic aperture radar (SAR) and ground moving target indicator (GMTI) as discussed in [6]. The pattern shown is interesting from the types of new radar operations that it might support. For example, the pattern might help to combat glint, which has degraded patterns at specific angles. There might also be applications in electronic warfare where a fast-moving target might egress from air defense along a diagonal line. The pattern in Figure 28 has the main peak varying in both range and angle, so diagonal tracking might be enhanced.

The array patterns given in Figures 27 and 28 are the spatial patterns. However, to see the time varying far electric field, one should define the electric fields radiated from the array elements in terms of time and frequency increment Δf. Now, assume that there is an array of *N* elements where elements are separated by a distance of d meters and excited with a frequency shift of Δf. In Chapter II, when array antenna theory was introduced, phasor notation was used and the time-dependent term $e^{j\omega t}$ was omitted. In this chapter, time dependency is taken into account. Therefore, the electric field radiated from each element in the far field can be rewritten using Equation (11) as

$$E = \sum_{n=0}^{N-1} \frac{a_n}{R_n} \, e^{j(\omega_n t - k_n R_n)} f_e(\theta, \phi) \tag{86}$$

where $\omega_n = \omega_0 + n\Delta\omega$, $k_n = k_0 + n\Delta k$, $\Delta k = \dfrac{\Delta\omega}{c} = \dfrac{2\pi}{\Delta k}$, $R_n \approx R_0 - nd\cos\theta$, and $f_e(\theta, \phi)$ is the element factor, which is in fact a function of frequency. Substituting these equations in Equation (86) yields

$$E = \sum_{n=0}^{N-1} \frac{a_n}{R_n} f_e(\omega_0 + n\Delta\omega) \; e^{j(\omega_0 + n\Delta\omega)t} \; e^{-j(k_0 + n\Delta k)R_n} \tag{87}$$

where $k_0 = \frac{\omega_0}{c}$. In this equation, current excitations of all elements are assumed to be in phase coherence. Due to this reason, the $e^{j\psi_n}$ term is dropped from Equation (11). The $\frac{1}{R_n}$ term in Equation (87) is the fall-off factor of the far electric field due to range. In the far field, the distances from the individual array elements to the observation point can be considered as equal, and this term can be pulled out of the summation. However, the same assumption cannot be made for the phase associated with the R_n term in the exponent. A small change in phase can generate a big change in radiation pattern. However, an approximation can be made using simple trigonometry: $R_n \approx R_0 - nd\cos\theta$. Taking into account all the approximations and assuming that the array is uniformly excited where $a_n = 1$, Equation (87) turns out to be

$$E = \frac{1}{R_0}\sum_{n=0}^{N-1} f_e\left(\omega_0 + n\Delta\omega\right)\, e^{j(\omega_0 + n\Delta\omega)t}\; e^{-j(k_0 + n\Delta k)(R_0 - nd\cos\theta)} \tag{88}$$

and

$$E = \frac{1}{R_0}\sum_{n=0}^{N-1} f_e\left(\omega_0 + n\Delta\omega\right)\, e^{j(\omega_0 + n\Delta\omega)t}\; e^{-j\left(k_0R_0 - k_0nd\cos\theta + n\Delta kR_0 - n^2kd\cos\theta\right)} \tag{89}$$

Combining the terms dependent on n yields

$$E = \frac{1}{R_0}\sum_{n=0}^{N-1} f_e\left(\omega_0 + n\Delta\omega\right)\, e^{j(\omega_0 t - k_0R_0)}\; e^{jn\left(k_0d\cos\theta - \Delta kR_0 + nkd\cos\theta + \Delta\omega t\right)} \tag{90}$$

Since $e^{j(\omega_0 + k_0R_0)}$ does not depend on n, it can be pulled out of the summation and Equation (90) can be written as

$$E = \frac{1}{R_0}e^{j(\omega_0 t - k_0R_0)}\sum_{n=0}^{N-1} f_e\left(\omega_0 + n\Delta\omega\right)\, e^{jn\left(k_0d\cos\theta - \Delta kR_0 + \Delta\omega t + n\Delta kd\cos\theta\right)} \tag{91}$$

The following assumptions can be made to further simplify Equation (91). First, it can be assumed that $(N-1)d \ll R$, which means array length is much less than the distance to the far field in terms of spatial units. Second, using the fundamental frequency

diverse array constraint that $\omega_0 \gg \Delta\omega$, the element factor $f_e(\omega_0 + n\Delta\omega)$ can be approximated by $f_e(\omega_0)$. In the same fashion, $(N-1)\Delta\omega \ll \omega_0$. Lastly, in the amplitude sense, $R_n \approx R_0$.

Let the exponent in Equation (91) be named γ and defined as

$$\gamma = k_0 d\cos\theta - \Delta k R_0 + \Delta\omega t + n\Delta k d\cos\theta \tag{92}$$

The last term $n\Delta k d\cos\theta$ is much less than the other three terms in Equation (92). If this equation is examined, one can see that $t \gg \frac{nd\cos\theta}{c}$, which means any observation time t is much greater than the time delay experienced by the signals arriving at the different array elements. It is also obvious that the distance to the observation point R_0 is much greater than the projection of the aperture length $nd\sin\theta$ in the direction of the observation point; in other words $R_0 \gg nd\cos\theta$. Lastly, since $\omega_0 \gg \Delta\omega$, then $k_0 d\cos\theta \gg n\Delta k d\cos\theta$. Taking into consideration all the assumptions made, Equation (93) can be rewritten as

$$E = f_e(\omega_0)\frac{1}{R_0}e^{j(\omega_0 t - k_0 R_0)}\sum_{n=0}^{N-1} e^{jn\gamma} \tag{93}$$

where γ is now

$$\gamma = k_0 d\cos\theta - \Delta k R_0 + \Delta\omega t \tag{94}$$

In Equation (93), the summation $\sum_{n=0}^{N-1} e^{jn\gamma}$ is a geometric series and the result of this summation is equal to $\frac{1-e^{j\gamma N}}{1-e^{j\gamma}}$. Applying Euler's identities to this result, Equation (93) can be written in the form of the Dirichlet function as

$$E = f_e(\omega_0)\left(\frac{1}{R_0}\right)\left(e^{j\frac{\gamma}{2}(N-1)}\right)\left(\frac{\sin\left(\frac{N\gamma}{2}\right)}{\sin\left(\frac{\gamma}{2}\right)}\right) \tag{95}$$

and the absolute value of the far electric field is

$$|E| = \left(\frac{1}{R_0}\right)\left|\frac{\sin\left(\frac{N\gamma}{2}\right)}{\sin\left(\frac{\gamma}{2}\right)}\right| \tag{96}$$

in which the element factor is omitted since the array pattern is the subject of this analysis.

In Equation (93), the maximum field is obtained when the exponent in the summation is equal to zero or the multiple of 2π. This can be expressed mathematically as [6]

$$\gamma = k_0 d\cos\theta - \Delta k R_0 + \Delta\omega t = 2\pi m, \quad m = 0, \pm 1, \pm 2, \ldots \tag{97}$$

Now, if Equation (97) is solved for time t, the result is

$$t = \frac{m}{\Delta f} + \frac{d\cos\theta}{\lambda f} + \frac{R_0}{c} \tag{98}$$

It should be noted that Equation (98) shows the periodic nature of the array pattern in time where the fundamental period is $\frac{1}{\Delta f}$ and the range R_0 and angle θ is fixed [17]. Similarly, solving for R_0 yields

$$R_0 = ct + \frac{d\cos\theta}{\lambda\Delta f} - m\frac{c}{\Delta f} \tag{99}$$

and it reveals that the array pattern is also a periodic function of range assuming both θ and t are fixed and where the fundamental period is $\frac{c}{\Delta f}$ [17]. By the same token, solving for $\cos\theta$ results in

$$\cos\theta = \left(\frac{\lambda}{d}\right)m - \left(R_0 - ct\right)\frac{\Delta f}{fd} \tag{100}$$

The periodicity of the angle-dependent pattern is the inverse of the spacing in terms of wavelength, which corresponds to the location of the grating lobes [17]. It is clearly seen from Equation (97) that when only one parameter is fixed, there are an infinite number of solutions for the unfixed parameter couple. On the other hand, when two parameters are fixed, the periodicity of the array pattern is revealed depending on the unfixed variable.

2. Periodicity of the Angle-, Range- and Time-dependent Patterns

The periodic nature of the array pattern on range, time and angle can be illustrated using MATLAB. First, the periodic nature of the pattern in time will be illustrated while keeping the range and angle θ fixed. The parameters used for the simulation are operating frequency $f_0 = 10$ MHz, interelement frequency increment $\Delta f = 10$ kHz, and number of array elements $N = 10$ with a spacing of $\frac{\lambda}{2}$. Figure 29 shows the time-dependent array pattern at the range of $R_0 = 10$ km and the broadside of the array where $\theta = 90^\circ$ and both parameters are fixed. It can be clearly seen that the time difference between the two peaks in Figure 29 is around 100 μsec and it verifies that the period of the time-dependent array pattern is 100 μsec, which matches the result of Equation (98) where the period was found to be $\frac{1}{\Delta f}$. Since the frequency increment Δf used for this simulation is 10 kHz, $\frac{1}{\Delta f}$ yield 100 μsec as expected. Figure 29 also reveals that the main beam of the antenna illuminates a target at a fixed range and angle (R_0, θ_0) every $\frac{1}{\Delta f}$ seconds. Therefore, the scanning speed can be increased by using a higher value of frequency increment without violating the fundamental frequency diverse array constraint $\omega_0 \gg \Delta\omega$.

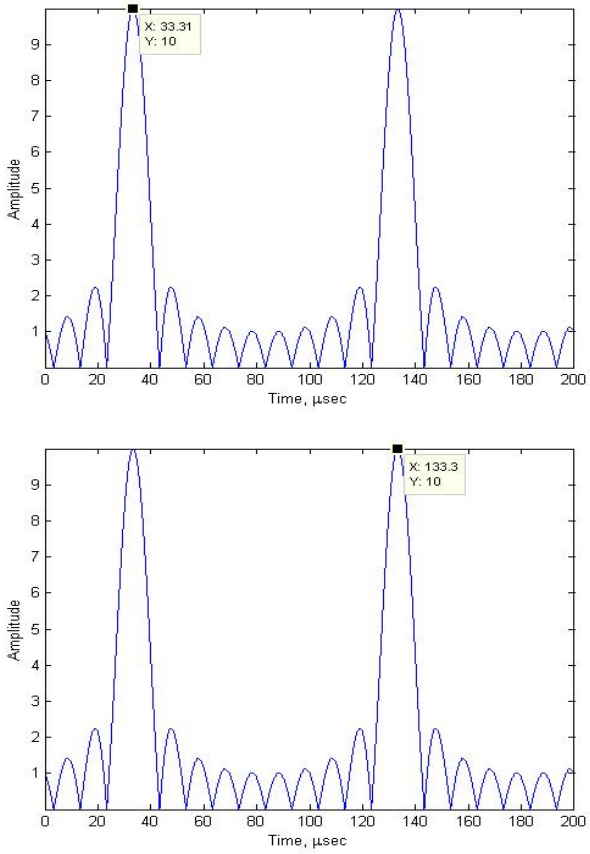

Figure 29. Time-dependent Array Pattern when the Range R_0 and Angle θ are Fixed

Using the same array configuration, the range-dependent array pattern can be plotted for a fixed time $t = 233\ \mu\text{sec}$ and angle $\theta = 90^\circ$.

Figure 30 shows the periodicity of the range-dependent array pattern. The period of the pattern is measured to be approximately 30 km from Figure 30, which is compatible with the period defined in Equation (99). The period in Equation (99) was found to be $\frac{c}{\Delta f}$ and it yields 30 km for the array configuration used in MATLAB. Therefore, it can be concluded that for fixed time and angle values, the pattern reaches its peak value every 30 km for this configuration.

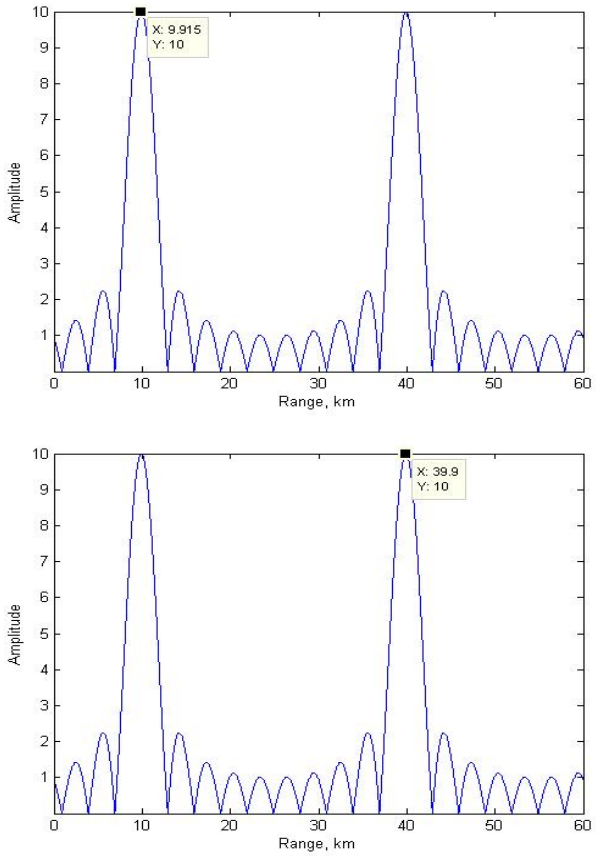

Figure 30. Range-dependent Array Pattern when the Time t and Angle θ are Fixed.

Lastly, the angle-dependent array pattern is plotted in MATLAB for a fixed value of time $t = 233\ \mu\text{sec}$ and range $R_0 = 10$ km. The resulting plots are given in Figure 31.

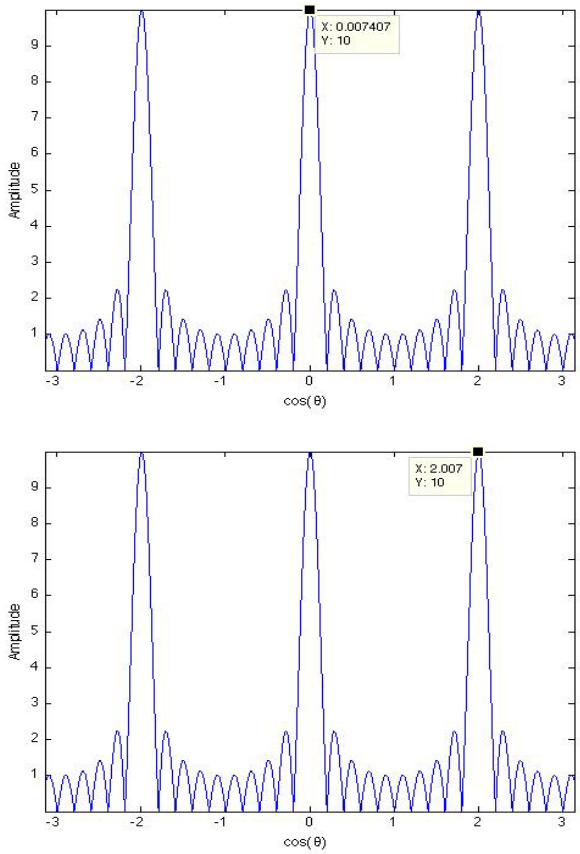

Figure 31. Angle-dependent Array Pattern when the Range R_0 and Time t are Fixed

Based on Figure 31, the period of the angle-dependent pattern turns out to be two. In Equation (100) it was found to be $\frac{\lambda}{d}$ radians, which is exactly the same value where $d = \frac{\lambda}{2}$. The locations of the peaks (excluding those at zero radians) correspond to the grating lobes that are not in the visible region of the antenna.

The patterns as a function of time, angle and range modulation have the same functional shape as shown in Figures 29, 30 and 31. Taking all these figures into consideration, it can be concluded that for an array with uniform distribution in amplitude and phase, all parameters have the same type of modulation by setting the other parameters constant.

B. SIMULATION OF A FREQUENCY DIVERSE ARRAY

1. Simulation of a FDA

In Section A of this chapter, the theory of a frequency diverse array was presented. Next, the simulation of a general FDA with isotropic radiators and a FDA above a perfectly conducting plane, where half-wave dipoles are used, is presented.

Consider a linear array of ten elements along the *z*-axis. The array coordinate system is the same as defined in Figure 26. The interelement spacing is $d = \frac{\lambda}{2}$ and the frequency increment $\Delta f = +10$ kHz. To simulate this array configuration and plot the resulting radiation pattern, MATLAB is used. In these patterns the free space attenuation due to the range, in other words $\frac{1}{R_0}$, is suppressed to clearly see the pattern's local maxima. A binomial distribution is used to excite the array elements at the lowest possible sidelobe levels. At a fixed time of $t = 200$ μsec, the resulting pattern is given in Figure 32. In this plot, only the $x > 0$ half-space is shown.

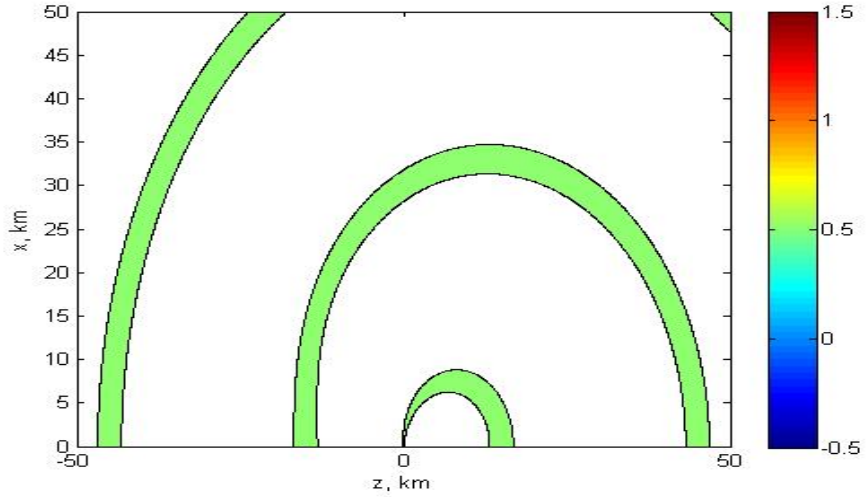

Figure 32. Normalized Radiation Pattern of the FDA for Time Instance $t = 200$ μsec

As seen from Figure 32, the radiation pattern of the FDA reaches its maxima at all angles but different ranges [8]. This is what was expected according to Equation (92), where it was concluded that for a fixed time parameter there would be an infinite number of solutions for the other pair of parameters; in this case the range and the angle pair (R_0, θ_0). Next, the same pattern is plotted at the time instances of $t = 225\ \mu\text{sec}$ and $t = 250\ \mu\text{sec}$. The resulting patterns are depicted in Figures 33 and 34, respectively.

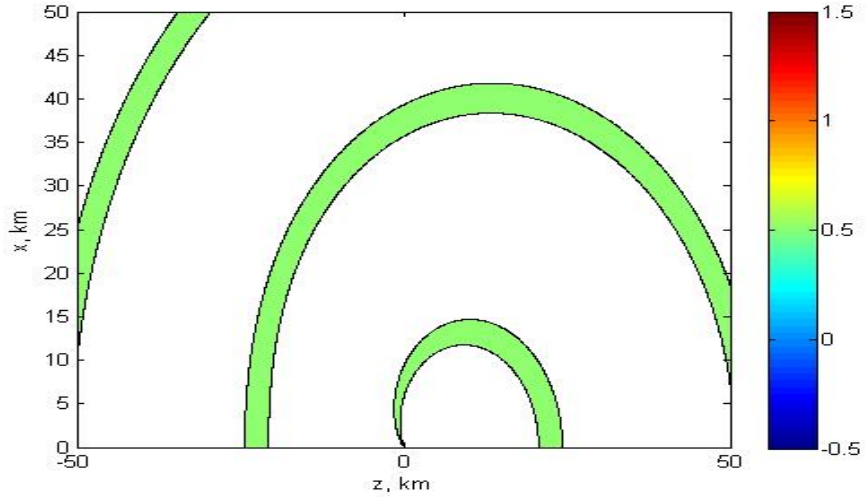

Figure 33. Normalized Radiation Pattern of the FDA for Time Instance $t = 225\ \mu\text{sec}$

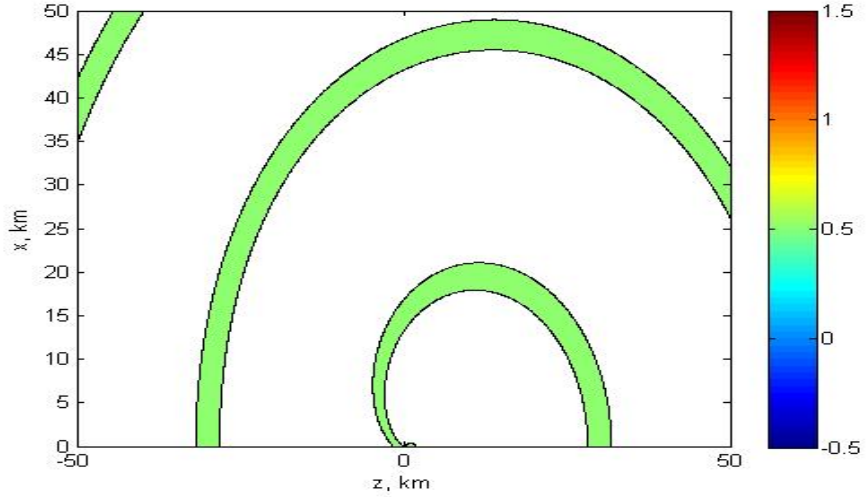

Figure 34. Normalized Radiation Pattern of the FDA for Time Instance $t = 250\ \mu\text{sec}$

Figures 32, 33 and 34 show that for a frequency increment, the time varying radiation pattern rotates in angle in the counterclockwise direction. If frequency decrement is applied instead of frequency increment, the pattern rotates in angle in a clockwise fashion. Figures 35 and 36 reveal the clockwise rotation of the radiation pattern where the time instances of $t = 200\ \mu\text{sec}$ and $t = 250\ \mu\text{sec}$ are used.

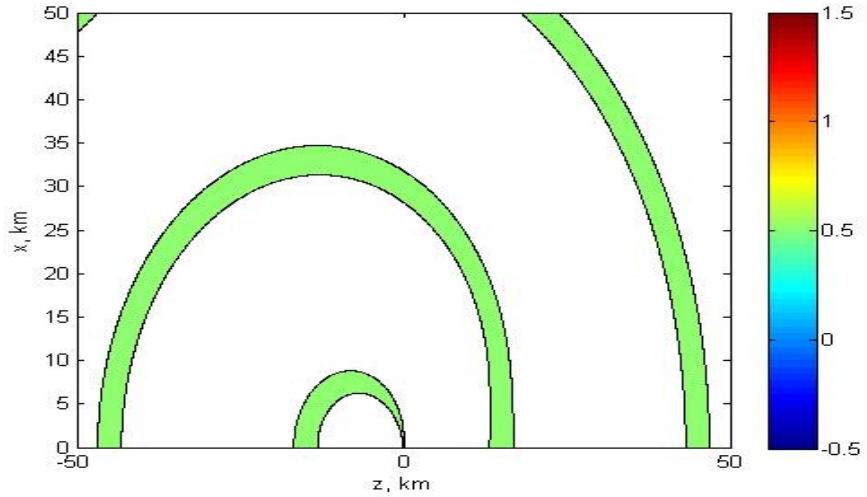

Figure 35. Normalized Radiation Pattern of the FDA for Time Instance $t = 200\ \mu\text{sec}$

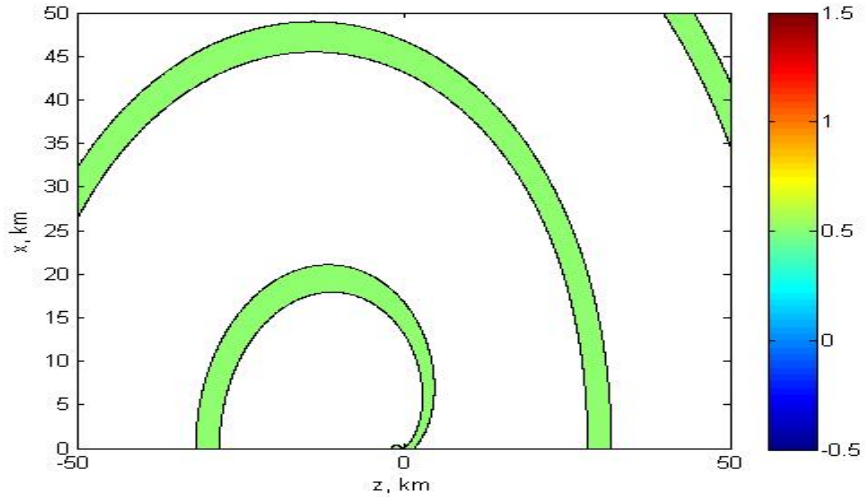

Figure 36. Normalized Radiation Pattern of the FDA for Time Instance $t = 250\ \mu\text{sec}$

Similarly, for a fixed range of $R_0 = 30$ km at $t = 200$ μsec and $t = 225$ μsec the normalized radiation pattern can be plotted on a polar plot to see the angle scanning of the array. It should be noted that the free space attenuation factor $\frac{1}{R_0}$ is again suppressed for these plots. The resulting polar plots are shown in Figures 37 and 38.

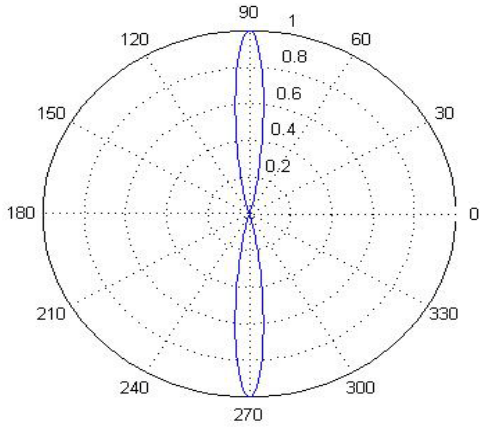

Figure 37. Polar Plot of the Normalized Radiation Pattern at Range $R_0 = 30$ km and $t = 200$ μsec for Angle θ where $\phi = 0^\circ$

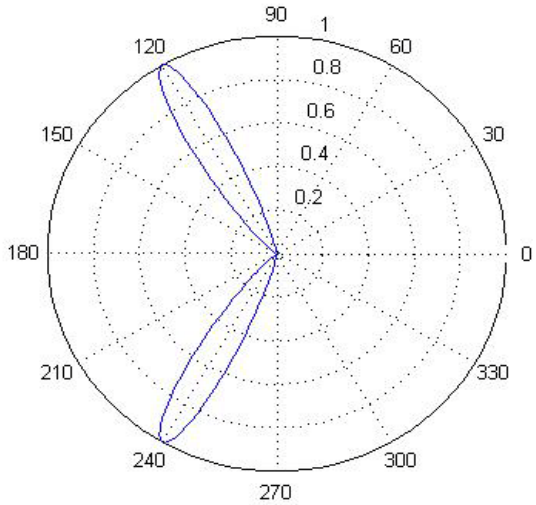

Figure 38. Polar Plot of the Normalized Radiation Pattern at Range $R_0 = 30$ km and $t = 225$ μsec for Angle θ where $\phi = 0^\circ$

It is clearly seen from Figures 37 and 38 that the time varying pattern scans all angles in a counterclockwise fashion for frequency increment as expected. For a frequency decrement, the pattern scans all angles in a clockwise direction as seen in Figures 39 and 40.

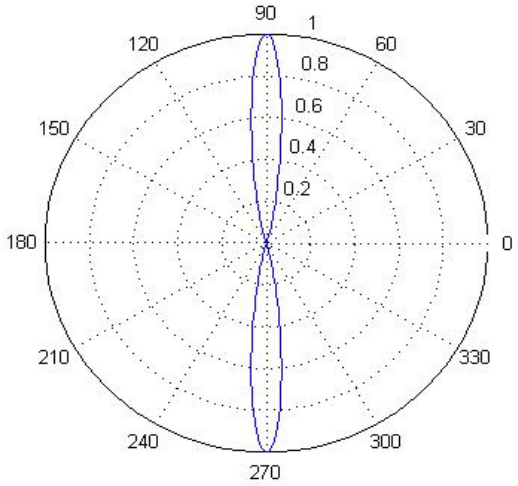

Figure 39. Polar Plot of the Normalized Radiation Pattern at Range $R_0 = 30$ km and $t = 200$ μsec for Frequency Decrement where $\phi = 0^\circ$

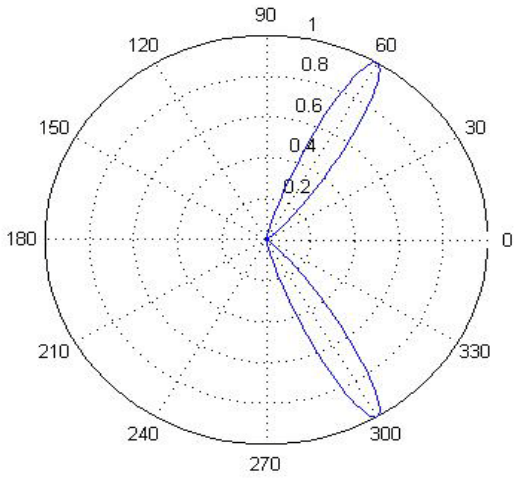

Figure 40. Polar Plot of the Normalized Radiation Pattern at Range $R_0 = 30$ km and $t = 225$ μsec for Frequency Decrement where $\phi = 0^\circ$

The time varying patterns plotted for this simulation repeat every $\frac{1}{\Delta f}$ seconds due to the periodicity of the pattern. In [8], the angular velocity of the pattern is defined as

$$\frac{d\theta}{dt} = \frac{\Delta f}{\left(\frac{d}{\lambda}\right)\sin\theta} \tag{101}$$

and 180 degrees is swept at a time interval of

$$\Delta t = \frac{2d}{\lambda \Delta f} \tag{102}$$

2. Simulation of FDA Above a Ground Plane

In the final section of this chapter, the frequency diverse array of *y* directed dipoles above a perfectly conducting plane is examined. As mentioned previously, an array above a ground plane of infinite extent can be approximated with use of image theory. Even though in reality an infinite, perfectly conducting ground plane does not exist, the use of image theory still provides a useful means of determining the radiated field from an array above a ground plane of finite extent. In this simulation frequency, the diverse array is placed at a height of $h = 0.25\lambda$ and the half-wave dipole Equations (35) and (36) are used where the current flows in the *y*-axis. The observation point is assumed to be in the *x*-*z* plane (i.e., $\phi = 0^\circ$ in Equation (31)). The resulting pattern is computed according to the principle of pattern multiplication as given in Equation (34). Three different excitations in Table 1 and a binomial distribution are used in the simulation. First, uniform excitation is applied to ten array elements and the pattern is plotted for the time snapshots of $t = 225\ \mu\text{sec}$ and $t = 250\ \mu\text{sec}$. Figure 41 and 42 show two time snapshots obtained from MATLAB for uniform excitation.

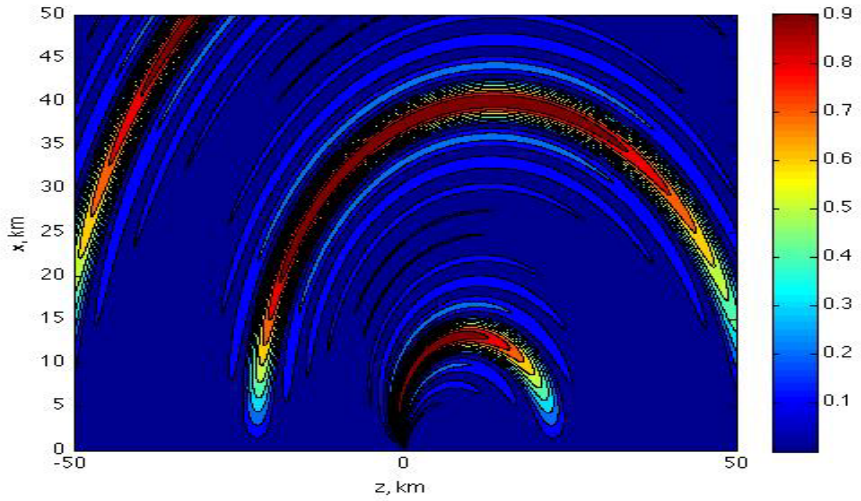

Figure 41. Radiation Pattern of a Linearly Excited FDA Above a Ground Plane $(t = 225\ \mu\text{sec})$

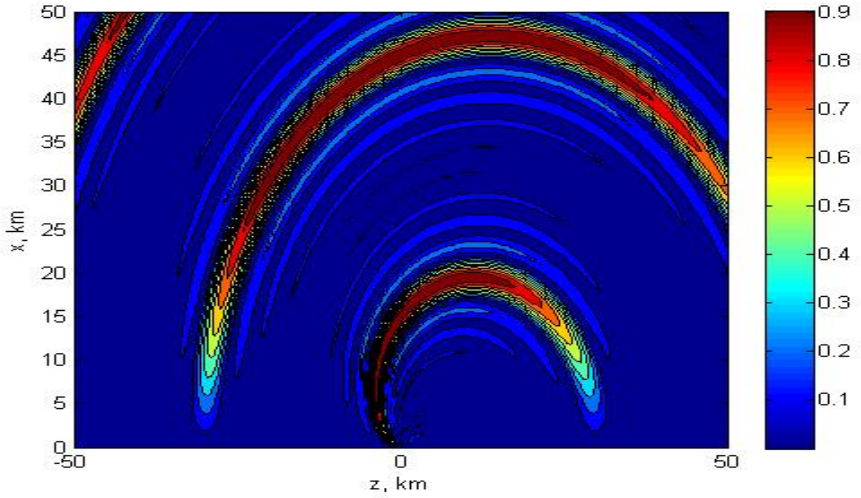

Figure 42. Radiation Pattern of a Linearly Excited FDA Above a Ground Plane $(t = 250\ \mu\text{sec})$

The pattern still exhibits the same characteristics and rotates in the counterclockwise direction. However, the tangential electric field is zero at the ground plane, thus eliminating the beams at the end fire of the array. It is also seen that due to linear excitation, the sidelobe levels are high. This might be problematic for radar and cause false alarms due to the high sidelobe level.

Secondly, a cosine amplitude tapering is applied to the array. This excitation gives rise to the following plots in Figure 43 and 44.

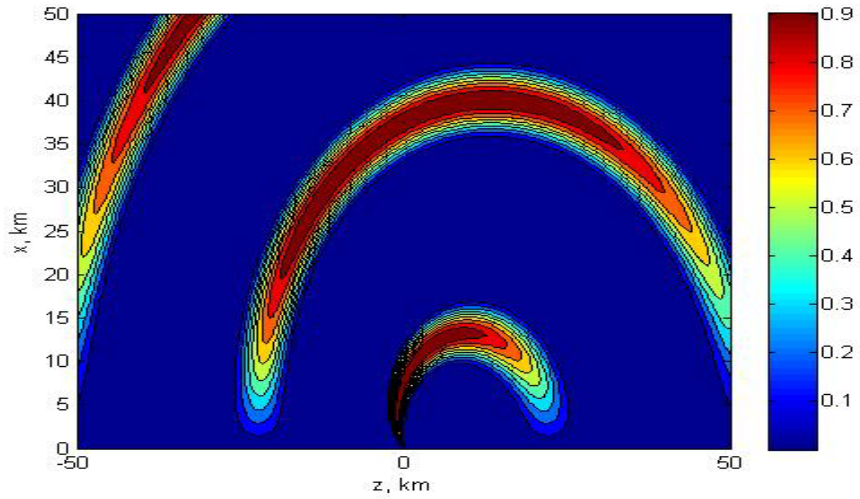

Figure 43. Radiation Pattern of a Cosine Tapered FDA Above a Ground Plane $(t = 225\ \mu\text{sec})$

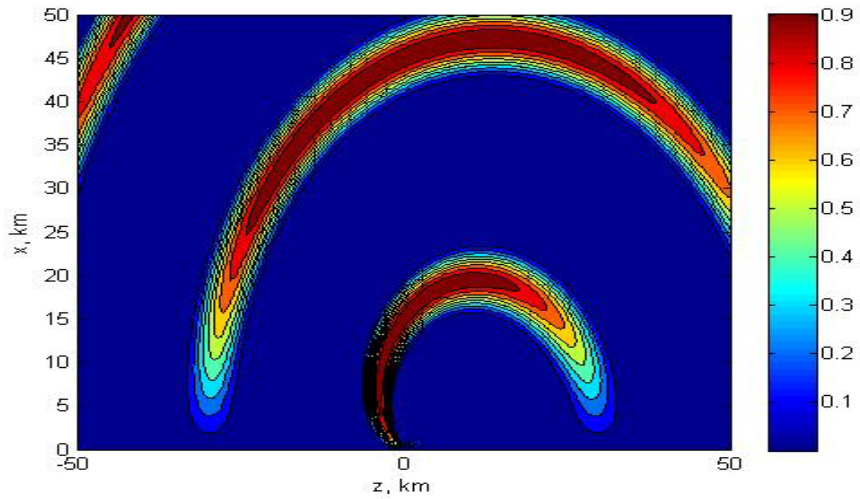

Figure 44. Radiation Pattern of a Cosine Tapered FDA Above a Ground Plane $(t = 250\ \mu\text{sec})$

It is clearly seen that the sidelobes represented by the spirals around the main lobe spirals vanished and are at a level close to zero, which can be read from the colored bar. However, as expected the main beam is broadened and covers wider range than in

Figures 41 and 42. Again, due to the ground plane and destructive interference, the power of the main beam is decreased considerably close to angles $\pm 90^{\circ}$.

Next, a cosine-squared-on-a-pedestal excitation $\left(A(z) = 0.33 + 0.66\cos^2(\pi z / 2)\right)$ and binomial excitation, which is an extreme case where no sidelobes are generated, are used in the simulation. The resulting patterns for the cosine-squared taper are plotted against the range in the *xz*-plane in Figures 45 and 46.

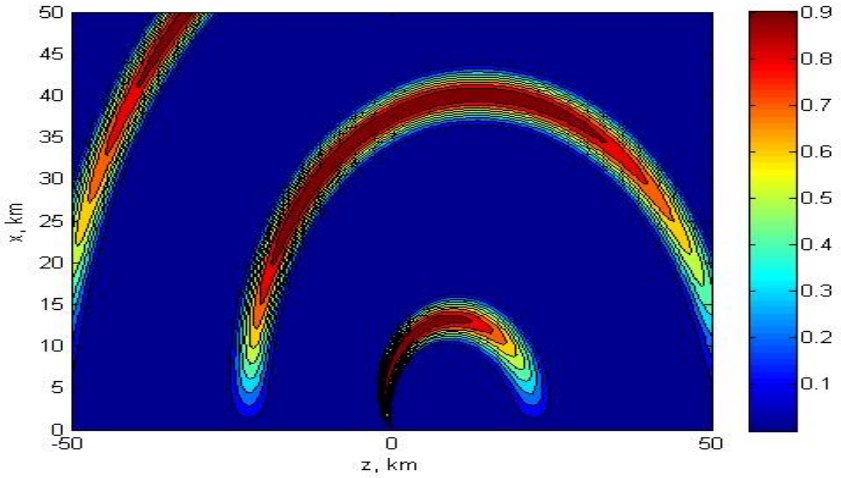

Figure 45. Radiation Pattern of the FDA Above a Ground Plane Excited with a Cosine-squared-on-a-pedestal Excitation $\left(t = 225\ \mu\text{sec}\right)$

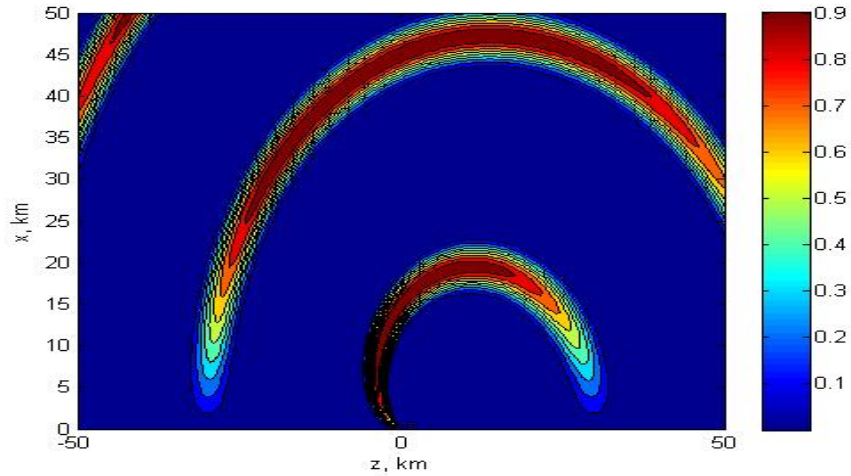

Figure 46. Radiation Pattern of the FDA Above a Ground Plane Excited with a Cosine-squared-on-a-pedestal Excitation $\left(t = 250\ \mu\text{sec}\right)$

Figures 47 and 48 show that when a binomial distribution is used for excitation of the elements, the main beam has the broadest width compared to the previous cases. However, the sidelobe level is zero. This is the tradeoff between ultra-low sidelobe level and the width of the main beam as seen from the figures. In these simulations, the number of elements used was ten $(N=10)$.

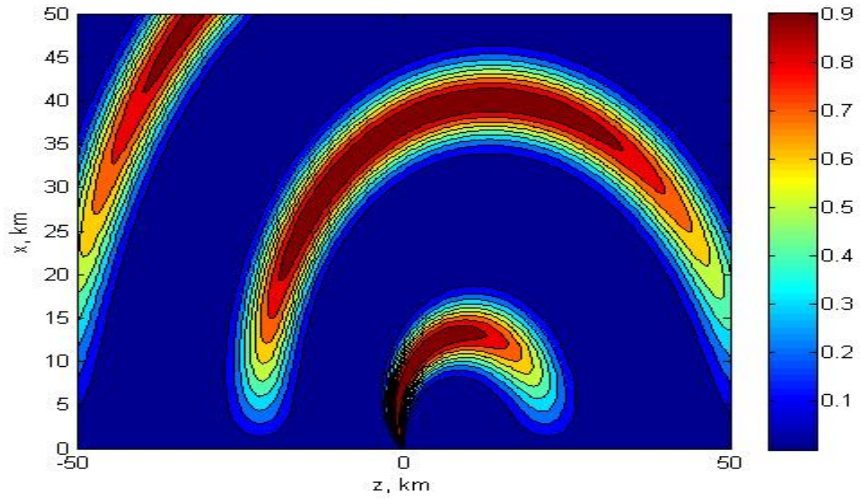

Figure 47. Radiation Pattern of the FDA Above a Ground Plane Excited with Binomial Excitation $(t=225\ \mu\text{sec})$

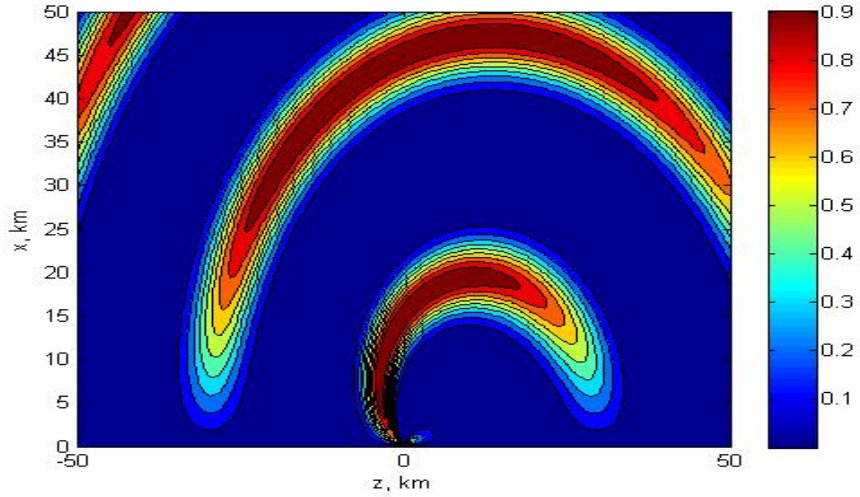

Figure 48. Radiation Pattern of the FDA Above a Ground Plane Excited with Binomial Excitation $(t=250\ \mu\text{sec})$

If one increases the number of the elements, then the width and the range coverage of the main beam can be decreased. Figure 49 shows the reduction in width of the main beam when the number of the elements is increased to fifty $(N = 50)$ with a cosine amplitude excitation at time $t = 250\ \mu\text{sec}$. The result can be verified by a comparison with Figure 44.

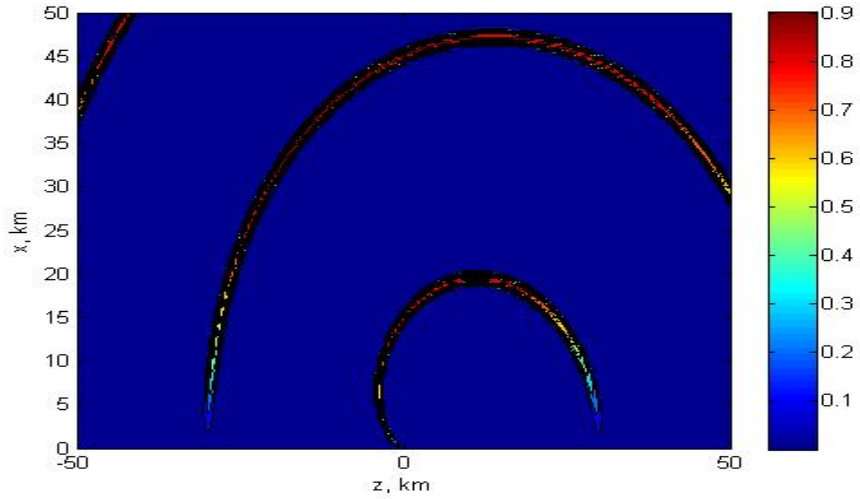

Figure 49. Radiation Pattern of a Cosine Tapered FDA Above a Ground Plane $(t = 250\ \mu\text{sec}, N = 50)$

In this chapter, the mathematical foundations of a frequency diverse array were established and the theory was presented. MATLAB simulations used to support the theory of FDAs showed that interelement frequency increment generates a range, time- and angle- dependent pattern. Since this pattern scans all angles, it can be considered as a novel electronic scanning method. Moreover, this pattern has its maxima at different ranges, which can lead to simultaneous, multiple target detection if the circuitry and right digital signal processing techniques are used. In addition to this, FDAs do not use phase shifters, which is a great advantage compared to conventional arrays, and they provide a way to reduce the cost of radar. In the next chapter, the system design aspects of FDAs such as SNR will be addressed briefly.

V. TIME DOMAIN RADAR PERFORMACE PREDICTION

A. INTRODUCTION

Signal detection on the basis of narrowband signals is commonly used in conventional radars. This method of performance analysis only works as long as frequency domain assumptions hold [18]. However, in Chapters III and IV, we took a time domain approach. The assumptions for frequency domain analysis may no longer hold and the performance of the radar in terms of time domain quantities needs to be reconsidered.

In signal processing terms, a function of time is a representation of a signal with perfect time resolution, but no frequency information, while the Fourier transform has perfect frequency resolution, but no time information. The magnitude of the Fourier transform at a point is how much frequency content there is, but location is only given by phase, and standing waves are not localized in time—a sine wave continues out to infinity, without decaying. This limits the usefulness of the Fourier transform for analyzing signals that are localized in time, notably transients, or any signal of finite extent.

Now, consider a rectangular pulse waveform, which has an infinite bandwidth and produces a transient due to its rise and fall time. Any sudden change in a signal is regarded as a transient, and transients in an input signal disturb the steady-state operation of a filter, resulting in a transient response at the filter output. Mathematically, a signal is said to contain a transient whenever its Fourier expansion requires an infinite number of sinusoids. Conversely, any signal expressible as a finite number of sinusoids can be defined as a steady-state signal. Thus, waveform discontinuities are transients, as are discontinuities in the waveform slope, curvature, etc. Any fixed sum of sinusoids, on the other hand, is a steady-state signal [19].

Fourier decomposing a transient signal and then trying to reconstruct it without knowing the exact phase relation will not work due to the global nature of the Fourier

transform. The point is that Fourier decomposition of a pulse is a steady-state description of a transient state and does not adequately address causality conditions. The problem arises in the use of global methods for description of local events and when there is a requirement to either transmit or receive instantaneous frequencies and phases [18]. Therefore, in order to get the instantaneous frequency content of a signal, one can use short-time Fourier transform or wavelets. This problem also can be addressed with the use of Cauchy Problem which is a system of partial differential equations of order *m* from the prescribed values of the solution and of its derivates of order less than *m* on a given surface [18]. Since this concept is mathematically tedious, it will not be discussed in this thesis.

A stationary signal has the same statistical characteristics by the shift in the time origin. In other words, it has fixed mean and the autocorrelation function is a function of time lag. A non-stationary signal does not satisfy the rules defined for the stationary signal, and it has different statistical characteristics for the different time lags. In time domain signal processing, it is extremely important to know the precise return time of the signal at the receiver. Since the Fourier transform is defined from negative infinity to positive infinity, the frequency spectrum of the signal will not show the instantaneous frequency contents and the local information about the target's point scatterers will be obscured and not be resolved.

B. FREQUENCY DOMAIN AND TIME DOMAIN RECEIVER PROCESSOR DESIGN

From statistical signal processing, it is accepted that one usually deals with random signals which are random processes. Signal processing techniques one uses for deterministic signals such as sinusoids do not hold. When the target is at an unknown distance, the temporal location of the echo pulse is not predictable [18]. If one takes the autocorrelation of a random signal, then valuable information can be extracted. It is well known that the Fourier transform of an autocorrelation function gives the power spectral density of the signal, which also shows the frequency content of the signal.

In [18], it is stated that Fourier transform cannot be applied directly on the threshold–detected returned signal due the fact that in the absence of prior knowledge regarding the target, the Fourier transformation will not converge. However if time domain signal is sampled, what basically happens in autocorrelation, and then another type of convergence can be achieved. This condition dictates the use of autocorrelation function for the detection of time domain signals. After acquisition of the signal by autocorrelation methods, applying the Fourier transform gives the power spectral density of the signal. Autocorrelation function and power spectral density together describe the signal.

In the following sections, a brief comparison of time domain and frequency domain radar processing is given.

1. Frequency Domain Receiver

In the frequency domain, the presence of a target is detected by threshold amplitude detection. When the amplitude of the returned signal exceeds the predefined threshold value, it is declared as a target on the radar scope. Radar designer needs to optimize the threshold for the desired probabilities of false alarm and detection. Defining a too low threshold may increase the number of the false alarms where the noise can exceed the given threshold value. On the other hand, defining a too high threshold may miss targets when they are present. This concept is depicted in Figure 50.

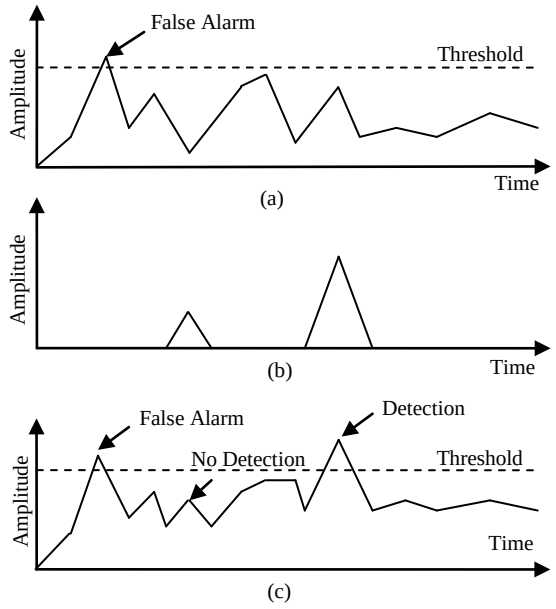

Figure 50. Illustration of the Detection Process and the Effect of the Detection Threshold (a) Noise (b) Target Signals (c) Signal Plus Noise

From the viewpoint of detecting frequency domain signals in noise, preserving the shape of the signal is of no importance, however for time domain signals in noise, it is extremely important. Threshold detection is a local time event. However, autocorrelation places a local time event in a global time context. It is this characteristic of the autocorrelation that preserves the shape of the signal [18].

In a frequency domain receiver, the received signal is first amplified with a low noise amplifier (LNA) and then down converted to the intermediate frequency or baseband by a mixer. The output of the mixer is processed to produce in-phase and quadrature baseband signals. A block diagram of a frequency domain receiver is illustrated in Figure 51.

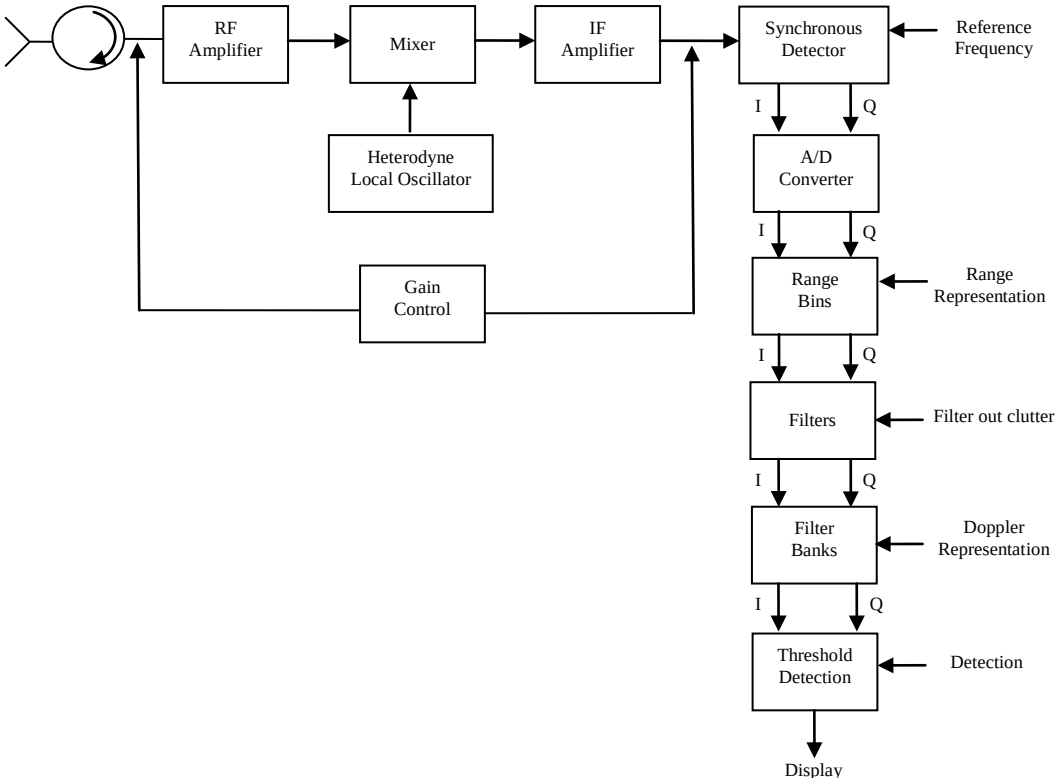

Figure 51. Frequency Domain Receiver Block Diagram (After [18])

2. Time Domain Receiver

Time domain receiver can detect and characterize a target much better than a frequency domain receiver. However, the right receiver processor design is required. In a time domain receiver the target can be detected when the power spectral line corresponding to the target exceeds noise or clutter level by a given amount. This process is analogous to the threshold detection in frequency domain; but in time domain power spectral density is used. For this reason, in time domain analysis power spectral density computation is a must.

Time domain receiver is not only capable of detecting, but also characterizing the target. In order to characterize a target, one needs to use further signal processing to recognize the target. The only difference between time domain detection and frequency detection is that time domain detection depends on the power spectral density, whereas frequency domain detection depends on the signal envelope. In time domain detection,

autocorrelation is a key, as power spectral density can be computed from autocorrelation. Figure 52 shows the block diagram of a time domain receiver where the time signal first correlated with homodyne autocorrelator. After the autocorrelation process, the Fourier transform is applied and power spectral density is computed.

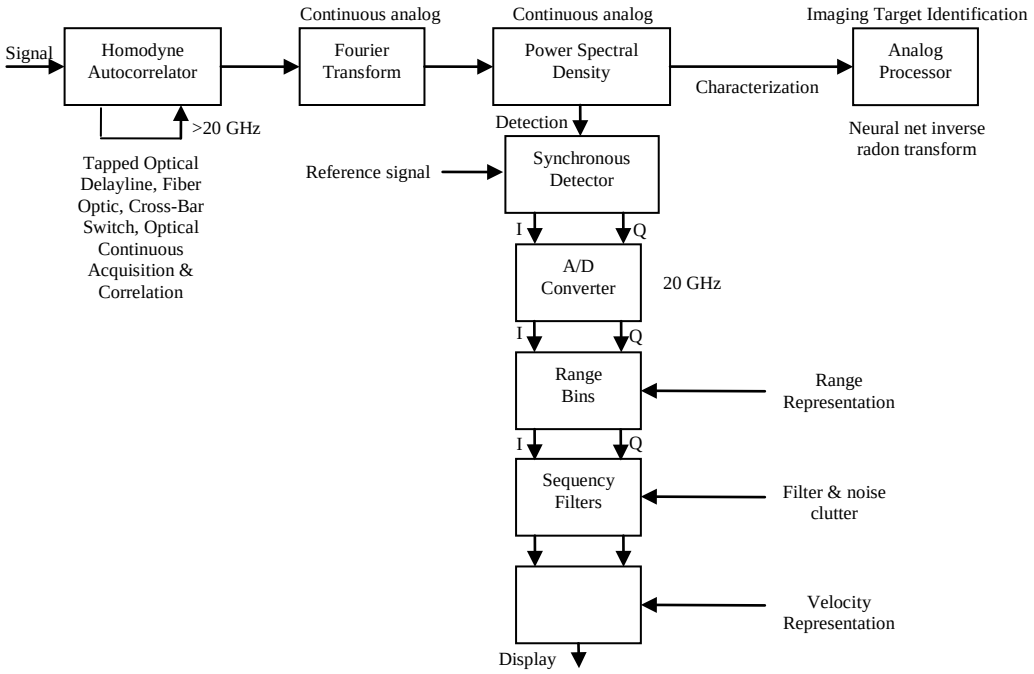

Figure 52. Time Domain Receiver Block Diagram (After [18])

In the frequency domain radar range equation, transmitted energy, transmitter gain, effective aperture of the antenna, and the receiver sensitivity in terms of SNR play an important role. These parameters are equally important in the time domain. However, time domain signals carry much more information than frequency domain signals and due to the need to process time domain signals an additional receiver gain parameter must be added to the time domain radar range equation.

Autocorrelation can be applied to periodic and aperiodic signals; however, this is not necessary to determine the power and energy spectrum densities. On the other hand, autocorrelation is the only means to calculate the power spectral density of a random signal. Frequency domain signals can be detected by envelope detection threshold

methods, whereas time domain signals can only be detected by power spectral density threshold methods if the characterization information of the target is to be preserved.

Cross-correlation methods can also be used for detection purposes because they preserve the signal phase information, as well as the timing information. Autocorrelation does not preserve the phasing information. Therefore, cross-correlation might be useful in cases where the phase information is critical. Whether autocorrelation or cross-correlation is used, time domain signals can provide more information than a frequency domain signal.

3. Time Domain Receiver Gain

In time domain signal processing, target can be considered as an information source and the receiver as an information processor. Therefore, the channel between the target and the receiver is an information channel. The amount of information the channel carries depends on the duration of the signal. Two signals of identical bandwidth but different in duration will carry different amounts of information. If these are two signals that have the same bandwidth, but one is shorter than the other one in duration, the amount of the information carried by the signal of shorter duration will be more than that of longer duration. The short signals do not interfere with the resolved target individual scatterers and the contribution from each scatterer can be separated in time. On the other hand, if a long duration signal is used, the components form elementary scatterers will overlap and cannot be resolved in time.

The more information about the target that is transmitted to the receiver the more signal-to-noise (SNR) gain, if that information can be accessed and displayed in the power spectral density [18]. One can access that information by using receiver-processor gain, which is also known as time scale conversion. The receiver processor gain is defined in [18] as

$$\upsilon = \frac{p}{p_{\min}} = \frac{\Delta t_c}{\Delta t} = \frac{\left(S_o / N_o\right)_{out}}{\left(S_o / N_o\right)_{in}} \tag{103}$$

where p is the time scale conversion factor, Δt is the duration of the signal, Δt_c is the receiver-processor initial sampling rate. We can see that when the processing gain υ is greater than 1, there is an increase in SNR.

C. TIME DOMAIN RADAR RANGE EQUATION

The simplest form of the radar range equation was given in Chapter I with Equations (9) and (10). This is the frequency domain form of the radar range equation. Often it is more convenient to deal with frequency diverse arrays in the time domain. Thus, we need to derive a new radar range equation in the time domain. The following paragraphs develop the time domain radar range equation as explained in [18].

Consider a target at a distance R from source that transmits a power of P_t watts with gain of G_t. The received power from a target with radar cross section (RCS) σ at range R is

$$\text{Power received} = \left(\frac{P_t G_t}{4\pi R^2}\right)\left(\frac{\sigma}{4\pi R^2}\right) A_e = \left(\frac{P_t G_t G_r \lambda^2 \sigma}{(4\pi)^3 R^4}\right) \text{W} \tag{104}$$

which, at this point, is the same as the frequency domain version of Equation (9).

The thermal noise at a receiver with $T_0 = 290^\circ$ K is

$$N = k_B T B \tag{105}$$

where k_B is the Stefan Boltzman's constant and B is the bandwidth of the receiver. At the same temperature, the system noise figure is

$$F_n = \frac{(N_o / N_i)}{(S_o / S_i)} = \frac{SNR_i}{SNR_o} \tag{106}$$

where "i" denote the input and "o" denote the output. If we use L for all signal loses, then SNR before processing can be written using Equations (104), (105) and (106) as

$$\frac{S_o}{N_o} = \frac{P_t G_t G_r \lambda^2 \sigma}{(4\pi)^3 R^4 L F_n k_B T_0 B} \tag{107}$$

The maximum detection range is then

$$R_{\max} = \left(\frac{P_t G_t G_r \lambda^2 \sigma}{(4\pi)^3 (S_o / N_o)_{\min} L F_n k_B T_0 B} \right)^{1/4} \tag{108}$$

If the effective aperture of the antenna is used, Equation (108) gives

$$R_{\max} = \left(\frac{P_t G_t A_e \sigma}{(4\pi)^2 (S_o / N_o)_{\min} L F_n k_B T_0 B} \right)^{1/4} \tag{109}$$

The maximum range can be defined in terms of energy by simple adding the signal duration τ to Equation (109).

$$R_{\max} = \left(\frac{P_t \tau G_t A_e \sigma}{(4\pi)^2 (S_o / N_o)_{\min} L F_n k_B T_0 B} \right)^{1/4} \tag{110}$$

Equation (109) is the radar range equation in the frequency domain and what is commonly seen in textbooks. In frequency domain equation, the maximum range depends on the total transmitted energy, transmitter gain, and effective aperture of the antenna and receiver noise figure. But, it does not depend on the receiver gain.

In the time domain radar range equation, the receiver gain has to be considered. If the signal is summed coherently and the noise incoherently, then SNR of the summed signal can be written as

$$\beta = \frac{P_{signal}}{P_{noise}} \tag{111}$$

and $\beta_{\min}$ is the SNR of the sampling window:

$$\beta_{\min} = \left(\frac{P_{signal}}{P_{noise}} \right)_{\min} \tag{112}$$

Then the processing gain can be written as

$$\upsilon = \frac{\beta}{\beta_{\min}} \tag{113}$$

Substituting the receiver processor gain equation into Equation (110) gives the time domain radar range equation as

$$R_{\max} = \left(\frac{E_t G_t A_e \sigma \upsilon}{(4\pi)^2 (S_o / N_o)_{\min} L F_n k_B T_0 B} \right)^{1/4} \tag{114}$$

where $E_t = P_t \tau$ is the total transmitted energy.

Equation (114) shows that when the receiver gain is equal to 1 (i.e., $\upsilon = 1$), we get the radar range equation in the frequency domain. Even though this range equation seems to be similar to frequency domain range equation, in reality they are quite different. As explained in [18] to count for the characteristics of the target, the constraint

$$\frac{K}{\upsilon} = 1 \tag{115}$$

must be met, where *K* is the ratio of the target's maximum length $(\alpha_{\max})$ to the target's minimum length $(\alpha_{\min})$:

$$K = \frac{\alpha_{\max}}{\alpha_{\min}} \tag{116}$$

Equation (115) shows that when $K = 1$, then , $\upsilon = 1$ which means no processing gain is achieved. However, when $K = 2$, the constraint given in Equation (115) forces the processing gain to be 2. Due to the increase in processing gain, greater target resolution and greater range can be achieved either by a decrease in the sampling by a half or by decreasing the duration of the signal by a half. Thus, the processing gain can be written as a function of

$$\upsilon = \frac{\tau}{\tau_s} \tag{117}$$

where τ is the pulse duration and τ_s is the sampling window duration. Substituting Equations (116) and (117) into Equation (115) gives

$$\frac{K}{\upsilon} = \left(\frac{\alpha_{\max}}{\alpha_{\min}}\right)\left(\frac{\tau_s}{\tau}\right) \tag{118}$$

Equation (114) is simulated in MATLAB for increasing energy up to 100 Joules. The maximum ranges obtained from this equation are plotted against the energy of the signal. In the simulation, the following values were used: $G_t = 47$ dB, $A_e = 1\ \text{m}^2$, $\sigma = 0.1\ \text{m}^2$, $k_B T_0 = 4\text{x}10^{-21}$, $F_n = 3$ dB, $L = 4$ dB, $\left(S_o / N_o\right)_{\min} =$ 13 dB. The results are shown in Figure 53.

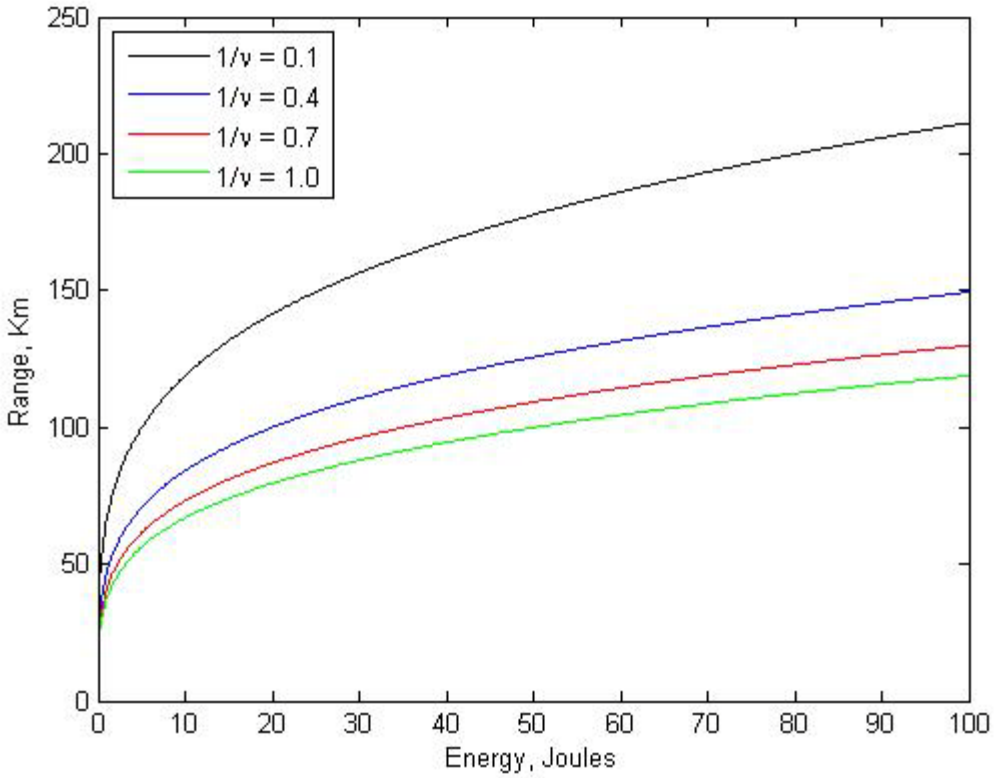

Figure 53. Ranging and Detection for $K > 1$, $G_t = 47$ dB, and $\frac{K}{\upsilon} = 1$

The importance of the processing gain in time domain radar range equation is evident from the curves. As the processing gain, υ, increases the greater maximum range is achieved. In Figure 53, $\frac{1}{\upsilon}=1.0$ corresponds to the frequency domain radar range equation. This figure also illustrates the advantages of time domain signals against frequency domain signals.

In this chapter, the performance of a radar, which employs a time domain signal and the basic principles of receiver design in the time domain, is presented. Since the frequency diverse array radar deals with time domain signals, the performance of the frequency diverse array radar should be considered in the time domain. The key features of time domain detection are: (1) the autocorrelation of the signal in time domain which preserves the shaping of the signal; (2) power spectral density which basically allows us to detect and characterize the target, and (3) the processing gain which increases the maximum range of the radar significantly.

In the next chapter, conclusions about frequency diverse array and the recommendations for the further research will be presented.

VI. CONCLUSIONS AND RECOMMENDATIONS

A. CONCLUSIONS

The focus of this thesis has been on the investigation of frequency diversity among the elements of a linear array which is in literature called frequency diverse array. This new and novel electronic scanning technique has been popular for the last 10 years and several papers were published concerning this promising electronic scanning technique.

First, the concept of frequency diverse array as a time modulated antenna was validated with the MATLAB simulations. It turns out that using a periodic travelling pulse waveform and exciting the antenna elements in an on-off-keying fashion generates simultaneous pencil beams in the desired directions where each beam is tagged with a different frequency. We should also note that the frequency tagging is a function of the modulation frequency, which depends on the period of the travelling pulse waveform. In Chapter III, several amplitude tapering functions were applied to the time modulated frequency diverse array and the results obtained from MATLAB simulation justified the given theoretical values.

Applying a continuous waveform and a small frequency increment compared to the carrier frequency generates a range, time and angle dependent array pattern. The most important feature of the frequency diverse array is that no phase shifters are needed. This unique feature can provide an inexpensive way of accomplishing electronic scanning. It can also be used in SAR and GMTI applications as explained in [7]. The periodic nature of the pattern in range, angle and time was validated with MATLAB simulations. The spiral plot obtained in Chapter IV shows the promising electronic scanning of the frequency diverse array where the main beam reaches its maximum value at all angles but in different ranges. Although this novel electronic scanning method has advantages over conventional arrays, having range dependent pattern may introduce range ambiguity problems.

The use of the frequency diverse arrays in radar applications can be considered in the time domain since time domain signals are used. In the last chapter of this thesis, the performance of the time domain receiver was discussed and radar range equation was presented. We clearly saw that the processing gain plays a key role in the time domain range equation. Therefore, the frequency diverse array receiver antenna can be considered as a time domain antenna and the time domain techniques can be applied.

B. RECOMMENDATIONS FOR FUTURE WORK

This thesis basically provides the theory of the frequency diverse array antenna. Throughout this thesis, theory was supported with MATLAB simulations. Therefore this thesis can be considered as an introductory thesis. Due to time limitations, hardware implementations could not be done. A future effort may focus on the simulation of the frequency diverse array in a computer-aided-design environment such as Microwave Studio, Agilent ADS or Labview. The results obtained from these simulations can be compared with the results provided in this thesis.

Another effort may include the implementation of the frequency diverse array with hardware. The FDA elements may be placed over a perfectly conducting electric ground plane and the results can be compared with the results given in this thesis.

One can also examine the use of frequency diverse array antenna in radar applications and try to derive a specific radar range equation for frequency diverse array radar. A further study may also include the definition of signal-to-noise ratio and examine how to avoid ambiguities due to the multiple maxima that occur in range and angle for FDA.

APPENDIX. MATLAB SOURCE CODES

This appendix lists all MATLAB programs used in this work.

ArrayFactor.m

```
clear all
close all
clc

theta = -180:0.01:180;
lambda = 1;
d = lambda/2;
k = 2*pi/lambda;

N = 6;
a = ones(1,N);

theta0 = pi/9;
gamma = k*d*(sind(theta)- sin(theta0));

sum = 0;
for n = 0:N-1
    AF = a(n+1)* exp(1i*n*gamma);
    sum = sum + AF;
end

AF = abs(sum);
normAF = AF./max(AF);

figure(1)
plot(theta,normAF);
xlim([-2 2])
axis tight
grid on
xlabel('\theta, deg');
ylabel('Magnitude');


%%
AF2 =
sin((pi/lambda).*N.*d.*sind(theta))./(N*sin((pi/lambda).*d.*sind(theta)
));
AF2 = abs(sum);
normAF2 = AF2./max(AF2);

figure(2)
plot(theta/180,normAF2);
```

ApparentAngle.m

```
clear all
close all
clc

f1 = 1e5;
c = 3e8;
d = (c/f1)/2;
df = 350;

R = 0:1e3:5e5;
th = -90:0.1:90;

lR = length(R);
lth = length(th);
N = 10;
th0 = 0;
psi = zeros(lR,lth);

for n = 1:lR
    for m = 1:lth
        psi(n,m) =
(2*pi*f1*d*sind(th(m))/c)+(2*pi*R(n)*df/c)+(2*pi*df*d*sind(th(m))/c)-
(2*pi*f1*d*sind(th0)/c);
    end
end


sum = 0;

for k = 0:N-1
    E = exp(1i*psi*k);
    sum = sum + E;
end

AbsSum = abs(sum);
maxsum = max(max(AbsSum));
normsum = AbsSum/maxsum;
dBsum = 10*log10(normsum);

for n= 1:lR
    for m = 1:lth
        if dBsum(n,m)<-50
            dBsum(n,m) = -50;
        end
    end
end


[U,V] = meshgrid(th,R);

mesh(U,V,dBsum);
```

```
title('\Deltaf = 0 Hz');
xlabel('\theta,deg');
ylabel('Range,m');
zlabel('Relative Power,dB');
```

TDAFourSeries.m

```
clear all
close all
clc

N = 115;     % Number of antenna elements
nmax = 10;   % Number of beams
nvec = -nmax:nmax;

theta = -90:0.1:90;  % scan angle
Nx = length(theta);  % length of the scan angle vector

f_opr = 1e7;         % operating frequency
f_mod = 1e4;         % modulation frequency
T = 1/(f_mod);       % Duration of the signal

c = 3e8;             % speed of light
lambda = c/f_opr;    % wavelength
d= lambda/2;         % Spacing between antenna elements
k = 2*pi/lambda;     % wavenumber
omg_opr = 2*pi*f_opr; % operating frequency in radians
omg_mod = 2*pi*f_mod; % modulation frequency in radians


fs = 2*(f_opr  + max(abs(nvec))*f_mod); % Sampling frequency which ...
%must be at least twice the highest frequency content of the signal...
%(Nyquist rate)
dt = 1/fs;  % time increment
len = T/dt; % length of the signal

if mod(len,N)~=0            % adjustment for the length of the signal
    dur = ceil(len/N);      % in order to have equal data points for
    len = dur * N;          % each antenna element
else
    dur = len/N;
end

tvec = linspace(0,T-dt,len);  % time vector is adjusted according to
the new length defined above


for m = 0:N-1
    rect(m+1,:) = [zeros(1,m*dur) ones(1,dur) zeros(1,len -
((m+1)*dur))];
end
```

```
figure(1)

for m = 0:N-1
    plot(tvec, rect(m+1,:));hold on
end
axis tight
hold off
%% Amplitude Tapering
A = zeros(1,N);% amplitude
n = 2;
for j = 1:N
    s = ((2*j-(N+1))*d/2)/(d*(N-1)/2);
    S(j)=s;
    A(j) = 0.66* cos(pi/2*s)^n;
end
A = A + 0.33;
figure(11)
plot(A);
xlabel('Element Number');
ylabel('Amplitude');
%title ('Cosine Amplitude Tapering, (A(z) = cos^n(\piz/2)) ');
axis tight


%%
for x = 1:Nx
    toplam = 0;
    for m = 0:N-1
        z = A(1,m+1)* rect(m+1,:).*exp(1i.*k.*m.*d.*sind(theta(x)));
        toplam = toplam + z;
        clear z
    end
    h (x,:) = toplam;
    clear toplam
end

%% Fourier Series
clear rect

fourierMat=exp(i*2.0*pi*((nvec.'/T) *tvec));
for x = 1:Nx
    f(:,x) = (1/T) * conj(fourierMat) * h(x,:).'* dt;% Fourier
Coefficients
end

absf = abs(f);
maxf = max(max(f));
normf = absf/maxf;
dBf = 20*log10(normf);

figure(2)
Ny = length(nvec);
```

```
for y = 1:Ny
    plot(theta, dBf(y,:));hold on
end
axis([-90 90 -60 0]);
hold off
ylabel('Relative Power, dB');
xlabel('\theta, deg');


%%
clear h
clear fourierMat
clear tvec
clear dBf
clear A

deltaf = 0.5e3;
T = 1/deltaf;
newtvec = 0:dt:T;


for x = 1:Nx
    toplam = 0;
    for y = 1:Ny
        z = f(y,x)* exp(1i*(omg_opr+nvec(y)*omg_mod).*newtvec);
        toplam = z+toplam;
        clear z
    end
    g(x,:)=toplam;
    clear toplam
end

%%
clear absf N Nx Ny S T c d dt dur f_mod f_opr j k lambda len m maxf ...
    n nmax nvec omg_opr omg_mod s x y
clear f
clear newtvec
clear normf
clear freq


GF = fft(transpose(g));
GF = transpose(GF);
clear g
%%
freq = 0:deltaf:fs;
[U,V] = meshgrid(freq(1,19750:20250),theta);

figure(4)
mesh(U,V, abs(GF(:,19750:20250)));
axis tight

absGF = abs(GF(:,19750:20250));
```

```
maxGF = max(max(absGF));
normGF = absGF./maxGF;
GFdb = 20*log10(normGF);
sizeGF = size(GFdb);
for g = 1:sizeGF(1)
    for h = 1:sizeGF(2)
        if GFdb (g,h) < -50
            GFdb(g,h) = -50;
        end
    end
end

figure(5)
mesh(U,V,GFdb);
xlabel('Frequency, Hz');
ylabel('\theta, deg');
zlabel('Relative Power, dB');
axis tight
```

TDAClosedForm.m

```
clear all
close all
clc

N = 115;
n = -10 : 10;
theta = -90:.01:90;
f_opr = 1e7;
f_mod = 1e4;
c = 3e8;
lambda = c/f_opr;
d= lambda/2;
k = 2*pi/lambda;
omg_opr = 2*pi*f_opr;
omg_mod = 2*pi*f_mod;

deltaf = 2e3;
T = 1/deltaf;

Fmax = 2*(f_opr  + max(abs(n))*f_mod);
dt = 1/Fmax;
tvec = 0:dt:T;


Ny=length(n);
for y= 1:Ny
    a = pi* (sind(theta)-(2*n(y)/N));
    f(y,:) = ((-1)^n(y))* sinc(n(y)/N)* exp(1i*(N-
1/2)*pi*sind(theta)).* diric(a,N)*N;
end
```

```
absf=abs(f);
fmax=max(max(absf));
fdb=20*log10(absf/fmax);
for y=1:Ny
    plot (theta,fdb(y,:));
    if y==1, hold on; end
end
xlabel('\theta, deg')
ylabel('dB')
axis([-90,90,-60,0])
title('Closed Form')

%% Complex Pattern
close all
clear f
clear a
clear absf
clear fdb

theta = -90:0.1:90;
Nx=length(theta);
Ny=length(n);


for x = 1:Nx
    toplam = 0;
    for y = 1:Ny
        a = pi* (sind(theta(x))-(2*n(y)/N));
        f = ((-1)^n(y))* sinc(n(y)/N)* exp(1i*(N-
1/2)*pi*sind(theta(x))).* diric(a,N)*N;
        h = f * exp(1i*(omg_opr+n(y)*omg_mod).*tvec);
        toplam = h+toplam;
        clear h
    end
    g(x,:)=toplam;
    clear toplam
end


GF = fft(transpose(g));
clear g
GF = transpose(GF);
freq = 0:deltaf:Fmax;

figure(2)
plot(freq(4950:5050),abs(GF(:,4950:5050)));
axis tight
%%
clear tvec

[U,V] = meshgrid(freq(4950:5050),theta);
figure(3)
mesh(U,V,abs(GF(:,4950:5050)));
xlabel('Frequency, Hz');
```

```
ylabel('\theta, deg');
zlabel('Amplitude');
axis tight

absGF = abs(GF(:,4950:5050));
maxGF = max(max(absGF));
normGF = absGF./maxGF;
GFdb = 20*log10(normGF);
sizeGF = size(GFdb);

for g = 1:sizeGF(1)
    for h = 1:sizeGF(2)
        if GFdb (g,h) < -50
            GFdb(g,h) = -50;
        end
    end
end

figure(4)
mesh(U,V,GFdb);
xlabel('Frequency, Hz');
ylabel('\theta, deg');
zlabel('Relative Power, dB');
axis tight
```

FDA1.m

```
clear all
clc
close all

%-------------------------------------------------------------------------%
% ------------- Time(t) and Scan Angle (Theta) Fixed -------------- %
%-------------------------------------------------------------------------%

N = 17;                % Number of antenna elements


c = 3e8;              % speed of light
f_opr = 1e7;          % operating frequency
omg_opr = 2*pi*f_opr; % operating frequency in radians
lambda = c/f_opr;     % wavelength
d = lambda/2;         % Spacing between antenna elements
ko = 2*pi/lambda;     % wavenumber
deltaf = 1e4;
deltaw = 2*pi*deltaf;
deltak = deltaw/c;

tvec = 0;
theta = 0;
Ro = 0:1:60000;
```

```
fe = 1;

phi = (deltaw *tvec)+(ko*d*cosd(theta))-(deltak*Ro);
E = fe* abs(cos((omg_opr*tvec)- (ko*Ro))).* abs(diric(phi,N)*N);
plot(Ro./1e3,E);
title('Electric Field vs Range Plot(Time(t) and Scan Angle (\theta_0)
fixed )');
xlabel('Range,km');
ylabel('Amplitude');
axis tight

%% R and theta fixed, time varying
clear tvec
clear theta
clear tvec
clear E

tvec = 0:1e-9:2e-4;
theta = 0;
Ro = 0;
fe = 1;

phi = (deltaw *tvec)+(ko*d*cosd(theta))-(deltak*Ro);
E = fe* abs(cos((omg_opr*tvec)- (ko*Ro))).* abs(diric(phi,N)*N);
figure
plot(tvec./1e-6,E);
title('Electric Field vs Time Plot(Range(R_0) and Scan Angle (\theta_0)
fixed )');
xlabel('Time,\musec');
ylabel('Amplitude');
axis tight
%% R and t fixed, theta varying

clear tvec
clear theta
clear tvec
clear E

tvec = 233e-6;
theta = -180:0.01:180;
%angvec = cosd(theta);
Ro = 15;
fe = 1;

phi = (deltaw *tvec)+(ko*d*cosd(theta))-(deltak*Ro);
E = fe* abs(cos((omg_opr*tvec)- (ko*Ro))).* abs(diric(phi,N)*N);
figure
plot(theta,E);
title('Electric Field vs Scan Angle Plot(Range(R_0) and Time (t) fixed
)');
xlabel('Scan Angle,(\theta)');
ylabel('Amplitude');
axis tight
```

```
figure
polar(theta*pi/180, E)
```

FDAspiral.m

```
clear all
clc
close all

%-------------------------------------------------------------------------%
% ------------- Time(t) and Scan Angle (Theta) Fixed -------------- %
%-------------------------------------------------------------------------%

N = 17;                % Number of antenna elements
c = 3e8;               % speed of light
f_opr = 1e7;           % operating frequency
omg_opr = 2*pi*f_opr; % operating frequency in radians
lambda = c/f_opr;      % wavelength
d = lambda/2;          % Spacing between antenna elements
ko = 2*pi/lambda;      % wavenumber
deltaf = -1e4;
deltaw = 2*pi*deltaf;
deltak = deltaw/c;
% a = ones(1,N);
a = binom(N-1);
tvec = 200e-6;
theta = -180:180;
Ro = 0:0.1:90;
fe = 1;

for n = 1: length(theta)
    phi(n,:) = (deltaw *tvec)+(ko*d*cosd(theta(n)))-(deltak*Ro*1e3);
    sum = 0;
    for m = 0: N-1
        AF = a(m+1)*exp(1i*m*phi(n,:));
        sum = sum + AF;
        clear AF
    end
    E(n,:) = (fe* exp(1i*((omg_opr*tvec)- (ko*Ro*1e3))).* sum);
end

% no plot of figure 1
iplt=0;
if iplt==1
    figure(1)
    absE = abs(E);
    maxE = max(max(absE));
    normE = absE./maxE;
    [U,V] = meshgrid(Ro,theta);
    %mesh(U,V,normE);
    title('Electric Field at a fixed time, t = 233\musec');
    xlabel('Range,km');
    ylabel('Scan Angle, \theta,degrees')
    zlabel('Normalized Amplitude of Electric Field, |E_N_O_R_M|');
```

```
end

% do a rectangular grid ----------------------------------------
z=[-50000:100:50000];   % range steps in km
x=[0:100:50000];
[X,Y]=meshgrid(x,z);
Ngx=length(x);
Ngz=length(z);
msg = ['Computing....'];
hwait=waitbar(0,msg);
% time snapshots from t1 to t2
t1=250e-6;
t2=550e-6;
dt=25e-6;
Nt=floor((t2-t1)/dt)+1;
for it=1:Nt   % time loop
    t=t1+(it-1)*dt;
    disp(['time ',num2str(it),' of ',num2str(Nt)])
    for i=1:Ngx
        waitbar(((it-1)*Ngx+i)/(Nt*Ngx),hwait);
        for n=1:Ngz
            R0=sqrt(x(i)^2+z(n)^2);
            ct=z(n)/(R0+1e-6);     % cos(theta) at grid points
            phi=deltaw*(t-R0/c)+ko*d*ct;
            arg=phi/2;
            SSinc=N;
            if abs(arg)>0.0001, SSinc=sin(N*arg)/sin(arg); end
            E(i,n)=abs(SSinc);
        end
    end
    Emax=max(max(E));
    normE=abs(E/Emax);
    normEdB = 20*log10(normE);
    figure(2)
    contourf(Y/1e3,X/1e3,normE',[.5,.5])
    colorbar
     xlabel('z, km')
    ylabel('x, km')
    Mov(it)=getframe;
end
disp('saving movie')
close(hwait);
movie(Mov,3)   % play the movie 10 times
movie2avi(Mov,'\\comfort\aaytun$\Desktop\ArrayMov3');
%% ---------------------------------------------------------------------
clear E

t1=225e-6;
t2=225e-6;
dt=10e-6;
Nt=floor((t2-t1)/dt)+1;
for it=1:Nt   % time loop
    t=t1+(it-1)*dt;
    theta = 0:0.01:2*pi;
    Ro = 30000;
```

```
    fe = 1;

    for n = 1: length(theta)
        phi = (deltaw *t)+(ko*d*cos(theta(n)))-(deltak*Ro);
        sum = 0;
        for m = 0: N-1
            AF = a(m+1)*exp(1i*m*phi);
            sum = sum + AF;
        end
        E(n,:) = fe* exp(1i*((omg_opr*tvec)- (ko*Ro))).* sum;
    end
    int_emp = 120*pi;
    absE = abs(E);
    S = (1/2)* (absE.^2)./int_emp;
    maxS = max(max(S));
    Fpat = S./maxS;

    figure(4)
    polar(theta,Fpat.')
%         M(it) = getframe;
end
disp('saving movie');
movie(M)
movie2avi(M,'\\comfort\aaytun$\Desktop\ArrayMov2');
```

FDA_GP.m

```
warning off
clear all
clc
close all

N = 10;               % Number of antenna elements
c = 3e8;              % speed of light
f_opr = 1e9;          % operating frequency
omg_opr = 2*pi*f_opr; % operating frequency in radians
lambda = c/f_opr;     % wavelength
d = lambda/2;         % Spacing between antenna elements
ko = 2*pi/lambda;     % wavenumber
deltaf = 1e4;
deltaw = 2*pi*deltaf;
deltak = deltaw/c;
beta = 2*pi/lambda;
h = 0.25*lambda ;
%% Amplitude Tapering
% a = binom(N-1);
% a = ones(1,N);
n = 1;
for j = 1:N
    s = ((2*j-(N+1))*d/2)/(d*(N-1)/2);
    S(j)=s;
    a(j) =  cos(pi/2*s)^n;
```

```
end
%   a = 0.33+a;
figure(1)
plot(a);
xlabel('Element Number');
ylabel('Amplitude');
title ('Amplitude Tapering');
axis tight

%%

fe = 1;
rad = pi/180;


z = -50000:500:50000;
x =  0:500:50000;
y =  0;

[X,Z] = meshgrid(x,z);

Ngz = length(z);
Ngx = length(x);

msg = 'Computing....';
hwait=waitbar(0,msg);
% time snapshots from t1 to t2
t1=250e-6;
t2=450e-6;
dt=25e-6;
Nt=floor((t2-t1)/dt)+1;

for it=1:Nt   % time loop
    t=t1+(it-1)*dt;
    disp(['time ',num2str(it),' of ',num2str(Nt)])
    for p = 1:Ngx
        waitbar(((it-1)*Ngx+p)/(Nt*Ngx),hwait);
        for q = 1: Ngz

            r0 = sqrt(x(p)^2 + y^2)+1e-6;
            R0 = sqrt(x(p)^2 + y^2 + z(q)^2)+1e-6;
            ct = z(q)/R0;
            st = r0/R0;
            cphi = x(p)/r0;
            sphi = y/r0;

            psi = (deltaw *t)+(ko*d*ct)-(deltak*R0);

            sum = 0;
            for m = 0: N-1
                Ssum = a(m+1)*exp(1i*m*psi);
                sum = sum + Ssum;
                clear Ssum
```

```
            end
            AF(p,q) = sum;
            E(p,q) = 2 * 1i * fe * exp(1i*(omg_opr*t - ko*R0))*
sin(ko*h*st)* AF(p,q);
        end
    end

    absE = abs(E);
    maxE = max(max(absE));
    normE = absE./maxE;

    figure (2)
    C=[0.5 0.5];
    contourf(Z'/1e3,X'/1e3,normE);
    colorbar
    xlabel('z, km');
    ylabel('x, km');
    M(it) = getframe;
end
disp('saving movie')
close(hwait);
movie(M,3)
movie2avi(M,'\\comfort\aaytun$\Desktop\GroundPlane');
```

TDRRE.m

```
clear all
close all
clc

GtdB = 47;
Gt = 10^(GtdB/10);
Ae = 1;
sig = 0.1;
kT = 4e-21;
FndB = -3;
Fn = 10^(FndB/10);
LdB = -4;
L = 10^(LdB/10);
SNRmindB = 13;
SNRmin = 10^(SNRmindB/10);
B = 1;
E = 0:.1:100;
invnu = 0.1:0.3:1;
nu = 1./invnu;
colorvec = ['k' 'b' 'r'  'g' ] ;
for n = 1:length(nu)
R(n,:) = (E*Gt*sig*Ae*nu(n))/(((4*pi)^2)*SNRmin*Fn*L*kT*1e3*B);
R(n,:) = R(n,:).^(1/4);
plot(E,R(n,:)/1e3,colorvec(n))
hold on
end
hold off
xlabel('Energy, Joules');
```

```
ylabel('Range, Km');
legend('1/\nu = 0.1','1/\nu = 0.4', '1/\nu = 0.7', '1/\nu = 1.0',...
    'location','northwest');
```

THIS PAGE INTENTIONALLY LEFT BLANK

LIST OF REFERENCES

[1] H. E. Shanks, "A new technique for electronic scanning," *IRE Trans. on Antennas and Propagation*, vol. 9, pp.162-166, March 1961.

[2] M. A. Richards, *Fundamentals of Radar Signal Processing*. New York: McGraw-Hill, 2005, pp. 1–22.

[3] M. I. Skolnik, *Introduction to Radar Systems*, 3rd ed. New York: McGraw-Hill, 2001, pp. 1-16, 540–589.

[4] Radartutorial.eu, "Receivers bandwidth," [Online]. Available: http://www.radartutorial.eu/09.receivers/rx10.en.html, [Accessed: Aug. 21, 2010].

[5] G. Li, S. Yang, Y. Chen, and Z. Nie, "A novel beam scanning technique in time modulated linear arrays," in *Antennas and Propagation Society International Symposium*, 2009, pp. 1–4.

[6] P. Antonik, M. C. Wicks, H. D. Griffiths, and C. J. Baker, "Frequency diverse array radars," in *IEEE Conference on Radar*, 2006.

[7] P. Antonik, M. C. Wicks, H. D. Griffiths, and C. J. Baker, "Multi-mission multi-mode waveform diversity," in *IEEE Conference on Radar*.

[8] M. Secmen, S. Demir, A. Hizal, and T. Eker, "Frequency diverse array antenna with periodic time modulated pattern in range and angle," *IEEE Conference on Radar*, 2007, pp. 427–430.

[9] J. Huang, K. Tong, and C. J. Baker, "Frequency diverse array with beam scanning feature," in *Antennas and Propagation Society International Symposium*, 2008, pp. 1–4.

[10] W. L. Stutzman and G. A. Thiele, *Antenna Theory and Design*, 2nd ed. New York: John Wiley & Sons, 1998, pp. 107–109.

[11] F. T. Ulaby, *Fundamentals of Applied Electromagnetics*, 5th ed. New Jersey: Pearson Prentice Hall, 2007, pp. 403–416.

[12] M. I. Skolnik, *Radar Handbook*, 2nd ed. New York: McGraw-Hill, 1990.

[13] D. C. Jenn, "Arrays with elements above a ground plane," lecture notes for EC4610 (Microwave Devices and Radar), Naval Postgraduate School, Monterey, CA, 2003.

[14] H. E. Shanks and R. W. Bickmore, "Four Dimensional Radiators," *Canadian Journal of Physics*, vol. 37, p. 263, 1959.

[15] D. C. Jenn, “Dipoles of arbitrary orientation,” lecture notes for EC4610 (Microwave Devices and Radar), Naval Postgraduate School, Monterey, CA, 2003

[16] J. H. McClellan, R. W. Schafer, and M. A. Yoder, *Signal Processing First*. New Jersey: Pearson Prentice Hall, 2003, pp. 47–50.

[17] P. Antonik, “An investigation of a frequency diverse array,” Ph.D. thesis, University College London, Bloomsbury, London, UK, 2009

[18] J. D. Taylor, *Introduction to Ultra-Wideband Systems*, Florida: CRC Press, 1995, pp. 609–644.

[19] Center for Computer Research in Music and Acoustics, ‘Transient and steady-state signals,” [Online]. Available: https://ccrma.stanford.edu/~jos/filters/Transient_Steady_State_Signals.html, [Accessed: Sep. 2, 2010].

INITIAL DISTRIBUTION LIST

1. Defense Technical Information Center
   Ft. Belvoir, Virginia

2. Dudley Knox Library
   Naval Postgraduate School
   Monterey, California

3. Dr. David C. Jenn
   Department of Electrical and Computer Engineering
   Monterey, California

4. Dr. Dan C. Boger
   Chairman
   Department of Information Sciences
   Monterey, California

5. Lt. Col. Terry Smith
   IW/EW Program Officer
   Monterey, California

6. Lt. J.G. Alper AYTUN
   Turkish Navy
   Ankara, Turkey

7. Kara Harp Okulu
   Kara Hap Okulu Kütüphanesi
   Ankara, Turkey

8. Deniz Harp Okulu
   Deniz Harp Okulu Kütüphanesi
   İstanbul, Turkey

9. Hava Harp Okulu
   Hava Harp Okulu Kütüphanesi
   İstanbul, Turkey

10. Deniz Kuvvetleri Komutanlığı Araştırma Merkezi Komutanlığı
    İstanbul, Turkey